CRANFIELD UNIVERSITY

LIHAO YAN

Wire and Arc Additive Manufacture (WAAM) reusable tooling investigation

SCHOOL OF APPLIED SCIENCE
MRes Welding Engineering

MRes THESIS
Academic Year: 2012 - 2013

Supervisor: Dr Jörn Mehnen & Dr Fude Wang
October 2013

CRANFIELD UNIVERSITY

SCHOOL OF APPLIED SCIENCE
MRes welding Engineering

MRes THESIS

Academic Year 2012- 2013

LIHAO YAN

Wire and Arc Additive Manufacture (WAAM) reusable tooling investigation

Supervisor: Dr Jörn Mehnen & Dr Fude Wang
October 2013

ABSTRACT

Composite materials have been extensively adopted by modern aircraft design and manufacture. This manufacturing process needs a forming mould. Invar alloy has been widely used to manufacture moulds for the fabrication of aeronautics and astronautics composite structures because of its unique low thermal expansion coefficient. However, Invar is very expensive and the machining and repair process is difficult and costly. Therefore, to find an alternative approach to manufacture and repair the Invar mould is would help to save costs.

Additive Manufacturing (AM) technology is an innovative technology which can manufacture components layer upon layer directly from a CAD file without the need of tooling. Unlike conventional machining technologies which remove materials from a solid block of metal, AM is an additive process which can significantly save materials. Dissimilar material components can be fabricated by Wire and Arc Additive Manufacturing (WAAM) process with good metallurgical joints.

A new, functional tooling approach combining Invar and steel using Wire and Arc Additive Manufacturing (WAAM) technology is introduced in this research. Invar is used to fabricate the top part of the tool as it has a uniquely low thermal expansion coefficient property while the base part of the tool is made of mild steel to supply strength and save costs.

The research showed that Invar can be successfully deposited on steel using the WAAM process with high integrity joint. In addition, an FEM model was built to simulate the deformation of multi-material moulds in the autoclave heating process. Following on from the results from the FEA-based mould's deformation prediction, a parameter compensation method was proposed for the bi-material mould design and optimisation. The FEM model was verified through a case study around a composite door from a commercial aeroplane. The results indicate that the mould deformation can be effectively controlled by parameter

compensation and the optimised mould will satisfy industrial tolerance requirements.

Keywords:

Autoclave mould, Invar alloy, Welding, composite tooling, Deformation compensation

ACKNOWLEDGEMENTS

The author would like to extend his thanks to his supervisors: Dr. Jörn Mehnen and Dr. Fude Wang for their support and guidance during the whole project.

The author would like to thank Dr. Jialuo Ding and Dr. Liuxian Wei for their support and feedback of tests during the project.

The author would like to thank the Cranfield Welding Engineering Research Centre for funding the project and Mr Flemming Niselsen for their assistance work in the laboratory.

TABLE OF CONTENTS

ABSTRACT i
ACKNOWLEDGEMENTS iii
LIST OF FIGURES viii
LIST OF TABLES xiv
LIST OF EQUATIONS xv
LIST OF ABBREVIATIONS xvi
1 Introduction 1
1.1 Background 1
1.2 Reasons for this Research 5
1.3 Main objective 6
1.3.1 WAAM Invar on steel substrate feasibility study 6
1.3.2 Advanced tooling design and optimisation 6
1.4 Methodology 6
1.5 Outline of Thesis 7
2 Literature Review 9
2.1 Introduction 9
2.2 Autoclave forming process for composite components 9
2.2.1 Main equipment used in autoclave forming process 9
2.2.2 Main steps in the autoclave forming process 13
2.3 Curing deformation of composite products 14
2.3.1 Factors that cause dimensional variations 14
2.3.2 Introduction of the parameter compensation design method 15
2.4 Features of Invar alloy 18
2.4.1 Invar and its characteristics 18
2.4.2 Applications of Invar alloy 21
2.4.3 Welding capability of Invar alloy 22
2.5 Additive Manufacture (AM) 23
2.6 Cold Metal Transfer (CMT) 26
2.7 Challenges in welding dissimilar materials 27
2.8 Potential problems and possible solutions 29
2.8.1 Solidification cracking 29
2.8.2 Shielding gases 29
2.8.3 Microstructure influence 31
2.9 Summary 32
3 Experimental Procedures 33
3.1 Materials and equipment 33
3.1.1 Experimental materials 33
3.1.2 Welding facilities 33
3.1.3 Voltage and current recording device 34
3.2 Single-layer welding 35

3.2.1 Description of welding method 35
3.2.2 Parameters set up 36
3.3 Investigation into welding multi-layers 37
3.3.1 Description of welding method 37
3.3.2 Parameters set up 38
3.4 Wall Fabrication 38
3.4.1 Invar-Steel wall fabrication 38
3.4.2 Invar wall fabrication 42
3.5 Mechanical Test 42
3.5.1 Tensile test 42
3.5.2 Hardness test 43
3.6 Metallographic analysis 43
3.6.1 Optical microscope 44
3.6.2 SEM analysis 44
4 Results 45
4.1 Bead on plate deposition 45
4.1.1 Macroscopic analysis of specimens 45
4.1.2 Heat input with different shielding gases 46
4.1.3 Welding bead dimension measurement 47
4.2 Multi-layer welding 48
4.3 Microscopic analysis 49
4.3.1 Optical microscope analysis 49
4.3.2 SEM observation and EDS analysis 51
4.4 Mechanical properties Test 55
4.4.1 Tensile test 55
4.4.2 Hardness test 57
5 FEM analysis 59
5.1 Mould fabrication and set up of boundary conditions 59
5.1.1 Set up of the FE mould 59
5.1.2 Measurements 60
5.2 Numerical mould results 61
5.2.1 Typical example: Invar content = 60% 61
5.2.2 Result of 11 sets 62
5.3 Summary 63
6 Parameter compensation method in mould 65
6.1 The parameter compensation method 65
6.2 The implementation process 66
6.2.1 Mould deformation definition 66
6.2.2 Principle of the parameter compensation method 67
6.2.3 Principle of the calculation process 68
6.3 Application of parameter compensation method 69
6.3.1 Set up of the FE mould 69

6.3.2 Initial deformation result 70
6.3.3 Parameter compensation design 72
6.3.4 Compensated surface deformation results and analysis 73
6.4 Summary 75
7 Discussion 77
7.1 WAAM Invar on steel feasibility ability study 77
7.1.1 Bead on the plate deposition 77
7.1.2 Multi-layer welding 78
7.1.3 Microscopic analysis results 80
7.1.4 Mechanical properties 80
7.2 WAAM Invar on steel feasibility ability study 81
7.2.1 Factors that influence mould deformation 81
7.2.2 Mould's stress analysis 83
7.2.3 Effective way to control mould's deformation 84
8 Conclusions 87
REFERENCES 88
APPENDICES 93

LIST OF FIGURES

Figure 1-1 Composite material usage in civil aircraft (EADS Deutschland GmbH, June 2004)..... 1

Figure 1-2 Composite materials usage in the main structure of aeroplane (University of bath, 08 July 2004) 2

Figure 1-3 Autoclave curing process is still a dominated process in composite structure manufacture(Tom Moore, 6 Dec. 2012)..... 2

Figure 1-4 Autoclave curing process needs a forming mould to fabricated composite structure (Elbit Systems Ltd., 2010) 2

Figure 1-5 Current approach and proposal for the advanced mould 5

Figure 1-6 Flow chart of the methodology in this thesis 7

Figure 1-7 Main structure of the thesis..... 8

Figure 2-1 Schematic of an autoclave (University of Tennessee - Knoxville, 2010) 10

Figure 2-2 Schematic of the forming mould, material: Invar (Process Fab Inc., 2007) 10

Figure 2-3 Three types of forming mould: male mould, female mould and assembly mould (Shao, 2009)..... 12

Figure 2-4 Schematic diagram of the vacuum bag..... 13

Figure 2-5 main steps in autoclave fabrication processing(Hoa, 2009)..... 14

Figure 2-6 Sources of dimension variation for composite products..... 15

Figure 2-7 Typical design structures for composite components (Dong, 2003) 17

Figure 2-8 Typical design structures for composite components (Dong, 2003) 17

Figure 2-9 Chemical composition of Invar alloy and its thermal expansion coefficient 19

Figure 2-10 The Fe-Ni binary alloy phase diagram (Cacciamani et al., 2006).. 20

Figure 2-11 Invar used in telescopes for structural support systems(Wassermann, 1991)..... 21

Figure 2-12 Long-distance LNG pipeline can be designed as a straight line where Invar alloy is used (Otsuka, 2006)..... 22

Figure 2-13 Example of a method for produced manually a 3D metallic object layer by layer by shielded metal arc welding process (Baker, 1925) 24

Figure 2-14 Example of pressure vessel fabrication using SAW, electroslag and TIG process, also including multiwire with different wires to give functionally graded walls，(Ujiie，1972) 24

Figure 2-15 Example of using Shape Welding to manufacture high quality large nuclear structural steel ($_{20}MnMoNi_{55}$) parts, (Kussmaul et al., 1983) 25

Figure 2-16 The difference between GMAW and GTAW is that the tungsten electrode provides only the electricity, but not the filler (RobotWorx Co., 2009) 26

Figure 2-17 Fronius CMT-GMAW, As Viewed under High Speed Photography (one cycle) (Fronius Ltd., 2005) 27

Figure 2-18 Average instantaneous power usage compared during different welding processes (Leinonen, 2011) 27

Figure 3-1 Pictorial representation of welding facilities 34

Figure 3-2 AMW 4000 welding monitor 34

Figure 3-3 Single-layer welding setup: a length of 100mm bead was welded each time and back shielding was used to enhance the protection of the weldment 36

Figure 3-4 Measurement of usable area efficiency(Leinonen, 2011); total area in red, usable area after machining in blue 38

Figure 3-5 Schematic diagram of Invar-steel wall building forming process 39

Figure 3-6 When the steel structure was fabricated, the top layer of steel had to be ground to obtain a flat layer for Invar deposition 39

Figure 3-7(a) The additive-bricks method was used to enhance the shielding gas protection effect 40

Figure 3-7(b) Schematic diagram of the additive-bricks method (from the end-view) 40

Figure 3-8 Invar-steel welded samples 41

Figure 3-9 Invar welded samples 42

Figure 3-10 21 points along a line perpendicular to the weld seam with interval 250μm 43

Figure 4-1 Average energy input measurement against change in WFS 47

Figure 4-2 Deposition shape comparison: WFS=8m/min, TS=0.4m/min, ... 48

Figure 4-3 Picture of sample 6, WFS=6 m/min, TS=0.48 m/min, layer height 2 mm shielding gas: Ar + 2.5% CO2 48

Figure 4-4 Picture of cross section from sample 6, WFS=6 m/min, TS=0.48 m/min, layer height 2 mm shielding gas: Ar + 2.5% CO2 48

Figure 4-5 picture of sample 2 cross section, WFS=6 m/min, TS=0.48 m/min, layer height 2 mm shielding gas: Ar + 2.5% CO2 49

Figure 4-6 Measurement of usable area efficiency coefficient with different shielding gases 49

Figure 4-7 Optical microstructure observation of Invar/steel joint 50

Figure 4-8 Optical microstructure image of deposited Invar alloy by WAAM process 50

Figure 4-9 BSE image of WAAM Invar/Steel joint 51

Figure 4-10 SEM image of WAAM Invar/Steel joint 52

Figure 4-11 SEM image of WAAM deposited Invar alloy 52

Figure 4-12 SEM image of grain boundary precipitation of WAAM deposited Invar alloy 53

Figure 4-13 SEM analysis of the sample (pure Argon used) 53

Figure 4-14 Composition of Fe and Nickel versus location for a graded interface between Invar and steel, shielding gas: Ar 54

Figure 4-15 Composition of Fe and Nickel versus location for a graded interface between Invar and steel, shielding gas: Ar+2.5%CO2 54

Figure 4-16 Invar-steel samples failed within the Invar remote from the weld .. 56

Figure 4-17 Fracture morphology of tensile specimen images by SEM. (a) Invar/steel joint with Argon shielding gas; (b) Invar/steel joint with Argon + 2.5% CO2 shielding gas; (c) Pure Invar tested longitudinally; (d) Pure Invar tested transversely. 56

Figure 4-18 Interface hardness measurement, the points were set perpendicularly to the weld seam 57

Figure 4-19 Vickers hardness across steel to Invar joint 57

Figure 5-1 Two-dimensional rectangular model, Invar volume fraction varied from 0% to 100% 59

Figure 5-2 The mould initial and deformed shape when FEM wad used for numerical simulation of the curing process 60

Figure 5-3 Strain contours of the deformed shape, Invar content =60%, deformation scale factor=40, unit: m. 61

Figure 5-4 Stress distribution diagram of the deformed mould, Invar content =60%, deformation scale factor=40, unit: Pa 62

Figure 5-5 Measurement of mould’s bend angle change according to Invar content in the heating process. 63

Figure 5-6 Measurement of mould's bend length change according to Invar content in the heating process. 63

Figure 6-1 Parameter compensation design method flowchart 66

Figure 6-2 Deformation Schematic of the mould's surface 67

Figure 6-3 Basic calculation process of the mould surface 68

Figure 6-4 APU (auxiliary power unit) door from commercial aircraft 70

Figure 6-5 Female mould used for APU door forming 70

Figure 6-6 Strain contours of the deformed shape, ... 71

Figure 6-7 Stress contours of the deformed shape, ... 71

Figure 6-8 Node positions 72

Figure 6-9 New design shape of the mould 72

Figure 6-10 Shape created 73

Figure 6-11 Partial enlarged view of Model modification 73

Figure 6-12 Strain contours of compensated surface deformation, deformation scale factor=2, unit: m 74

Figure 6-13 Stress contours of compensated surface deformation deformation scale factor=2, unit: Pa 74

Figure 7-1 Cross section of the multi-layer welding 79

Figure 7-2 Sandwich model for bimetal mould 85

Figure A-1 Certification of Invar material 93

Figure B-1 Dog-bone sample dimension 94

Figure C- 1 SEM image of Invar-steel sample 95

Figure C- 2 Composition of Fe and Nickel versus location for a graded interface between Invar and steel 95

Figure C- 3 SEM image of Invar-steel sample 96

Figure C- 4 Composition of Fe and Nickel versus location for a graded interface between Invar and steel 96

Figure D- 1 Invar-steel wall, shielding gas of Argon; Invar 35 layers, steel 40 layers (Invar part waviness is higher due to less effective protection) 97

Figure D- 2 Image of Invar-steel wall cut from the substrate 97

Figure D- 3 Invar-steel wall, shielding gas of Argon+2.5%CO2;..... 98

Figure D- 4 Image of Invar-steel wall cut from the substrate 98

Figure D- 5 Invar-steel wall; Invar 65 layers 99

Figure D- 6 Image of Invar wall cut from the substrate 99

Figure E-1 Strain contours of the deformed shape, Invar content =0%, deformation scale factor=40, unit: m…… 100

Figure E-2 Stress distribution diagram of the deformed mould, Invar content =0%, deformation scale factor=40, unit: Pa 100

Figure E-3 Strain contours of the deformed shape, Invar content =10%, deformation scale factor=40, unit: m..... 101

Figure E-4 Stress distribution diagram of the deformed mould, Invar content =10%, deformation scale factor=40, unit: Pa 101

Figure E-5 Strain contours of the deformed shape, Invar content =20%, deformation scale factor=40, unit: m..... 102

Figure E-6 Stress distribution diagram of the deformed mould, Invar content =20%, deformation scale factor=40, unit: Pa 102

Figure E-7 Strain contours of the deformed shape, Invar content =30%, deformation scale factor=40, unit: m..... 103

Figure E-8 Stress distribution diagram of the deformed mould, Invar content =30%, deformation scale factor=40, unit: Pa 103

Figure E-9 Strain contours of the deformed shape, Invar content =40%, deformation scale factor=40, unit: m..... 104

Figure E-10 Stress distribution diagram of the deformed mould, Invar content =40%, deformation scale factor=40, unit: Pa 104

Figure E-11 Strain contours of the deformed shape, Invar content =50%, deformation scale factor=40, unit: m..... 105

Figure E-12 Stress distribution diagram of the deformed mould, Invar content =50%, deformation scale factor=40, unit: Pa 105

Figure E-13 Strain contours of the deformed shape, Invar content =60%, deformation scale factor=40, unit: m..... 106

Figure E-14 Stress distribution diagram of the deformed mould, Invar content =50%, deformation scale factor=40, unit: Pa 106

Figure E-15 Strain contours of the deformed shape, Invar content =70%, deformation scale factor=40, unit: m..... 107

Figure E-16 Stress distribution diagram of the deformed mould, Invar content =50%, deformation scale factor=40, unit: Pa 107

Figure E-17 Strain contours of the deformed shape, Invar content =80%, deformation scale factor=40, unit: m..... 108

Figure E-18 Stress distribution diagram of the deformed mould, Invar content =50%, deformation scale factor=40, unit: Pa 108

Figure E-19 Strain contours of the deformed shape, Invar content =90%, deformation scale factor=40, unit: m..... 109

Figure E-20 Stress distribution diagram of the deformed mould, Invar content =50%, deformation scale factor=40, unit: Pa 109

Figure E-21 Strain contours of the deformed shape, Invar content =100%, deformation scale factor=40, unit: m..... 110

Figure E-22 Stress distribution diagram of the deformed mould, Invar content =50%, deformation scale factor=40, unit: Pa 110

Figure E-23 Strain contours of original surface deformation, deformation scale factor=2, unit: m..... 111

Figure E-24 Stress contours of original surface deformation, deformation scale factor=2, unit: Pa 111

Figure E-25 Strain contours of compensated surface deformation (heated), deformation scale factor=2, unit: m..... 112

Figure E-26 Stress contours of compensated surface deformation (heated), deformation scale factor=2, unit: Pa 112

LIST OF TABLES

Table 1-1 Performance of materials for mould manufacture (Huang, 2011)..... 3

Table 2-1 Chemical composition of Invar36 alloy (W %) 18

Table 2-2 Thermal expansion coefficient of Invar 36 alloy 18

Table 2-3 Strength properties of Invar36 alloy and Austenitic stainless steel at ambient temperature (Takehiko, 2006)..... 20

Table 3-1 Invar chemical composition 33

Table 3-2 S355 mild steel chemical composition..... 33

Table 3-3 Preliminary CMT parameters set-up in single-layer welding 37

Table 3-4 Parameters used in the multi-layer Investigation..... 38

Table 3-5 Parameters for bimetal wall fabrication 41

Table 3-6 Parameters for Invar wall fabrication 42

Table 4-1 Macroscopic quality of specimens..... 45

Table 4-2 Macroscopic quality of specimens..... 46

Table 4-3 tensile test result 55

Table 5-1 Measurement parameters 60

Table 5-2 Measurement values of the deformed shape 62

Table 6-1 Angle change 71

Table 6-2 Compensated surface deformation result and comparison 74

LIST OF EQUATIONS

(2-1)..... 16
(3-1)..... 35
(6-1)..... 67
(6-2)..... 67
(6-3)..... 67
(6-4)..... 68
(6-5)..... 68
(6-6)..... 69
(7-1)..... 79

LIST OF ABBREVIATIONS

AM	Additive Manufacturing
Ar	Argon
$\angle A'B'C'$	Angle of $A'B'C'$
CTE	Coefficient Of Thermal Expansion
CMT	Cold Metal Transfer
CO_2	Carbon Dioxide
EBM	Electron Beam Melting
EDS	Energy-Dispersive Spectroscopy
FEM	Finite Element Method
GTAW	Gas Tungsten Arc Welding
GMAW	Gas Metal Arc Welding
He	Helium
H2	Hydrogen
HAZ	Heat Affect Zone
LAM	Laser Additive Manufacturing
LNG	Liquefied Natural Gas
$l_{A'B'C'}$	Length of $A'B'C'$
MIG	Metal Inert-Gas Welding
N2	Nitrogen
O2	Oxygen
RP	Rapid Prototyping
SDM	Shape Deposition Manufacturing
SEM	scanning electron microscope
SMAW	Shielded Metal Arc Welding
SAW	Submerged Arc Welding
TS	Travel Speed
UTS	Ultimate Tensile Strength
TIG	Tungsten Inert-Gas Welding
UAE	Useable Area Efficiency
WFS	Wire Feed Speed

WAAM	Wire And Arc Additive Manufacturing
3DP	Three-Dimensional Printing

1 Introduction

1.1 Background

Composite materials have been extensively adopted by modern aircraft design and manufacture, such as Boeing 787 and Airbus 350 because of its low-density and high-strength (Figure 1-1 and Figure 1-2)(EADS Deutschland GmbH, June 2004)Figure 1-1 Composite material usage in civil aircraft (EADS Deutschland GmbH, June 2004)

The use of composites in civil aircraft has grown from 3% to nearly 50% by weight from 1975 till now (EADS Deutschland GmbH, June 2004). For composite structure manufacture, autoclave curing is still the dominant process. This process needs a mould for forming composite structure, as shown in Figure 1- 3 and Figure 1- 4.

With the staggering growth in the use of composite materials used, demands for the forming moulds are also increasing rapidly. More importantly, composite materials are used in main structure components of aircraft such as the fuselage and wings (see Figure 1-2). This needs correspondingly larger moulds.

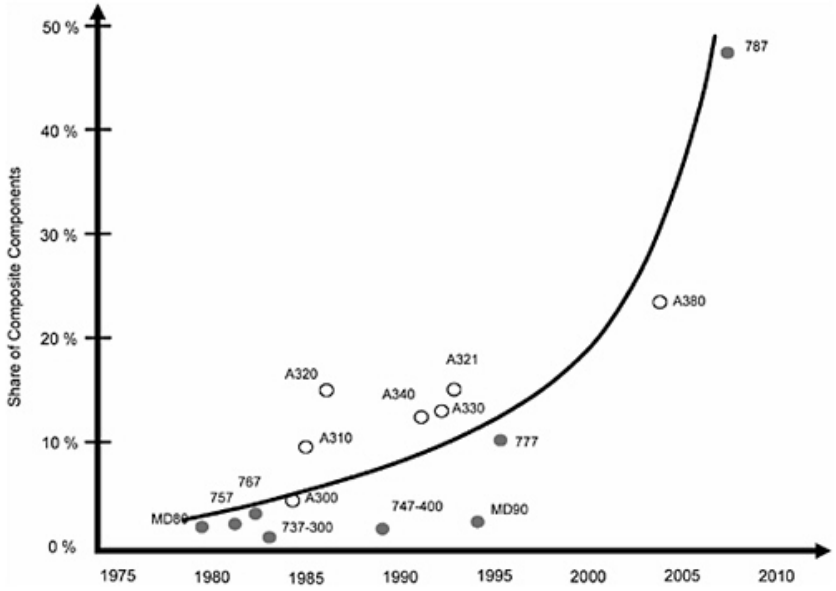

Figure 1-1 Composite material usage in civil aircraft (EADS Deutschland GmbH, June 2004)

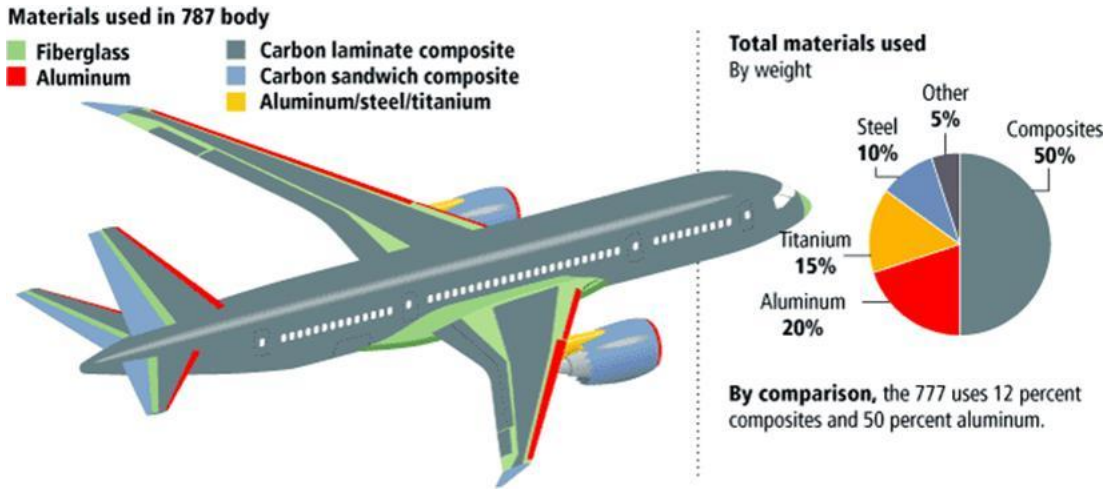

Figure 1-2 Composite materials usage in the main structure of aeroplane (University of Bath, 08 July 2004)

Figure 1-3 Autoclave curing process is still a dominated process in composite structure manufacture (Tom Moore, 6 Dec. 2012)

Figure 1-4 Autoclave curing process needs a forming mould to fabricated composite structure (Elbit Systems Ltd., 2010)

Currently, most of the forming mould is made of carbon steel, aluminium alloy, composite material and Invar (Huang, 2011). Carbon steel and aluminium alloy moulds have a significantly different thermal expansion coefficient with composite material (see Table 1-1), which results in distortion during composite structure fabrication. This makes it difficult for steel and aluminium alloy moulds to achieve the dimensional accuracy required by aerospace industry.

The characteristics of composite moulds are low thermal expansion coefficient，light weight and low thermal capacity. However, the composite material matrix is easily damaged and the mould's service life is relatively short. Furthermore, tooling for composite moulds is irreversible which makes it impossible to repair once the mould has been formed.

Invar alloy has a very similar thermal expansion coefficient (from room temperature to 230°) to composite material (see Table 1-1). Therefore, it has been widely used to manufacture moulds for fabrication of aeronautics and astronautics composite structures.

Table 1-1 Performance of materials for mould manufacture (Huang, 2011)

	carbon steel	aluminium alloy	Invar	composite material
thermal expansion coefficient(/°C,RT-200°C)	12×10-6	26×10-6	2.5×10-6	3.6×10-6
Manufacturing method	Welding machining	Welding machining	Welding machining	Solidify Paving
Difficult level to manufacture	High	Low	High	High
Material cost	Low	High	High	High
Manufacturing costs	Low	Low	High	High
Manufacturing cycle (month)	3	2.5	4	3.5
Service life(times)	>500	200	500	100~200

However, it is difficult and costly to manufacture Invar moulds. The ability of Invar alloy to be machined is generally poor and it is a very expensive material

(University of Bath, 08 July 2004). Additionally, it is difficult and costly to repair Invar moulds. Table 1-1 shows the basic performance of this material for moulds.

Additive Manufacturing (AM) is a freeform manufacturing technology which can manufacture components layer upon layer directly from a CAD file without need of tooling (Mattias, 2011). It has been used in rapid prototyping, automotive and aerospace industry as well as military and many other fields (Yang, 2010). The main advantages of AM are short lead time, material saving and it can fabricate complex geometrical components which cannot be manufactured by traditional machining processes (Chen et al., 2012). Typically, the buy-to-fly-ratio of aircraft components is 10:1 or higher in conventional manufacturing processes. This value can be reduced by 35~45% using AM technology (Smock, 2010). AM can be used as an alternative method to manufacture components.

A number of additive processes are now available and they are different in heat source, material and material transportation methods (Sherman, 2007). Wire and arc additive manufacturing (WAAM) is a novel manufacturing technology which can directly fabricate large 3-D simple geometry near net shape and fully dense components, from metal wire. During fabrication, the wire is fed at a controlled rate into the welding arc where the wire is melted and the substrate or the previously deposited layer is partially melted. This forms the fully dense component layer by layer as the movement of the arc follows the pre-defined path from a CAD file. It has a much higher deposition rate (several kg/hr), higher alloy capture efficiency (approaching 100%), no powder handling requirement and lower cost comparing to the laser and powder based technology (Owusu-Ofori et al., 1997; RobotWorx Co., 2009). Leinonen's work shows components of dissimilar materials (use of CMT process to deposit Cu97Si3 wire onto structural steel) can be fabricated by WAAM and the joint gives high strength, good heat conductivity (Mattias, 2011). This showed that the WAAM technology has a potential capability to manufacture bi-metal components.

1.2 Reasons for this Research

During Invar mould manufacturing, the vast majority of the material is machined away during traditional Invar mould manufacture. Considering the high cost of Invar material and its poor machinability, this considerably increases the manufacturing and repair cost of Invar moulds. Therefore, finding an alternative approach to manufacture Invar mould would help industries to reduce their costs. One solution is to replace part of the Invar mould with steel.

Research has shown that WAAM technologies can build Cu97Si3 bronze on the top of steel (Mattias, 2011). Therefore it should be possible to build Invar on the top of steel.

The purpose of this research is to fabricate an advanced, functional tooling for composite material fabrication using WAAM technology. It also includes the repair of tooling through WAAM technology.

The proposed advanced functionally tooling contains Invar and steel as indicated in Figure 1-5. Invar will be used as a top part, as in conventional Invar tooling, to provide its uniquely low thermal expansion coefficient property while the base part is made of mild steel to supply strength and save costs.

The main objective of this project is to investigate the feasibility of fabricating a bi-metal mould which contains Invar and steel to reduce cost by WAAM technology.

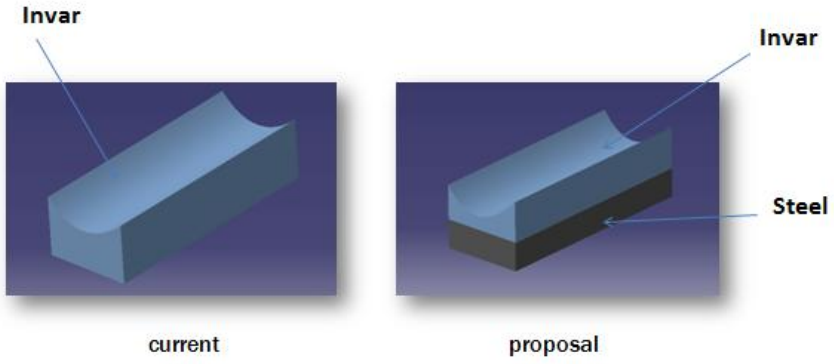

Figure 1-5 Current approach and proposal for the advanced mould

1.3 Main objective

This aims of this research are to investigate an innovative method to manufacture composite tooling for the aerospace industry.

The specific objectives of this project are:

1.3.1 WAAM Invar on steel substrate feasibility study

The Cold Metal Transfer (CMT) welding process is used to deposit Invar on steel. Macro and micro properties of the joining components are investigated in this phase, including mechanical and metallurgical investigation.

Two main steps will be carried in this phase:

1. Invar on steel deposition experiment will be carried out and the optimisation parameter is established.
2. The joining properties are investigated from both mechanical and metallurgical aspects.

1.3.2 Advanced tooling design and optimisation

A Finite Element Method (FEM) model containing different volume fractions of Invar and steel has been built to predict the mould dimensional deformation when it undergoes a use heat cycle. Based on the FEM model study, a deformation compensation method is developed to make the new mould thermal deformation meet the requirements of specified tolerances in the composite industry.

1.4 Methodology

According to the aim and main objects, a research strategy was developed (see in Figure 1-6). The first step is to investigate the welding capability of Invar and mild steel to make sure there is sufficient joining strength between the Invar and steel. The second step is to analyze the mould dimension deviation by Finite Element Method to make sure the bi-metal mould meets the composite industry requirements.

The whole task can be divided into two parts: experiment and FE model analysis. The project is carried out step by step according to the flow chart, as indicated in Figure 1-6. It has four parts. They are literature review, Invar on steel weldability investigation, FE model analysis and conclusion.

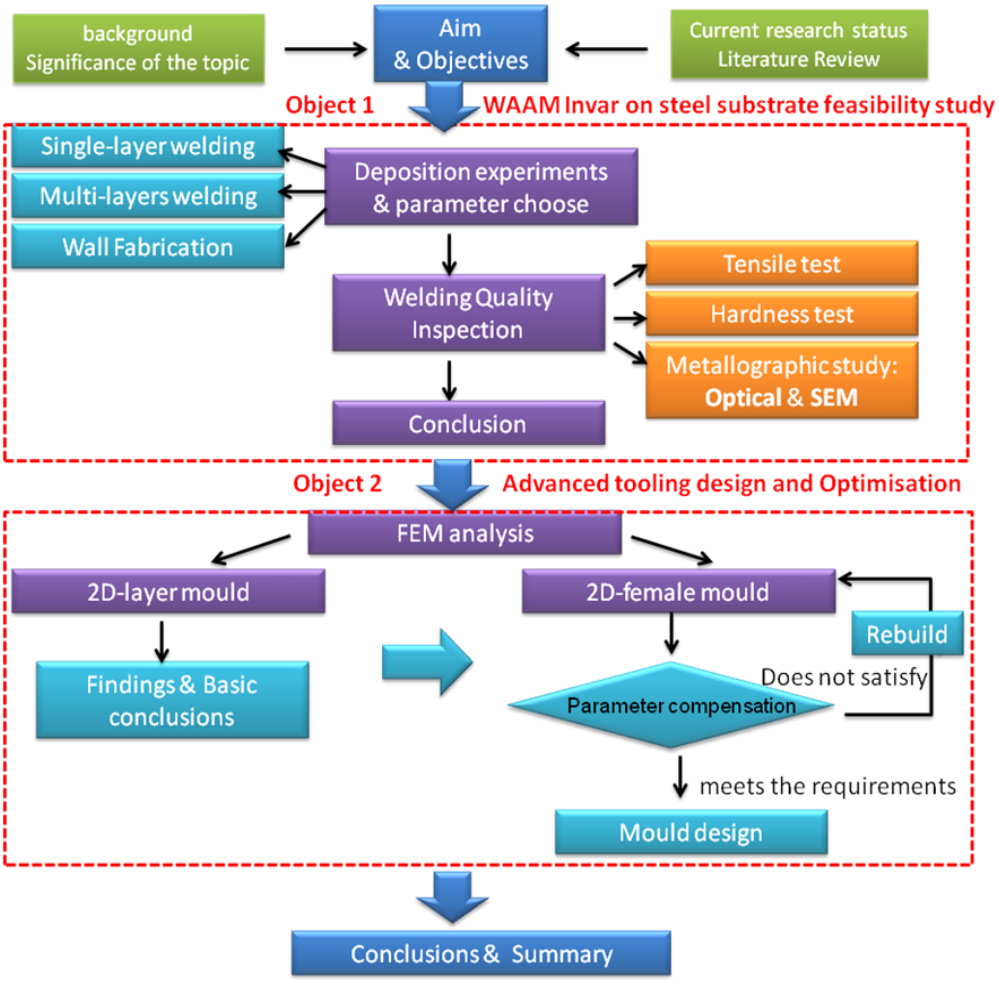

Figure 1-6 Flow chart of the methodology in this thesis

1.5 Outline of Thesis

Background information and reasons for research are outlined at the beginning of this thesis. In this part, the object and main steps are described together with the arrangement of thesis's structure. In Chapter 2, a literature review is given, including Invar properties, the Additive layer manufacture process, challenges in welding dissimilar materials and curing process for composite material. In Chapter 3, the experimental procedure including experimental methods,

parameters and facilities are presented. The metallographic analysis and mechanical property of WAAM Invar are also included in Chapter 3. Experimental results are presented in chapter 4. The finite element model analysis is reported in Chapter 5. Compensation design study is presented in Chapter Six. The whole structure of this thesis is shown in Figure1-7.

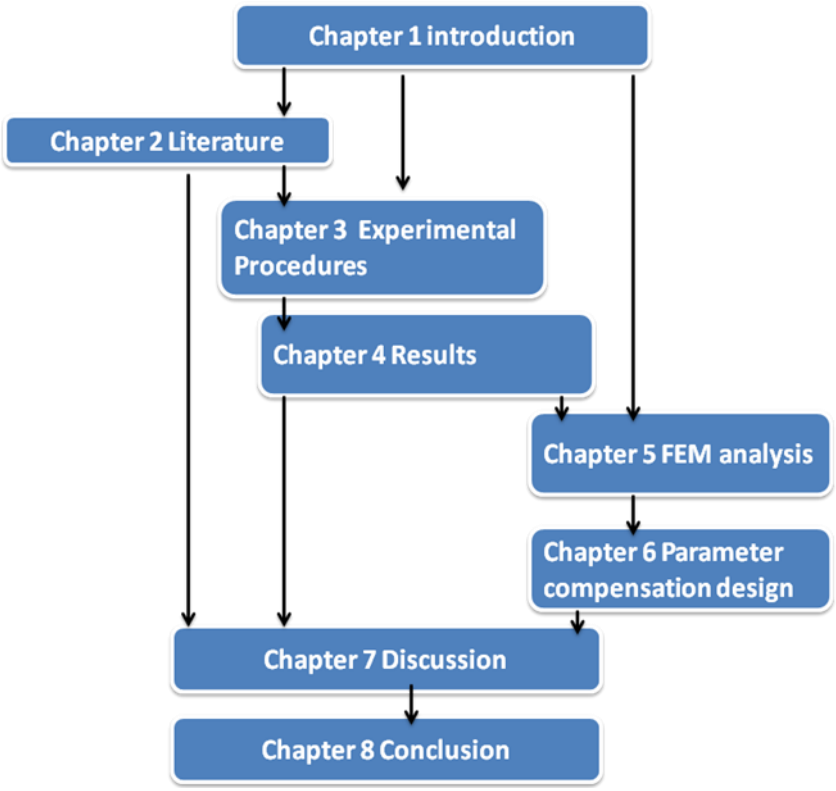

Figure 1-7 Main structure of the thesis

2 Literature Review

2.1 Introduction

A brief introduction about autoclave forming process and WAAM technology is given in this chapter. Invar alloy and potential problems of Invar welding are also included.

2.2 Autoclave forming process for composite components

Autoclave Moulding, Compression Moulding, Pultrusion, Filament Winding, Elastic Reservoir Moulding, Tube Rolling and Resin Transfer Moulding are the six main processes in making composite components at the present time (PK Mallick, 1993). The processing costs, component size, complexity of the parts and final requirements are the main considerations used in selecting an appropriate forming process (Owusu-Ofori et al., 1997).

The autoclave forming process is a special fabrication technology used to process resin-impregnated fabric composite materials. It includes heating, vacuum, pressure and other processes. It can fabricate high strength to weight ratio fibres and epoxy parts for load-bearing structures, such as beams, ribs, stringers, joints, as well as the entire body box section and other structural forms required in the aerospace industry (Luling, Li Guidong Zhou Laishui An and Xiaojing, 2010). In addition, this process is efficient; it can form a variety of composite structures using different forming moulds in the autoclave at the same time.

However, compared with other forming processes, the autoclave curing process is much more complex, it needs higher investment and running costs are also higher.

2.2.1 Main equipment used in autoclave forming process

2.2.1.1 Autoclave

An autoclave is a large pressure vessel with a heating system. It contains a pressure vessel, vacuum & pressure system, heating system, control system

and so on, as indicated in Figure 2-1.The function of the autoclave is to provide uniform temperature and pressure during a composite component forming process.

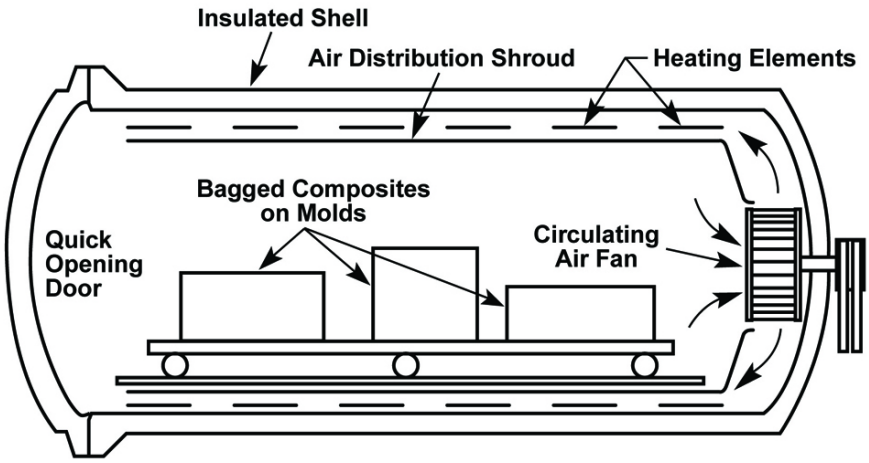

Figure 2-1 Schematic of an autoclave (University of Tennessee - Knoxville, 2010)

2.2.1.2 Forming mould

The function of the forming mould is to provide essential support and restraint for the composite components. Depending on the forming requirements, the forming mould is generally made of carbon steel, aluminium alloy, composite material or Invar. Figure 2- 2 is a typical Invar mould.

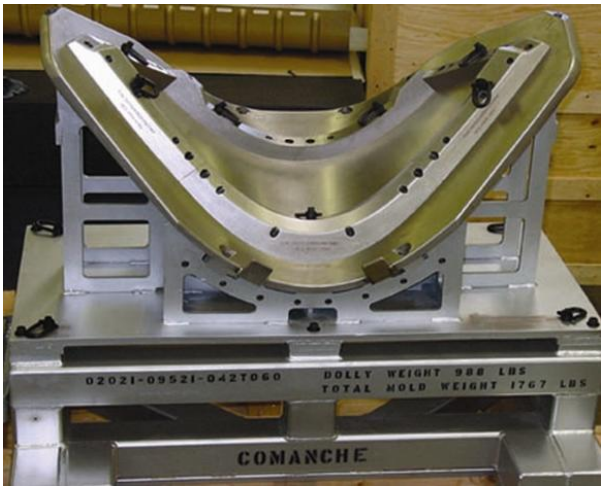

Figure 2-2 Schematic of the forming mould, material: Invar (Process Fab Inc., 2007)

Below are some basic requirements for the mould (HE et al., 2006):

1. Dimension and accuracy:

   The mould has to be accurate enough to meet the accuracy requirements of the dimensions of the composite component products. The difference between the thermal expansion coefficients for the composite component and the forming mould material has to be very small in order to minimize the thermal stress between the forming mould and the composite part. This can reduce the product deformation and guarantee dimensional stability.
2. Stiffness and strength:

   The mould must provide sufficient stiffness and strength to prevent any distortion occurring which will affect the product's quality and the mould's service life.
3. Good thermal conductivity and thermal stability:

   The mould must have enough heat resistance capacity to prevent deformation during the curing process. In addition, it must have good thermal conductivity. This enables it to achieve a uniform heating process which will reduce the curing cycle time of composite material and save energy costs.
4. Material and transport:

   The material of the forming mould should be easy to obtain and the tooling device should be easy to transport.
5. Manufacturing, maintenance and repair:

   Easy repairs and low-cost maintenance help extend the service life of the mould.

2.2.1.3 Main types of mould

There are three types of forming moulds (Shao, 2009): Male mould, female mould and assembly mould, as shown in Figure 2-3.

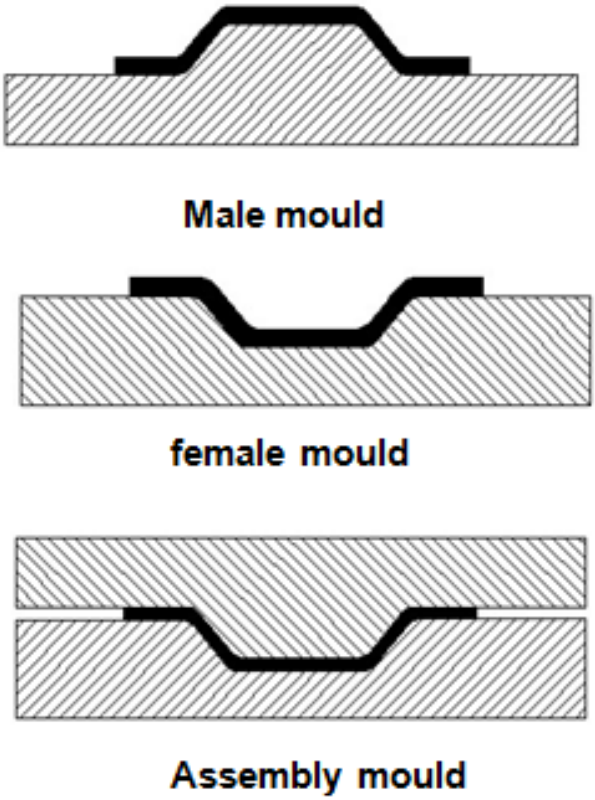

Figure 2-3 Three types of forming mould: male mould, female mould and assembly mould (Shao, 2009)

2.2.1.4 Auxiliary facilities

Auxiliary facilities include vacuum bag, re-mould agent, breathable material and so on. Layers of pre-impregnated fibres (prepreg) are piled using various fibre orientations, to form the desired thickness above the forming tool as shown in Figure 2-4. Vacuum bags are applied evenly to pressurise prepreg into complex shapes. During infusion, the resin flows across the surface of the mould to obtain the desired shape.

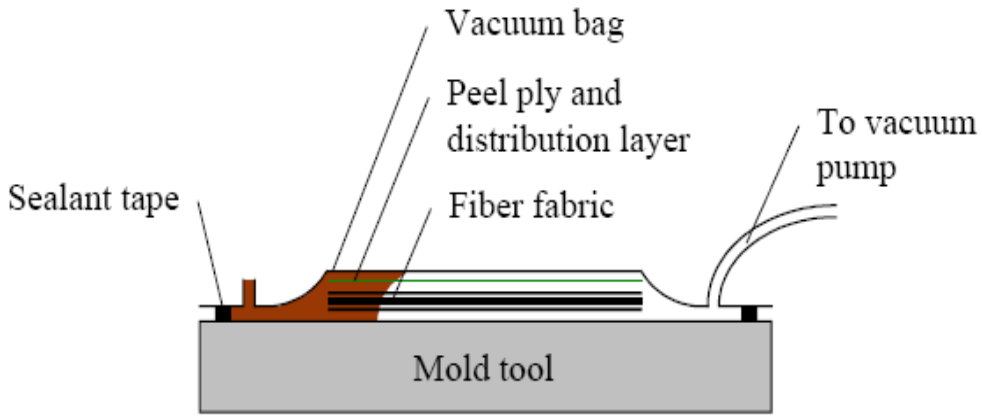

Figure 2-4 Schematic diagram of the vacuum bag

used in the forming process (Hoa, 2009)

2.2.2 Main steps in the autoclave forming process

In the autoclave forming process, prepreg materials are laid at different orientations for each layer. They lie on top of mould according to design requirements.

The main steps in autoclave processing are listed, as shown in Figure 2-5 (Hoa, 2009):

1. Prepregs
2. Tool preparation
3. Laying up prepregs on the tool to make the part
4. Curing of the part
5. Removal of the part from the tool
6. Inspection
7. Finishing steps

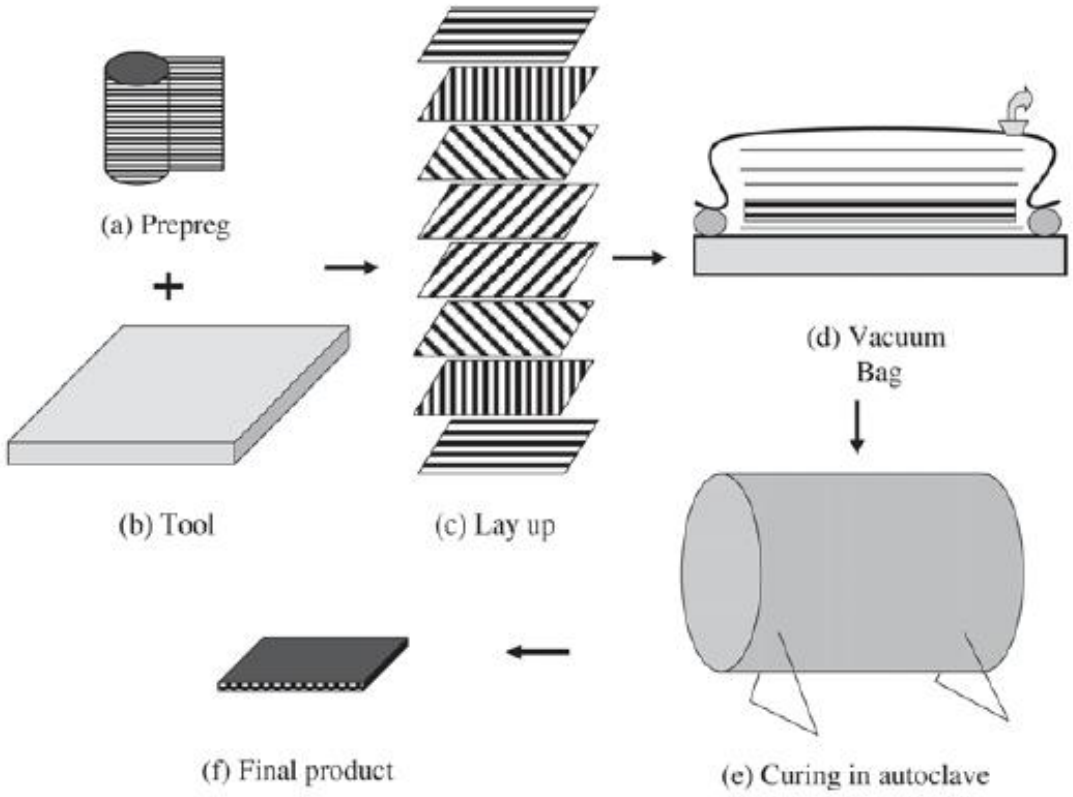

Figure 2-5 main steps in autoclave fabrication processing(Hoa, 2009)

After heateing→ pressurizing → thermal insulation →cooling and pressure relief processes, the resin will have completed the whole curing cycle.

2.3 Curing deformation of composite products

2.3.1 Factors that cause dimensional variations

The shape of composite products is determined by the forming mould's surface dimension. The product's final dimension depends on the forming mould's size at the curing temperature. The mould's dimension changes when the autoclave's temperature is changed. The maximum deformation happens when the curing temperature reaches its maximum. This not only affects the accuracy of the final composite product, but it is also adversely affects the product's assembly. Factors that cause deformation of the cured composite components can be divided into three categories (Dong, 2003):

1. mismatch in thermal expansion coefficients (CTE) between the forming mould and the composite material
2. interaction between the mould and composite component
3. shrinkage of the resin during curing process

Figure 2-6 shows the individual contributions of these categories in a typical composite material part. It indicates that the mismatch in thermal expansion coefficients between the forming mould and the composite material is the dominant factor influencing dimension variation.

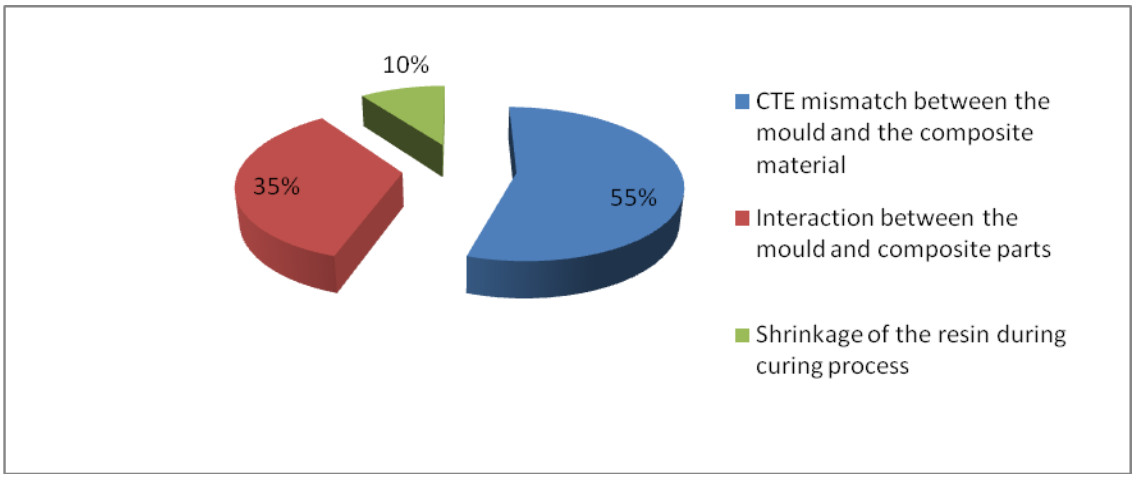

Figure 2-6 Sources of dimension variation for composite products

2.3.2 Introduction of the parameter compensation design method

2.3.2.1 Traditional mould design method

At present, optimisation of the curing parameters and compensation design for the mould are the main ways to solve the problem of dimensional variation (Shao, 2009). Optimisation of curing parameters is usually done by modifying temperature ramps and dwell times in the cycle to reduce residual stresses in the curing process.

Optimisation of curing parameters can to some extent relax curing deformation of composite components, but it cannot completely eliminate the problem. Usually the final solution requires a compensation design method of the mould's surface as well.

The traditional method is based on experience or an empirical formula, as shown in equation 2-1, to calculate the expansion value of the mould. Then the mould's surface can be offset according to the deformation value obtained.

$$\Delta L = L \times \alpha \times \Delta T \quad \textbf{(2-1)}$$

Where: ΔL is the value of the dimension variation

L is the original dimension

α is the thermal expansion coefficient of the mould's material

ΔT is the temperature variation between the initial and forming stages

The limitation of this approach is that it is only available for moulds with small size and simple geometry or surface and it will lead to a large deviation for a larger size mould. For a more complex shaped mould, the method is impossible to use.

2.3.2.2 Parameter compensation design method

The finite element method originated in the 1950s, it was first used in aeronautical engineering in aircraft structural and mechanical design and analysis. The essence of finite element analysis is the structure discretization; it means that an infinite continuum is discretized into in combination of a finite number of units. It is called Finite element analysis because of the limited number of cells and nodes. In 1960, Clough dealt with plane elasticity issues by the finite element method and the result was consistent with the experimental results (Huebner et al., 2008).In 1986, TJR Hughes and E Hinton used finite element methods for plate and shell structures (Hughes and Hinton, 1986). The U.S. Company MSC was involved in the computational structural analysis program funded by NASA, and based on this it first produced the commercial simulation software "Nastran". With the rapid development of computer technology, a large number of finite element simulation programs such as Abaqus, Ansys, Autoform, Dynaform and so on were applied in various industries. Therefore, a large number of virtual tests can replace physical

experiments, and methods that combine FEM analysis and the typical validation experiments together could be used with high efficiency and low cost.

Jain et al (Jain et al., 1998) adopted a spring-in mode to modify the design of the forming mould for an aileron rib. Dong, using FEM, developed regression-based dimension variation models for dimension variation prediction and control for mould design (da Costa Pépe, Nuno Vasco, 2010; Dong, 2003). The feasibility of this model was verified both by the experimental results and data from literature in a series of typical structural shapes, as shown in Figure 2-7 and 2-8.

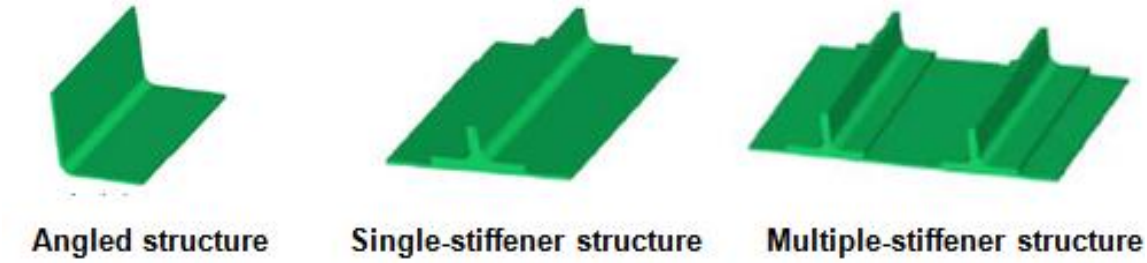

Figure 2-7 Typical design structures for composite components (Dong, 2003)

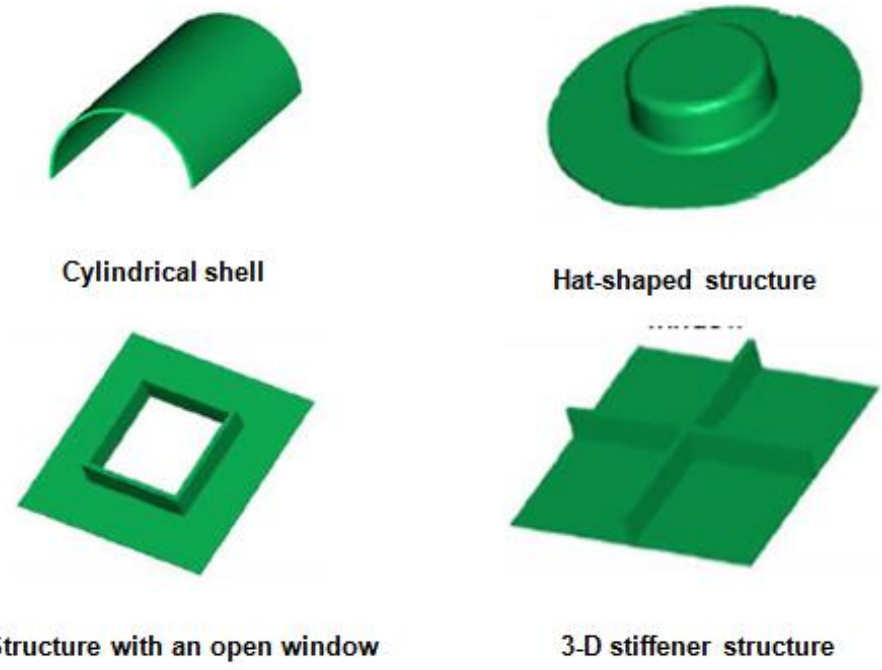

Figure 2-8 Typical design structures for composite components (Dong, 2003)

2.4 Features of Invar alloy

2.4.1 Invar and its characteristics

"Invar" is also called alloy 36, it is a nickel alloy notable for its unique low thermal expansion coefficient feature and its chemical composition is shown in Table 2-1. It was invented by Swiss scientist Charles Édouard Guillaume (Nobel Prize for Physics in 1920) in 1896 when he was looking for a dimensionally stable metallic material for geodesic equipment in land surveying. He discovered its property of lack of expansion even after temperature changes (Corbacho et al., 1998a). For instance, when an Invar sample is heated in a vacuum from 20 °C to 200 °C, its average thermal expansion coefficient is $2.5\times10^{-6}/°C$ (compared to most metallic materials which have a thermal expansion coefficient of $10\text{-}20\times10^{-6}/°C$).Table 2-2 shows Invar thermal expansion coefficients (CTE) at different temperature(Saito, 1978).

Table 2-1Chemical composition of Invar36 alloy (W %)

C	Si	P	S	Ni	Mn	Fe
≦						
0.05	**0. 2**	**0.02**	**0.02**	**35.0~37.0**	**0.20~0.60**	**balance**

Table 2-2 Thermal expansion coefficient of Invar 36 alloy at different temperatures

Temperature Range ($°C$)	Average CTE ($\times10^{-6}/°C$)	Temperature Range ($°C$)	Average CTE ($\times10^{-6}/°C$)
20~-60	1.8	20~250	3.6
20~-40	1.8	20~300	5.2
20~-20	1.6	20~350	6.5
20~0	1.6	20~400	7.8
20~50	1.1	20~450	8.9
20~100	1.4	20~500	9.7

Temperature Range ($^{\circ}C$)	Average CTE ($\times 10^{-6}/^{\circ}C$)	Temperature Range ($^{\circ}C$)	Average CTE ($\times 10^{-6}/^{\circ}C$)
20~150	1.9	20~550	10.4
20~200	2.5	20~600	11.0

It can be seen from Figure 2-9 that only at 36% nickel does the Iron-nickel alloy have a minimum thermal expansion. In addition, any deviation from this percentage of nickel leads to an increase in the thermal expansion coefficient, thus accurate control of nickel content is the key step to making Invar alloy.

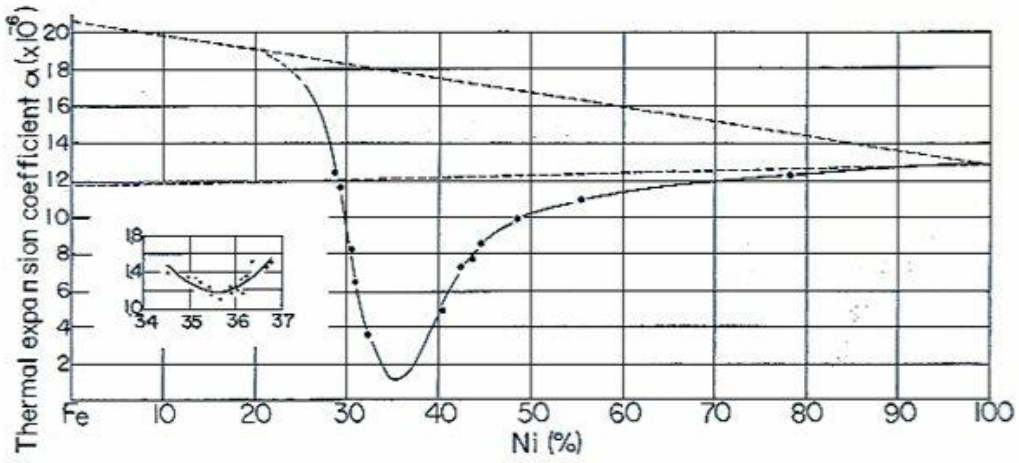

Figure 2-9 Chemical composition of Invar alloy and its thermal expansion coefficient

As shown in Figure 2-10, Invar has a single austenite microstructure at room temperature and its mechanical properties are very close to those of austenitic steels: high elongation with low hardness value and its Young's modulus is lower than that of common steel at ambient temperature (Takehiko, 2006) (see in Table 2-3).

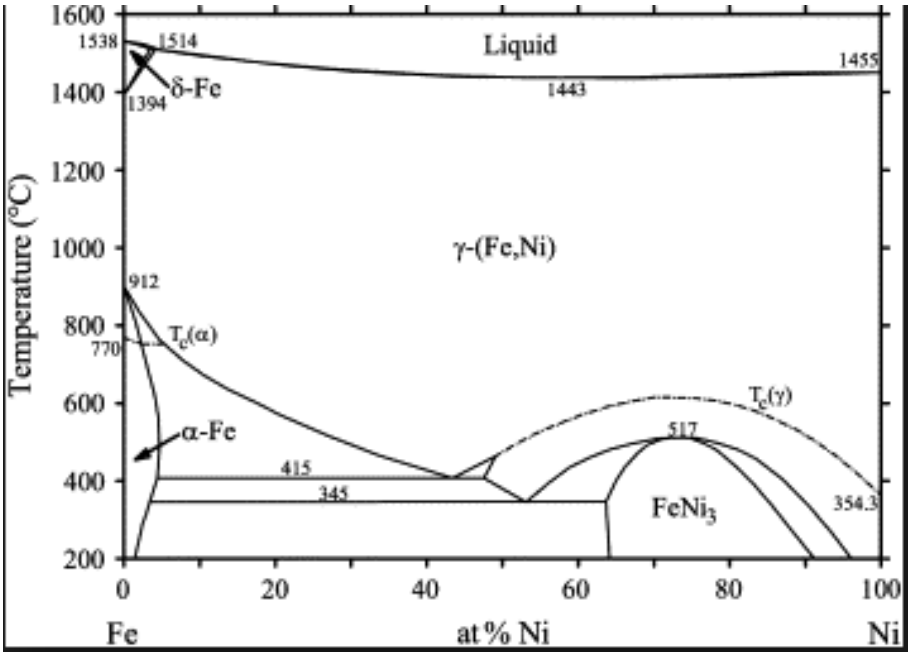

Figure 2-10 The Fe-Ni binary alloy phase diagram (Cacciamani et al., 2006)

Table 2-3 Strength properties of Invar36 alloy and Austenitic stainless steel at ambient temperature (Takehiko, 2006)

Property	Invar alloy	Austenitic stainless steel
0.2% proof stress	> 240 N/mm^2	> 205 N/mm^2
Tensile strength	> 440 N/mm^2	> 520 N/mm^2
Elongation	> 20 %	> 40 %

Compared with austenitic stainless steel, Invar alloy is more difficult to machine as it needs a large cutting force. This results in high cutting temperature which causes quick abrasion of the cutting tools (Sproule, 1990). Invar alloy is soft and sticky during the machining process. The machining swarf is not easy to cut off. It generates more frictional heat between the cutting tool and the workpiece. This will not only reduce the durability of the tool, but also the precision of machined parts.

2.4.2 Applications of Invar alloy

After it was invented, Invar has long been used as the material where high dimensional stability was needed, for instance precision instruments, geodesic equipment in land surveying, mechanical clocks. Since the 1920s, applications of Invar have gradually extended to valves in motors, antimagnetic watches, television shadow-mask frames and structural components in the electronics field (Sproule, 1990).

With the rapid development of aviation and aerospace technology, Invar was widely employed to make moulds for composite material fabrication, space remote sensors, man-made satellites, precision lasers, optical measurement systems and microscopes, structural support systems for telescopes (see in Figure 2-11), etc. (Wassermann, 1991).

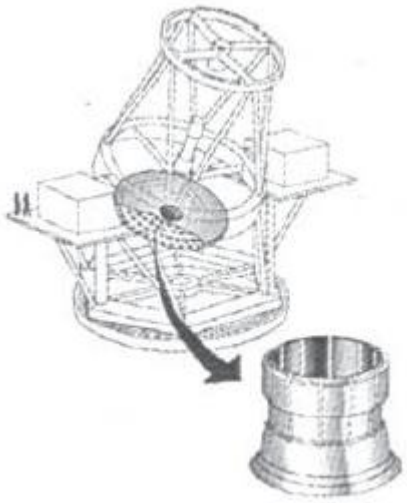

Figure 2-11 Invar used in telescopes for structural support systems(Wassermann, 1991)

In addition, because of its resistance in corrosive conditions, it can be used for LNG (liquefied natural gas) containers and pipelines for long-distance LNG transport (Otsuka, 2006).With steel, In order to minimise the expansion and shrinkage, a tube must be designed as a special "U" shape structure. With Invar alloy, the pipe line can be designed as a straight line because of its consistent low thermal coefficient, thus saving costs (see in Figure 2-12).

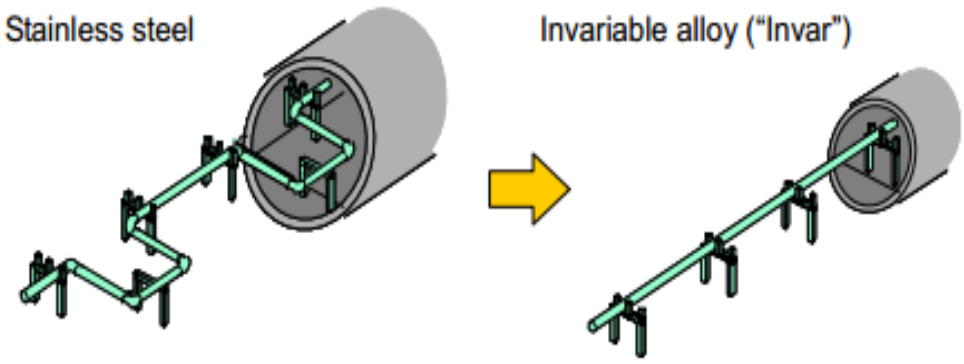

Figure 2-12 Long-distance LNG pipeline can be designed as a straight line where Invar alloy is used (Otsuka, 2006)

2.4.3 Welding capability of Invar alloy

In recent years, research about Invar alloys and its applications has increased dramatically. With the wide applications in Liquefied Natural Gas (LNG) containers, composite forming moulds for large aircraft, and other aspects such as microelectronics industry, the welding behaviour of Invar has become very important. The welding properties and methods of welding Invar alloys have therefore been extensively researched.

As a single austenite phase microstructure of Iron-Nickel alloy, Invar is sensitive to reheat cracking, which often leads to poor welding performance and cracking phenomena in the welding pool in the solidification stage (Wang et al., 2013). Earlier studies reported that this issue can be solved by the addition of titanium, manganese and a higher carbon content (Corbacho et al., 1998a). The main reason to add Ti and Mn to Invar alloy is prevent weld hot cracking and to use as a deoxidizer to form high melting point stable sulphide. This may be caused by the pinning effect of Ti and Mn precipitates, which hinders the migration of grain boundaries during recrystallization (Corbacho et al., 1998b). However these elements may also have negative effect on the alloy’s thermal expansion coefficient and thus cause a mismatch of thermal expansion coefficients around the welding joint. Generally a compromise chemical composition is 36% Ni, 3%Mn, 1% Ti, 0.1% C, and balance Fe, which provides relatively good balance

between resistance to solidification cracking and keeping thermal expansion coefficient low (Corbacho et al., 1998a).

Traditional methods for welding austenitic steel are Shielded Metal Arc Welding (SMAW), Submerged Arc Welding (SAW) and Gas Tungsten Arc Welding (GTAW). These methods are characterized by low heat input to avoid excessive growth of grain size in the heat affect zone (HAZ) and reheat cracking problems(da Costa Pépe, Nuno Vasco, 2010). When a higher productivity is needed, higher heat input methods like gas metal arc welding (GMAW) can be used. In this case, very low S (0.002%) and P content are required to resist the solidification cracking problem (Chen, 2012).

Furthermore, due to high Nickel content, Invar is an easily oxidised metal during the welding process. Adequate shielding gas should be used, for instance, pure Argon, Argon +$CO_{2,}$ etc. (Chen, 2012) .

2.5 Additive Manufacture (AM)

Additive manufacturing (AM) or Rapid Prototyping (RP), 3D printing are the terms used to describe a process for rapidly manufacturing a three-dimensional solid component layer upon layer from a digital model. Unlike conventional machining technologies which involve removing materials from a solid block by machining or cutting (Pierre, 2009). AM is an additive process. This technology can be traced back to 1926, when Baker who serviced for *Westinghouse Electric & Manufacturing Company*, patented “The use of an electric arc as a heat source to generate 3D objects depositing molten metal in superimposed layers” which claimed to be a new method for producing manually a three-dimensional metallic object layer by layer with the shielded metal arc welding (SMAW) process (see in Figure 2-13) (BAKER, 1925). This was the first time that the AM technology was reported.

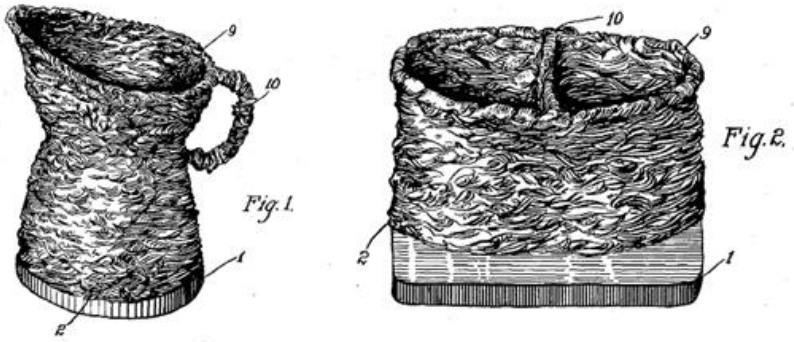

Figure 2-13 Example of a method for produced manually a 3D metallic object layer by layer by shielded metal arc welding process (Baker, 1925)

In 1971 Ujiie of *Mitsubishi Heavy Industries Co. Ltd* applied for a patent for pressure vessel fabrication using shielded arc welding (SAW), electroslag and tungsten inert gas welding (TIG) methods, it also included multiwire with different wires to give functionally graded walls(see in Figure 2-14) (Ujiie, 1972). It suggested that AM technology could be used to fabricate functionally graded structures.

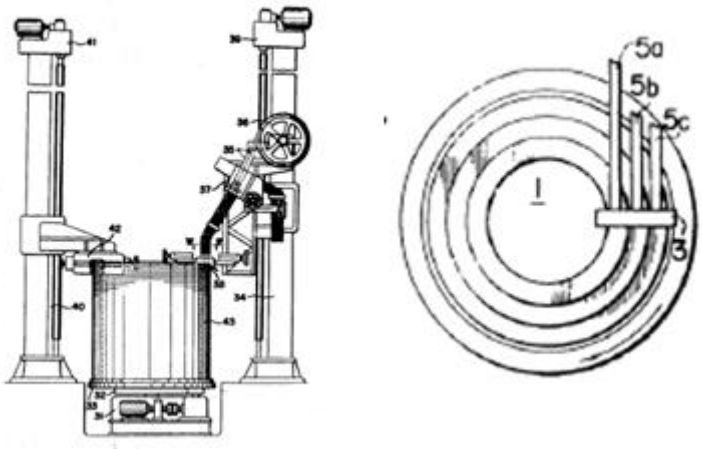

Figure 2-14 Example of pressure vessel fabrication using SAW, electroslag and TIG process, also including multiwire with different wires to give functionally graded walls，(Ujiie，1972)

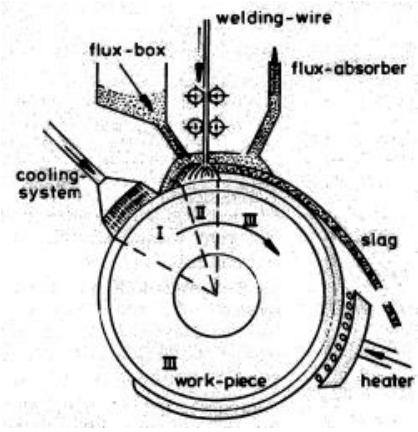

Figure 2-15 Example of using Shape Welding to manufacture high quality large nuclear structural steel ($_{20}MnMoNi_{55}$) parts, (Kussmaul et al., 1983)

Figure 2-15 described an example of using Shape Welding to manufacture high quality large nuclear structural steel parts. Deposition rate was 80kg/hr in this process and total weight was 79 tonnes (Kussmaul et al., 1983). This data showed the commercial viability of AM technology.

The AM technology discussed in this thesis is focused on metallic materials deposition. With the rapid development of industrial technology, many types of heat source can be used in the AM process, such as laser, electronic beam and arc. Hence AM is variously referred to as Laser Additive Manufacturing (LAM), Electron beam melting (EBM) and Wire and Arc Additive Manufacturing (WAAM) and so on.

WAAM uses an electronic arc to make the weld; wire is fed into the arc at a specific feed speed and then melted onto a substrate or the previously deposited layer (BAKER, 1925). Compared with powder based laser or electron beam additive manufacturing systems, WAAM has a higher deposition rate (several kg/hr)) and the part that is fabricated can approach nearly 100% density (Wang et al., 2013). Furthermore, the processing procedure is much simpler than laser system.

At present, gas tungsten arc welding (GTAW) and gas metal arc welding (GMAW) are two typical WAAM technologies. The main difference between them is the GTAW need a separate filler wire, as shown in Figure 2-16 (Varlowe

Ltd., 2006; RobotWorx Co., 2009). Compared to GMAW, GTAW welding has no spatter, but the deposition rate is lower than that of the GMAW process.

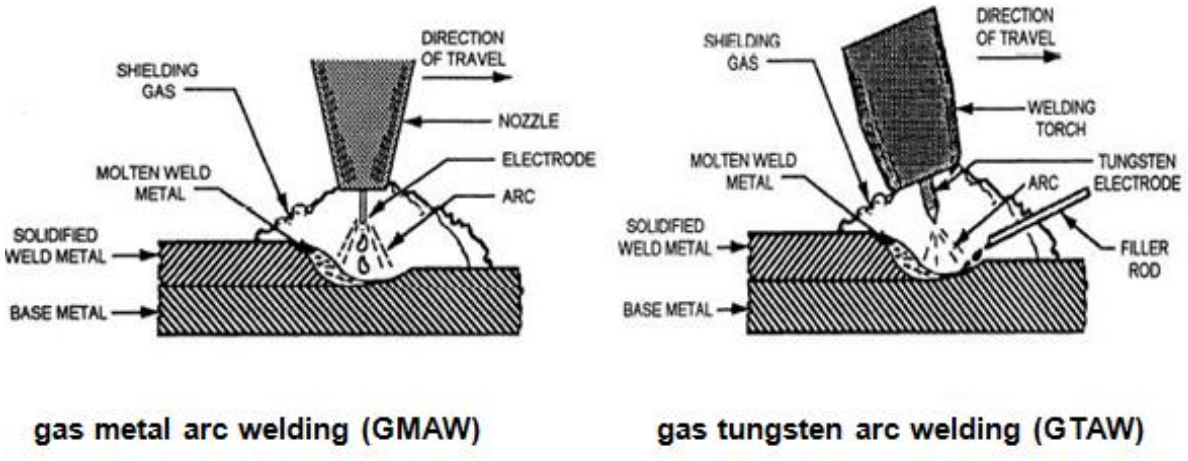

Figure 2-16 The difference between GMAW and GTAW is that the tungsten electrode provides only the electricity, but not the filler (RobotWorx Co., 2009)

2.6 Cold Metal Transfer (CMT)

Shielded Inert Gas Metal Arc (MIG) and Metal Active Gas (MAG) welding are the most common welding processes in use today. However, the high heat input and unavoidable spatter limits their application in some areas, such as thin sheet metal.

The concept of CMT was introduced to the public in 2005 by *Fronius International*. CMT is a fully digital, micro-processor-controlled inverter Gas Metal Arc Welding (GMAW) process (Fronius Ltd., 2005). It reduces the welding current when the droplet connects to the molten pool and at the same time it retracts the wire so as to help the droplet to transfer to the molten pool smoothly without spatter, as shown in Figure 2-17. Due to the mechanical adjustments of the arc length, the CMT process has a more stable arc than conventional GMAW (Mattias, 2011).

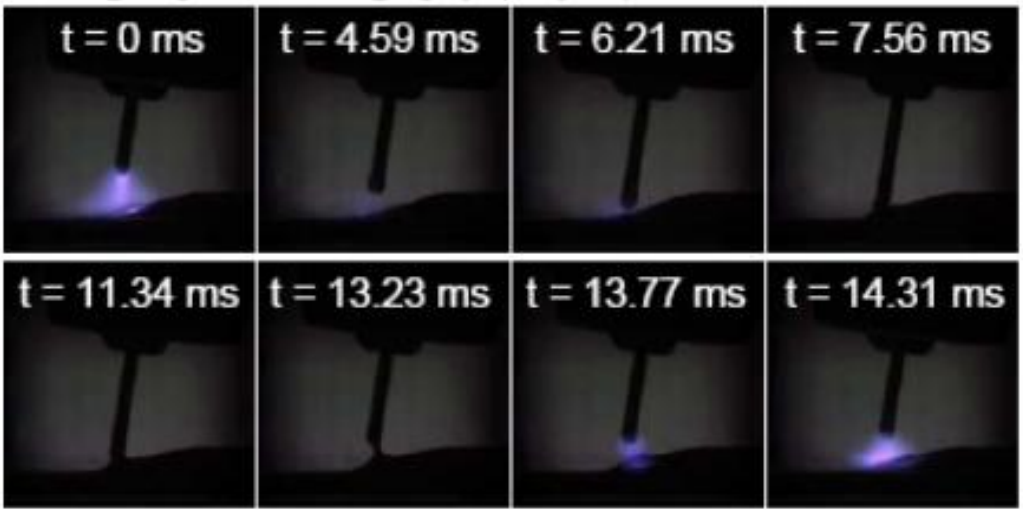

Figure 2-17 Fronius CMT-GMAW, As Viewed under High Speed Photography (one cycle) (Fronius Ltd., 2005)

Leinonen compared the average heat input during the welding process with Pulsed, Dip and CMT methods, and the results indicated that CMT has lower heat input and produces virtually no spatter (see Figure 2-18) (Mattias, 2011).

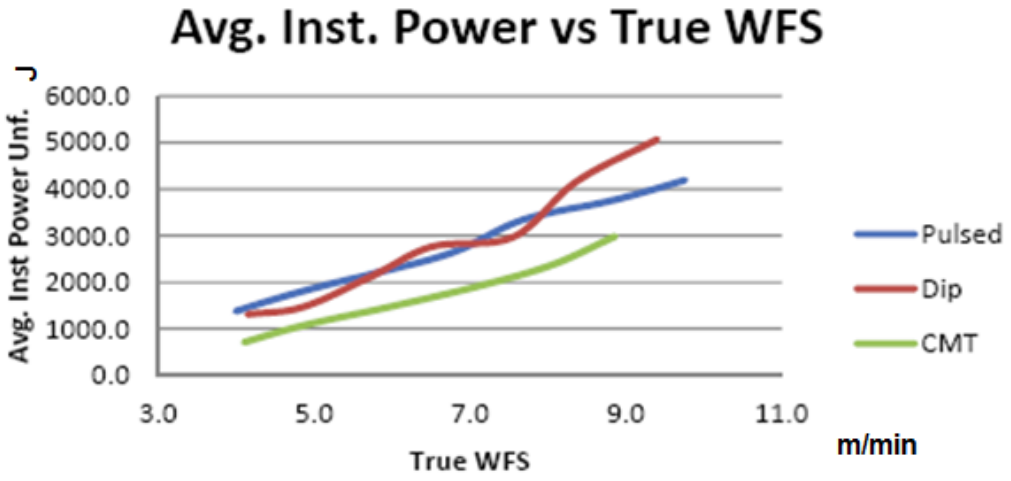

Figure 2-18 Average instantaneous power usage compared during different welding processes (Mattias, 2011)

2.7 Challenges in welding dissimilar materials

Dissimilar metal welding refers to joining metals of different chemical compositions. Many factors may influence the joint quality and a key factor that

needs to be considered is the solubility of two materials. For instance, for Iron and lead, they are crystallised individually because these two metals cannot dissolve in each other even in the liquid. It is therefore necessary to use a third metal which can be dissolved in the two base metals as a filler and it is usually known as the “inter-layer” (Wei and Chung, 2000). In addition, it is more difficult to weld dissimilar metal if they have widely different melting points. One metal melts while another is still in solid state; and this causes uneven heat flow and non-uniform dilution in the weld puddle (Wisconsin Wire Works, 2005). Loss or evaporation of lower melting point alloying elements also occurs in this process. In the solidification stage of the molten pool, material with higher melting point solidifies first while the lower-melting material is still fully or partially liquid. It has a negative impact on mechanical properties in the weld zone and it is prone to cracking in this area.

Furthermore, the material thermal expansion coefficient and thermal conductivity should also be considered. Since shrinkage of metal with a higher thermal expansion coefficient is larger in the cooling stage; high stresses can arise during and after welding due to large differences in thermal expansion between two joint metals. It is easy to cause cracking at solidification because of the brittleness from the internal stress. Two methods can be applied to avoid cracking caused by differences in thermal expansion. One is to choose an inter-metal with a thermal expansion coefficient which is intermediate between the two joint metals. Another approach is to use a preheating process that can reduce residual stress in the weld zone (Mattias, 2011).

In addition, differences in thermal conductivity between two base metals can result in different heating and cooling rates between two sides. The metal with the higher conductivity tends to absorb the heat away from the welding-pool; it results in a larger temperature difference in the welding metal and uneven heat flow. Not only does it affect fusion of the welding pool in solidification stage, but also causes distortion and thermal stresses in the finished assembly. To deal with this situation, preheating the base metal with the higher conductivity is helpful as it can reduce temperature difference between two welding materials.

So far, the monometallic fabrication processes have been studied by many researchers, such as Ti alloy (Huang, 2011; Almeida and Williams, 2010), Ni alloy (Clark et al., 2008), and steel (Skiba et al., 2011). However, a relatively small number of studies has been carried out on bimetallic area utilised AM technologies.

2.8 Potential problems and possible solutions

2.8.1 Solidification cracking

Study has shown that previously the main problem of welding Invar alloy is solidification cracking (Corbacho et al., 1998a). It has been reported that adding titanium, manganese and carbon into filler wire can reduce solidification cracking. This may relate to the pinning effect of Ti and Mn precipitates, which hinders the migration of grain boundaries during the recrystallization process (Corbacho et al., 1998b). In addition, porosity and loss of toughness can be observed in weldment with unmodified filler material(Clark et al., 2008). However, appropriate filler metal is a specialised metallurgical subject and is beyond the scope of the thesis.

In this paper, the quality of the welding parts has been checked and presence of porosity or cracking will be tested.

2.8.2 Shielding gases

The purpose of the shielding gas is not only to protect the molten weld pool from exposure to the atmosphere but also to isolate the impact from atmospheric gases such as oxygen, nitrogen, and water vapour, but it also can sustain a stable arc and promote the quality of the deposition (Cary and Helzer, 1979). Proper shielding gas selection is crucial to guaranteeing the ultimate quality of welded parts.

The fundamental pure shielding gases for welding are argon (Ar), helium (He), and carbon dioxide (CO_2) (Lyttle, 2005). An inert gas is a gas which does not undergo chemical reactions under a set of given conditions. These gases include helium, neon, argon, krypton, xenon and so on. But only two of them,

helium and argon are suitable for use in welding due to economic cost. In many cases, other gases for instance oxygen (O_2), nitrogen (N_2), and hydrogen (H_2) can be added in small quantities to improve weld qualities and modify arc characteristics [45]. For most materials, argon (Ar) and helium (He) ， or a mixture of them are compatible (Cary and Helzer, 1979).

Argon is heavier than air and when used as shielding gas; the main properties are low thermal conductivity and low ionization potential. It can produce a relatively narrow arc characteristic with good electrical conductivity, and easy arc-starting. Argon can be used alone or combined with other gases.

Helium is considerably lighter than air; it has good thermal conductivity and the highest ionization potential in shielding gases. Therefore, very high arc voltages accompany the use of helium which results in a high arc temperature in the welding process (Skiba et al., 2011). Because of its low density relative to air, helium easily drifts from the welding arc and molten weld pool, resulting in poor protection of the weld part. Thus, a higher helium gas flow rate is required than for Argon or carbon dioxide. With the higher arc temperature, helium has the advantage of offering deep bead. Because helium is in short supply and is very expensive; it is generally combined with other gases to promote required welding characteristics. Pure helium is not used for steel, as it provides erratic arc (Cary and Helzer, 1979).

Carbon dioxide is 1.5 times heavier than air; it dissociates at arc temperature (for example, nearly 99% of CO_2 deoxidises into CO and O_2 at 5000 K) and absorbs heat from the arc. When the gases make contact with the relatively cooler base material, they recombine and release heat. Through this process, arc energy is transferred to weld pool. Addition of carbon dioxide provides a wider welding bead. The oxidizing atmosphere produced within the arc zone results in more slag on the surface of the solidified GMAW bead (Haidar and Lowke, 1997). In this process, wire with high deoxidation capability should be used, and chemical element such as Si or Mn added into the wire. Carbon dioxide can be used alone for mild steel or as a component mixed with Argon to increase welding efficiency for GMAW (Lyttle, 2005).

When there is no shielding gas, oxygen, nitrogen, and water vapour from atmospheric gases will directly contact the arc and melting metal, which will not only destroy the arc stability, but produce harmful defects such as cracks, porosity, oxides, etc. In normal conditions, the use of a single protective gas may make the arc prone to instability and impact on the welding seam quality. This is the reason why pure Argon and helium are used only for some nonferrous metals. This problem can be overcome by mixed gases. From AWS handbook (2004), Small additions of Oxygen (O_2) or Carbon dioxide (CO_2) can improve fluidity of the melting puddle, reduce surface tension of the droplet and promote bead shape (Shanping et al., 2005). Leinonen investigated Argo-shield® Light (93% Argon， 2% Oxygen, 5% Carbon Dioxide) as a proper shielding gas for steel wire enhanced bead appearance and produced low spatter (Mattias, 2011). Chen's MSc work verified that Ar and Ar+2.5%CO_2 can be used for nickel alloy (Chen, 2012). Corbacho indicated that Invar is prone to surface and grain-boundary oxidation and defects appear in the weldment if is not properly protected (Clark et al., 2008).

2.8.3 Microstructure influence

Low heat input welding processes (GTAW, laser) are better for preventing problems related to excessive grain coarsening in the heat affect zone(Corbacho et al., 1998b). Nevertheless, to increase productivity, other processes with high deposition rates (SAW, GMAW) are needed.CMT is the appropriate technology which combines relatively lower heat input and higher deposition rate.

A report from University of Michigan (Shin et al., 2003) about fabrication of heterogeneous objects demonstrates the possibility of combining Invar and steel together. Projects on the Shape Deposition Manufacturing (SDM) at Stanford University and Three-Dimensional Printing (3DP) at Massachusetts Institute of Technology (MIT) have shown the possibility of creating artefacts with functionally graded materials with nickel alloy (Fessler et al., 1997). More specifically, an advance injection moulding tool, which was made of three materials, Invar, stainless steel, and copper, was presented (Fessler et al.,

1997). Though this SDM system used a laser powder deposition method, the principle is the similar for combinations of different materials.

2.9 Summary

This chapter summarised previous studies on WAAM technology and Invar alloy welding ability, reviewed the research status of autoclave forming process and mould design methods.

3 Experimental Procedures

3.1 Materials and equipment

3.1.1 Experimental materials

A 1.2 mm diameter Invar wire (supplied by *AirCraftMaterialsUK.com Ltd*) was used for the welding process. In this study, Invar was welded onto a piece of S355 mild steel; their chemical compositions are shown in Table 3-1and Table 3-2.

Table 3-1 Invar chemical composition

C	Si	Mn	P	S	Al	B	Cr	Cu	Fe	Ni	Ti	Nb
0.25	0.09	0.48	0.005	0.003	0.04	0.001	0.01	0.07	61.84	35.84	0.17	1.19

Table 3-2 S355 mild steel chemical composition

C	Si	Mn	P	S	Al	V	Cr	Cu	Fe	Ni	Ti	Nb	Mo	N
0.14	0.50	1.60	0.03	0.025	0.02	0.10	0.30	0.55	96.03	0.50	0.05	0.05	0.1	0.015

3.1.2 Welding facilities

A six-axis robot (ABB robot IRB 2000) was used to manipulate the torch. A mobile fume extractor was employed to extract dust during the welding process, as shown in Figure 3-1. A local back shielding device was used to protect the Invar weldment to avoid oxidization. In this study a Fronius CMT welding unit was employed for the Invar-on- steel investigation.

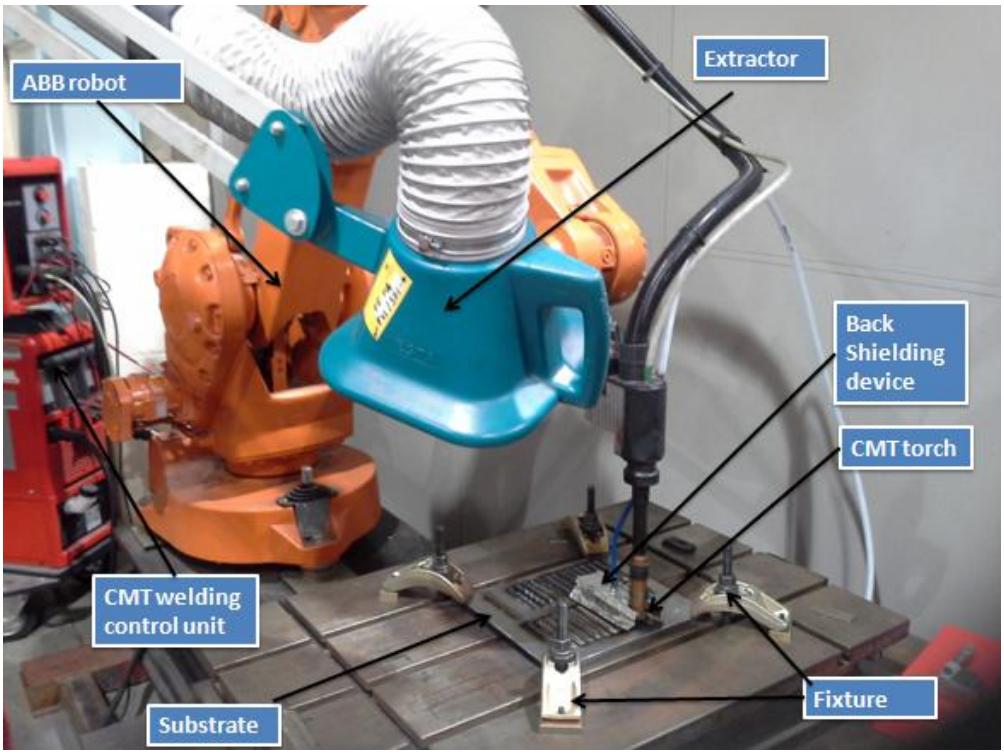

Figure 3-1 Pictorial representation of welding facilities

3.1.3 Voltage and current recording device

An AMV 4000 precision Welding Monitor (supplied by *Triton Electronics Ltd.*) was used to record the transient current and voltage in the experiment and the recording frequency is 20HZ, as shown Figure 3-2.

Figure 3-2 AMW 4000 welding monitor

The average energy input was calculated using the following equation(Sequeira Almeida, 2012):

$$\overline{E} = \eta \frac{\sum_{i=1}^{n} \frac{I_i * U_i}{n}}{TS} \quad \textbf{(3-1)}$$

Where

$\overline{E}$--------- Average energy input, J/mm;

TS-------- Travel speed, mm/s;

I_i --------- Transient Current, A;

U_i --------- Transient voltage, V.

η--------- Welding process efficiency factor. Throughout the work, the welding process efficiency factors is η=0.9 for CMT. This value was determined by the liquid nitrogen calorimetric method in recent studies (Hsu and Soltis, 2002) .

3.2 Single-layer welding

3.2.1 Description of welding method

The purpose of the single-layer welding experiment was to study how well Invar can be deposited on steel. Invar was deposited directly on the mild steel substrate at this stage. Each length of welding bead was 100mm, as shown in Figure 3-3 Single-layer welding setup: a length of 100mm bead was welded each time. After that, each bead was cut along the building direction including the substrate to get samples for bead geometries inspection and the subsequent metallographic analysis.

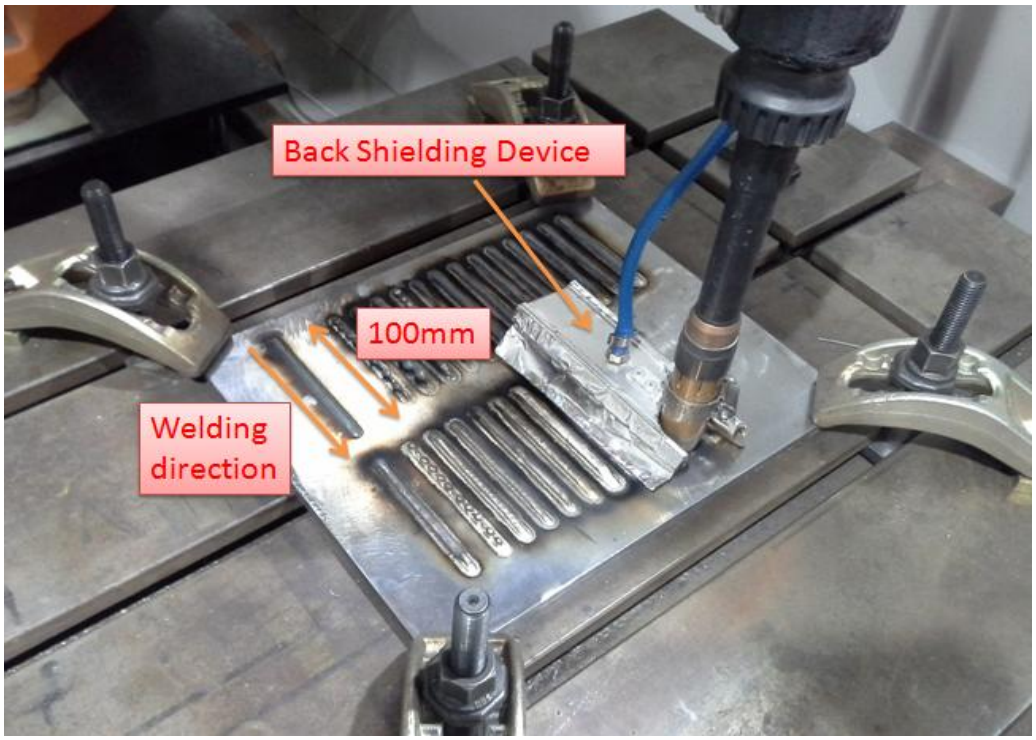

Figure 3-3 Single-layer welding setup: a length of 100mm bead was welded each time and back shielding was used to enhance the protection of the weldment

3.2.2 Parameters set up

Altogether 24 sets of welding parameters were investigated, as shown in Table 3-3. These 24 trials were divided into 2 groups in order to investigate the influence of two different shielding gases. In each group, 3 main Ratios (Wire feed speed (WFS)/Travel speed (TS)) were compared, using values of 8, 10 and 20.The main purpose of trials 1 to 4 was to study the effect of different Wire Feed Speed on the weldment's performance.

Table 3-3 Preliminary CMT parameters set-up in single-layer welding

Trial No.	CTWD (mm)	Shielding gas	Gas flow (L/min)	Ratio (RATIO (WFS/TS)	WFS (m/min)	TS (m/min)
1	13.5	Pure Ar	16	8	4	0.5
2			16		6	0.75
3			16		8	1.0
4			16		10	1.25
5			16	10	4	0.4
6			16		6	0.6
7			16		8	0.8
8			16		10	1.0
9			16	20	4	0.2
10			16		6	0.3
11			16		8	0.4
12			16		10	0.5
1	13.5	Ar+2.5%CO2	16	8	4	0.5
2			16		6	0.75
3			16		8	1.0
4			16		10	1.25
5			16	10	4	0.4
6			16		6	0.6
7			16		8	0.8
8			16		10	1.0
9			16	20	4	0.2
10			16		6	0.3
11			16		8	0.4
12			16		10	0.5

3.3 Investigation into welding multi-layers

3.3.1 Description of welding method

The purpose of the experiment was to find the appropriate parameters when Invar is welded layer upon layer. This was the basic experiment for the bi-metal wall building. Each trial was made of ten layers. As shown in Figure 3-4, due to the surface waviness, the rectangular area was the “real” material that could be used for dog-bone extraction. The usable area efficiency is the ratio of the usable area to the whole cross-sectional area of the wall.

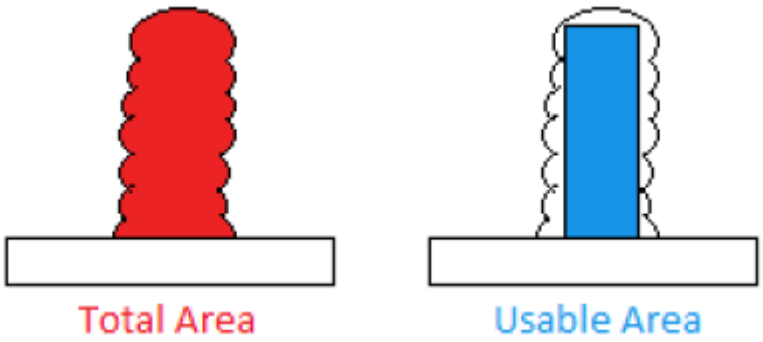

Figure 3-4 Measurement of usable area efficiency (Mattias, 2011); total area in red, usable area after machining in blue

3.3.2 Parameters set up

Eight trials were investigated in this phase; different ratios were compared from 10 to 20. WFS was always set as 6m/min to make sure the results from these trails were comparable. Two different shielding gases were used to investigate whether they have an impact on the product's effective wall thickness, as shown in Table 3-4.

Table 3-4 Parameters used in the multi-layer Investigation

Trial No.	Shielding gas	Ratio (RATIO (WFS/TS))	WFS (m/min)	TS (m/min)
1	Argon	10	6	0.6
2		12.5	6	0.48
3		15	6	0.4
4		20	6	0.3
5	Argon+2.5%CO2	10	6	0.6
6		12.5	6	0.48
7		15	6	0.4
8		20	6	0.3

3.4 Wall Fabrication

3.4.1 Invar-Steel wall fabrication

3.4.1.1 Forming Process

Two Invar-steel walls were built and the dog bone shape tensile test samples were extracted from them. The main difference between the two walls was that

the shielding gas was different. One was pure Argon and the other was Argon + 2.5% CO_2. Each wall was 300mm in length and 200 mm in height.

During the building of the Invar-steel wall, the wire was deposited layer upon layer onto a S355 steel substrate with a single bead without weaving. For each successive layer the deposition direction was reversed (see Figure 3-5).

When the steel wall was finished, the top layer was ground to remove the oxidization, as shown in Figure 3-6. Whilst the Invar part was built, a local shielding device was used to give further protection to avoid oxidization as shown in Figure 3-7(a). The outside and touching the AM wall a stacked wall of bricks was placed. The material of the bricks was stainless steel. The layers of bricks increased correspondingly with the height of the additive metal layers, as shown in Figure 3-7 (b). With this method, the latest metal layer can get more sufficient protection.

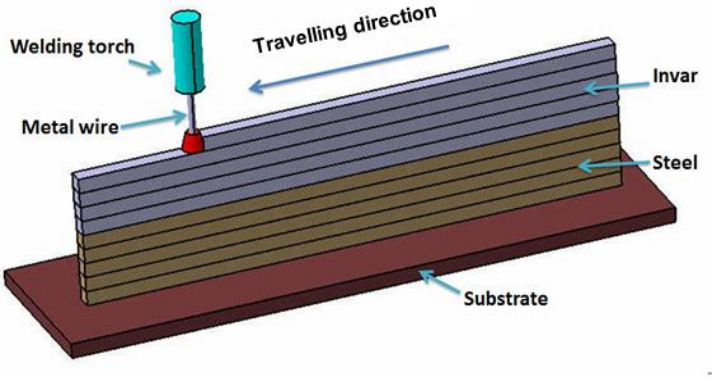

Figure 3-5 Schematic diagram of Invar-steel wall building forming process

Figure 3-6 When the steel structure was fabricated, the top layer of steel had to be ground to obtain a flat layer for Invar deposition

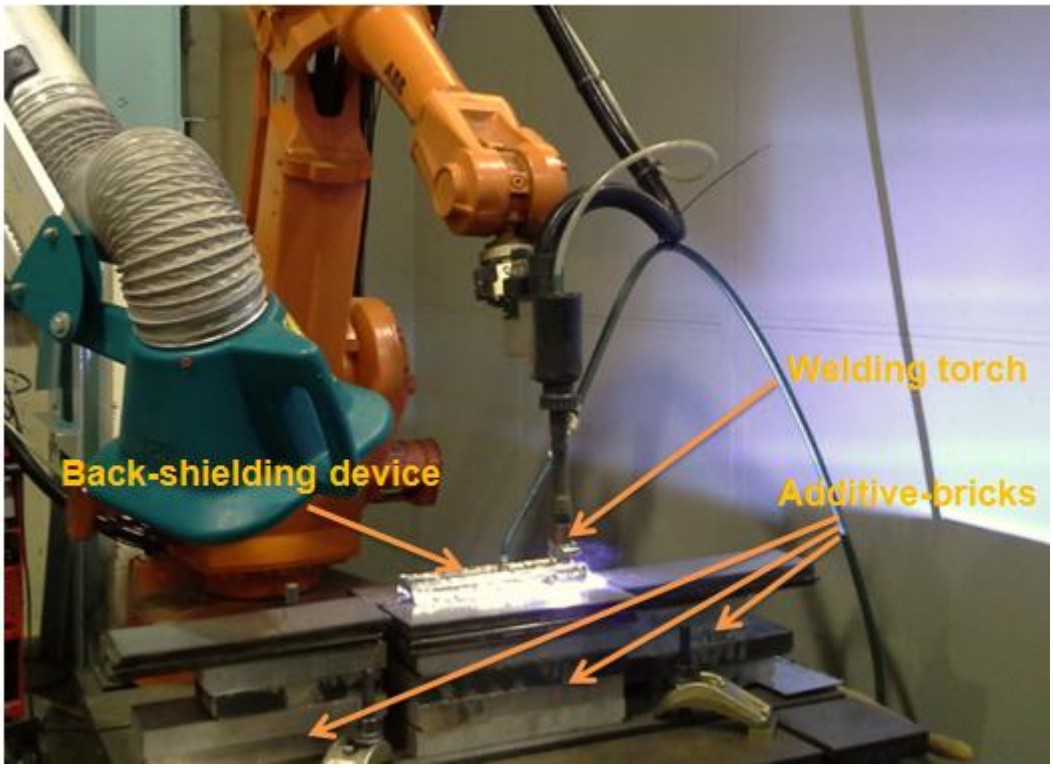

Figure 3-7(a) The additive-bricks method was used to enhance the shielding gas protection effect

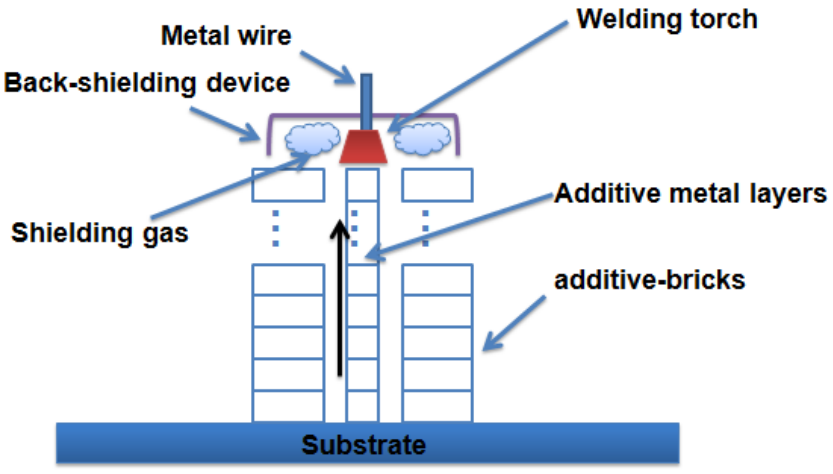

Figure 3-8(b) Schematic diagram of the additive-bricks method (from the end-view)

3.4.1.2 Forming parameters

To investigate the effect of different shielding gases on the Invar strength, pure Argon and Argon+2.5%CO_2 were used respectively for Invar layers of each wall, as shown in Table 3-5.

Table 3-5 Parameters for bimetal wall fabrication

Trial No.	composition	Shielding gas	WFS (m/min)	TS (mm/s)	Wire Diameter (mm)	Interval (sec)
Wall 1	Steel	93% Argon, 2% Oxygen, 5% Carbon Dioxide	4	5.33	1.0	180
	Invar	Argon	6	6.67	1.2	300
Wall 2	Steel	93% Argon, 2% Oxygen, 5% Carbon Dioxide	4	5.33	1.0	180
	Invar	Argon+2.5%CO2	6	6.67	1.2	300

3.4.1.3 “Dog-bone” samples

Tensile specimens were extracted perpendicular to the build direction according to the requirements of BS EN ISO 6892-1(2009). The tensile specimens had a dog-bone shape with a gauge length of 50 mm and a 12.5×2.5 mm cross-section, as shown in Figure 3-8 and Appendix B.

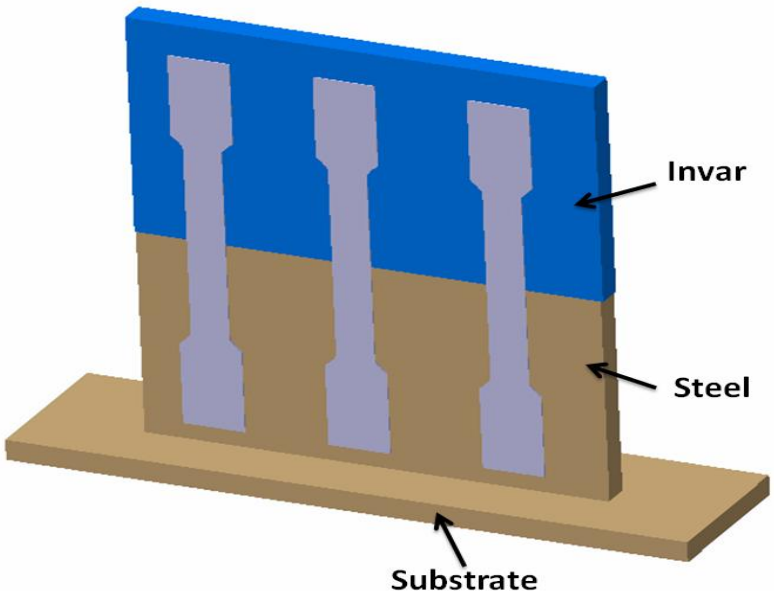

Figure 3-9 Invar-steel welded samples

3.4.2 Invar wall fabrication

3.4.2.1 Forming Process

A 300 mm by 350 mm pure Invar wall was built using the same procedure as described above. The parameters used to build the wall are shown in Table 3-6.

Table 3-6 Parameters for Invar wall fabrication

Trial No.	composition	Shielding gas	WFS (m/min)	TS (mm/s)	Wire Diameter (mm)	Interval (sec)
Wall 3	Invar	Argon+2.5%CO2	6	6.67	1.2	300

3.4.2.2 Dog-bone samples

Six tensile specimens were extracted parallel and perpendicular to the build direction, as shown in Figure 3-9.

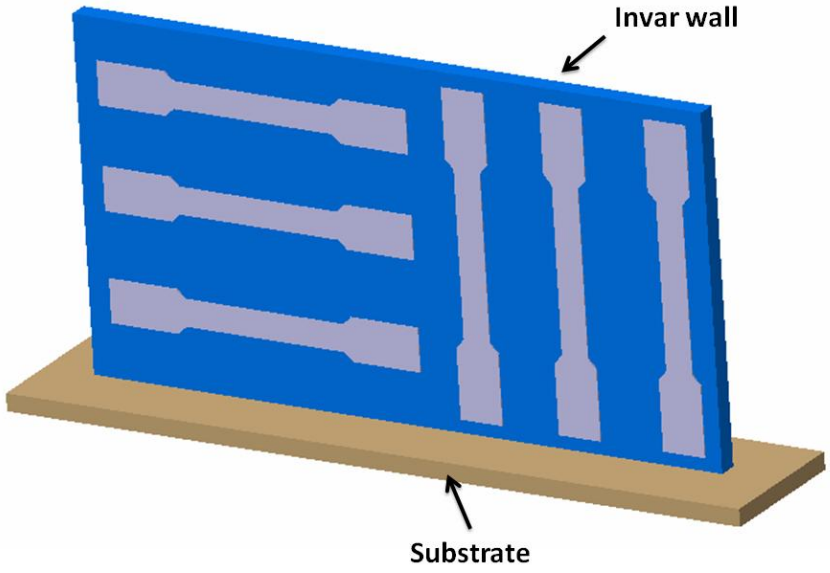

Figure 3-10 Invar welded samples

3.5 Mechanical Test

3.5.1 Tensile test

Tensile tests were carried out with an Instron 5500R Electromechanical (Instron, Coronation Road, High Wycombe, Bucks HP12 3SY, UK) machine with a 100kN load cell. The cross head displacement speed was 0.5 mm/min. An

Instron 2620-604 dynamic strain gauge extensometer was attached to each specimen while testing to measure ultimate tensile stress accurately. Tensile tests were based on BSTM E8/E8m-08.

3.5.2 Hardness test

The Vickers hardness was tested with a ZHVμ Micro Vickers hardness tester machine (supplied by Zwick Company). A force of 200g was applied to the Invar-steel welding sample for 15 seconds. In total 21 points along a line which was perpendicular to the weld seam were investigated. The distance between each point was 250μm, which is shown in Figure 3-10. Hardness Tests were based on BS EN 6507-1:1998.

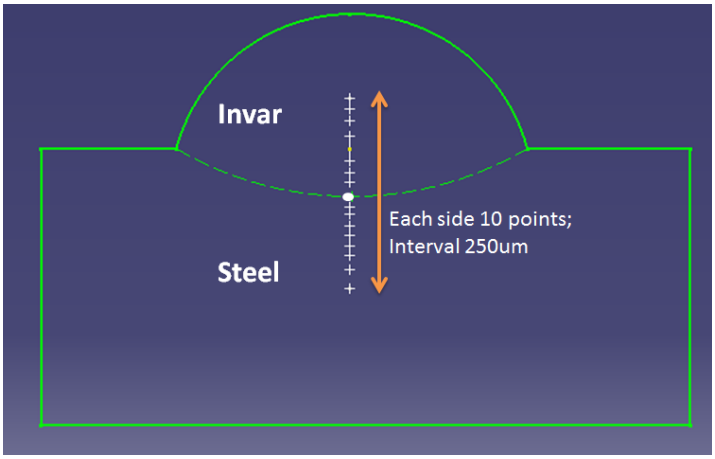

Figure 3-11 21 points along a line perpendicular to the weld seam with interval 250μm

3.6 Metallographic analysis

Samples for the observation of microstructure were cut perpendicular to the build direction including the substrate. They were ground by 240, 1200, 2500 grid emery paper respectively and then polished with 2.5μm diamond polishing paste for 3-5 minutes. After this the samples were finally polished with a 0.05mm particle size colloidal silica suspension. For bimetals it is usually difficult to get uniform etching results. As a type of corrosion-resistant metal, Invar was etched by copper chloride and mild steel side was etched by 25%

HNO_3 (ml %) for 10 seconds at room temperature. Samples were examined using an optical micrograph and a scanning electron microscope (SEM).

3.6.1 Optical microscope

An optical microscope (Nikon, Japan) was used to examine the macro-and microstructure of the samples. Magnifications of 10, 200 and 250 were used according to different observational requirements.

3.6.2 SEM analysis

A PHILIPS XL-30 scanning electron microscope (SEM) (Philips, Amsterdam, The Netherlands) operating at 20 KV was used for Energy-Dispersive Spectroscopy (EDS) analysis and fractograph observation.

4 Results

4.1 Bead on plate deposition

4.1.1 Macroscopic analysis of specimens

4.1.1.1 Bead on plate deposition with pure Argon

Table 4-1 shows the results of bead on the plate deposition with Argon shielding gas. It can be seen that a continuous welding bead cannot be achieved when the ratio (WFS/TS) is 8. Lack of fusion and discontinuous bead occur when the ratio (WFS/TS) is 8 as indicated in Table 4-1 a, b, c and d. Smooth and continuous deposition beads were observed when the Ratio (WFS/TS) is 10 and 20.

Table 4-1 Macroscopic quality of specimens

Trial No.	Ratio	WFS (m/min)	TS (m/min)	Weld appearance	Comments
a	8	4	0.5		△lack of fusion,
b		6	0.75		△lack of fusion
c		8	1		△Unstable arc occurred in the middle
d		10	1.25		△Unstable arc occurred in the middle
e	10	4	0.4		▲
f		6	0.6		▲
g		8	0.8		▲
h		10	1		▲
i	20	4	0.2		▲
j		6	0.3		▲
k		8	0.4		▲
l		10	0.5		▲

Remark: ▲= Surface quality was acceptable

△= quality defects

4.1.1.2 Bead on plate deposition with Argon + 2.5% CO_2

Table 4-2 shows the results of bead on the plate deposition with Argon + 2.5% CO_2 shielding gas. It can be seen that with Argon + 2.5% CO_2 shielding gas the quality of the welding beads has been improved. Only one trial has a discontinuous welding bead when ratio (WFS/TS) is 8, as shown in Table 4-2 (a).

Table 4-2 Macroscopic quality of specimens

Trial No.	Ratio	WFS (m/min)	TS (m/min)	Weld appearance	Comments
a	8	4	0.5		△lack of fusion, discontinuous
b		6	0.75		▲
c		8	1		▲
d		10	1.25		▲
e	10	4	0.4		▲
f		6	0.6		▲
g		8	0.8		▲
h		10	1		▲
i	20	4	0.2		▲
j		6	0.3		▲
k		8	0.4		▲
l		10	0.5		▲

Remark: ▲= Surface quality was acceptable

△= quality defects

4.1.2 Heat input with different shielding gases

Average heat input with different shielding gases was calculated according to the equation 3-1, as shown in Figure 4-1. The graph shows that average energy input grows when WFS is increased. The reason is that CMT is a synchronized

welding power source. When WFS is increased the welding current is also increased proportionally. It can be seen from Figure 4-1 that pure Argon has a higher heat input than Argon + 2.5% CO_2 at the same WFS. The reason is that Argon has a higher ionization potential. Cary et al. [44] pointed out that the ionising Voltage of Ar is 15.7V and CO_2 is 13.7V respectively. When CO_2 is added in to pure Argon, the ionisation potential is lower.

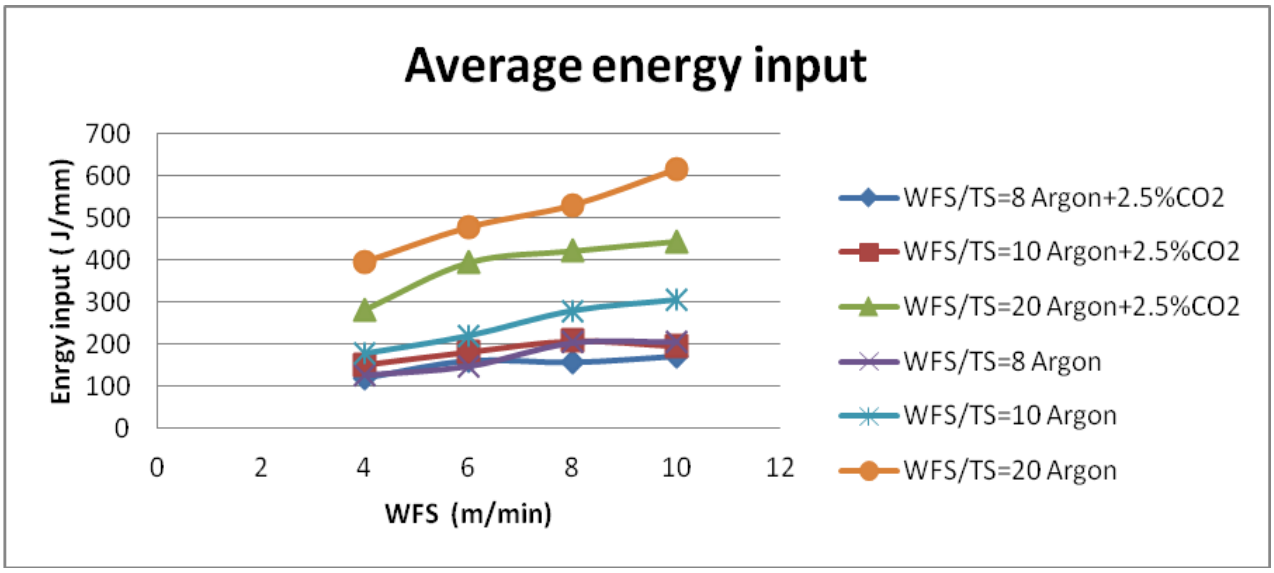

Figure 4-1 Average energy input measurement against change in WFS

4.1.3 Welding bead dimension measurement

The bead shape geometries were measured from samples cut in cross section of the bead on the plate deposition. One sample diameter at WFS 8 m/min and TS 0.4m/min with different shielding gas is shown in Figure 4-2. It can be seen that the bead shape is different.

Argon + 2.5% CO_2 generates a much better bead shape. It is wider and well spread on the substrate. The contact angle is 120 degrees.

The sample which was deposited using pure Argon shielding gas has a narrower and higher welding bead compared with the sample deposited with Argon + 2.5% CO_2 shielding gas. And its contact angle is less than 90 degrees which means it will not prevent fusion defects between two adjacent welding

beads when multi parallel welding bead deposition is used to produce a wide wall.

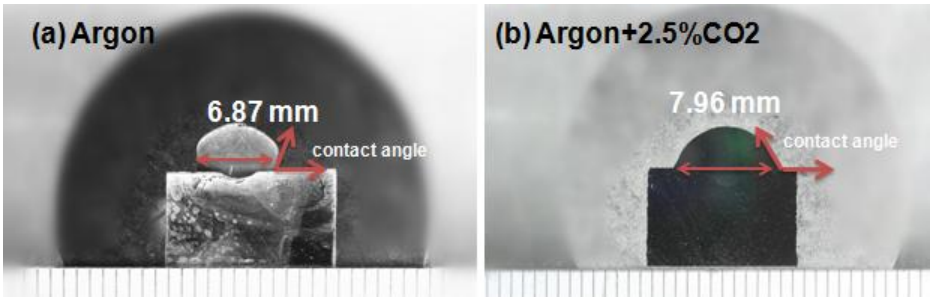

Figure 4-2 Deposition shape comparison: WFS=8m/min, TS=0.4m/min,

(a) Argon shielding gas (etched); (b) Argon+2.5%CO_2 Shielding gas.

4.2 Multi-layer welding

Eight multi-layer walls were built successfully using different parameters. One of them is shown in Figure 4-3. Cross sections were cut and two of them are shown in Figure 4-4 Figure 4-5 .

Figure 4-3 Picture of sample 6, WFS=6 m/min, TS=0.48 m/min, layer height 2 mm shielding gas: Ar + 2.5% CO2

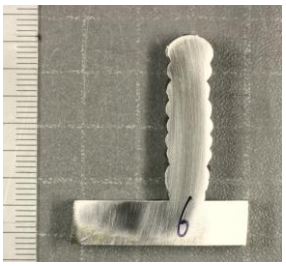

Figure 4-4 Picture of cross section from sample 6, WFS=6 m/min, TS=0.48 m/min, layer height 2 mm shielding gas: Ar + 2.5% CO2

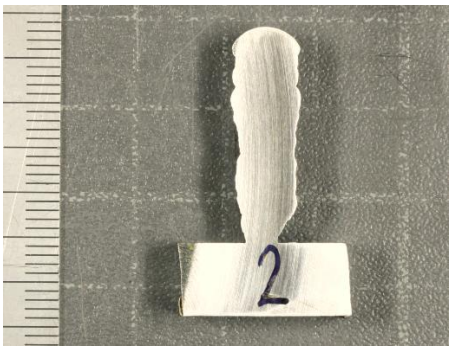

Figure 4-5 picture of sample 2 cross section, WFS=6 m/min, TS=0.48 m/min, layer height 2 mm shielding gas: Ar + 2.5% CO2

The usable area efficiency measurement for all 8 walls is shown in Figure 4-6. It can be seen that the samples which are built with Argon + 2.5% CO_2 have a higher usable area efficiency.

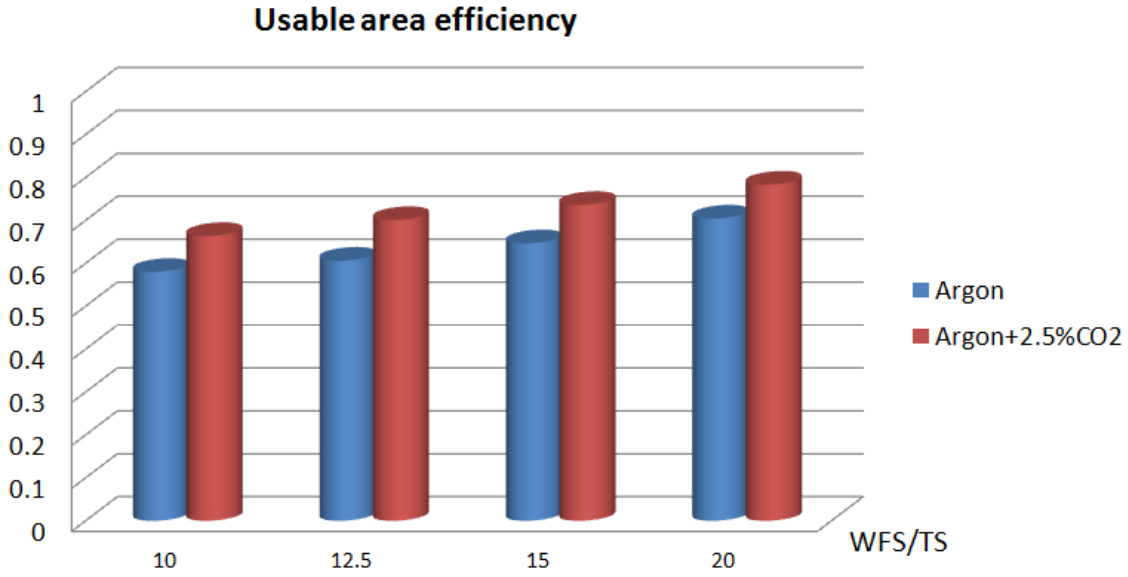

Figure 4-6 Measurement of usable area efficiency coefficient with different shielding gases

4.3 Microscopic analysis

4.3.1 Optical microscope analysis

The optical microstructure of the Invar and steel joint and the deposited Invar are given in Figure 4-7 and 4-8, respectively. There is no crack or porosity can be observed in the joint and Invar area. Typical dendrite characteristic

solidification microstructure is found in the Invar area and it is a single phase austenite (Cacciamani et al., 2006).

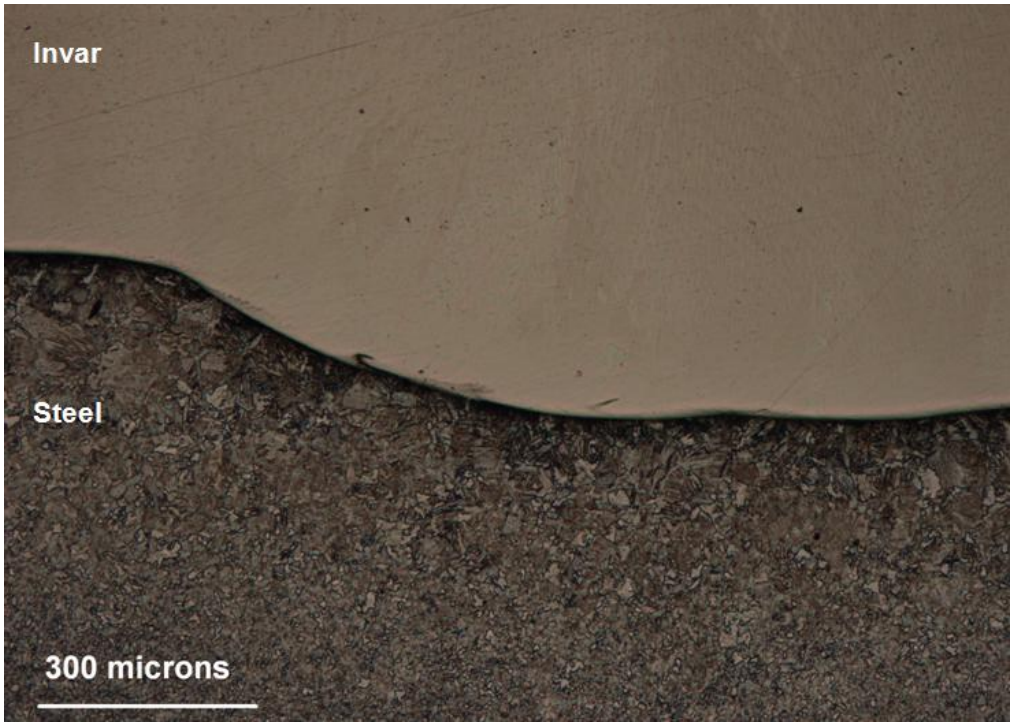

Figure 4-7 Optical microstructure observation of Invar/steel joint

Figure 4-8 Optical microstructure image of deposited Invar alloy by WAAM process

4.3.2 SEM observation and EDS analysis

Further detailed scanning electron microscope (SEM) observation of WAAM Invar/steel joint and Invar alloy are given in Figure 4-9 to 4-11. Energy-Dispersive Spectroscopy (EDS) analysis of precipitation along grain boundaries and element transition cross Invar/steel joint interface are shown in Figure 4-12 to 4-13. There is no crack or porosity is found in the Invar/steel joint and Invar alloy area. A joint line can be clearly observed in both the Back-Scattered Electron and Secondary Electron images, as shown in Figure 4-9 and 4-10. Precipitations can be observed along the Invar dendrite boundaries. EDS analysis results show it is $FeNi_3$ (Cacciamani et al., 2006). The results of element transition across Invar/steel joint interface with different shielding gases are shown in the Figure 4-14 and 4-15. A very narrow element transition zone is observed for two types of shielding gas: Argon (10 μm) and Argon + 2.5% CO_2 (30 μm).

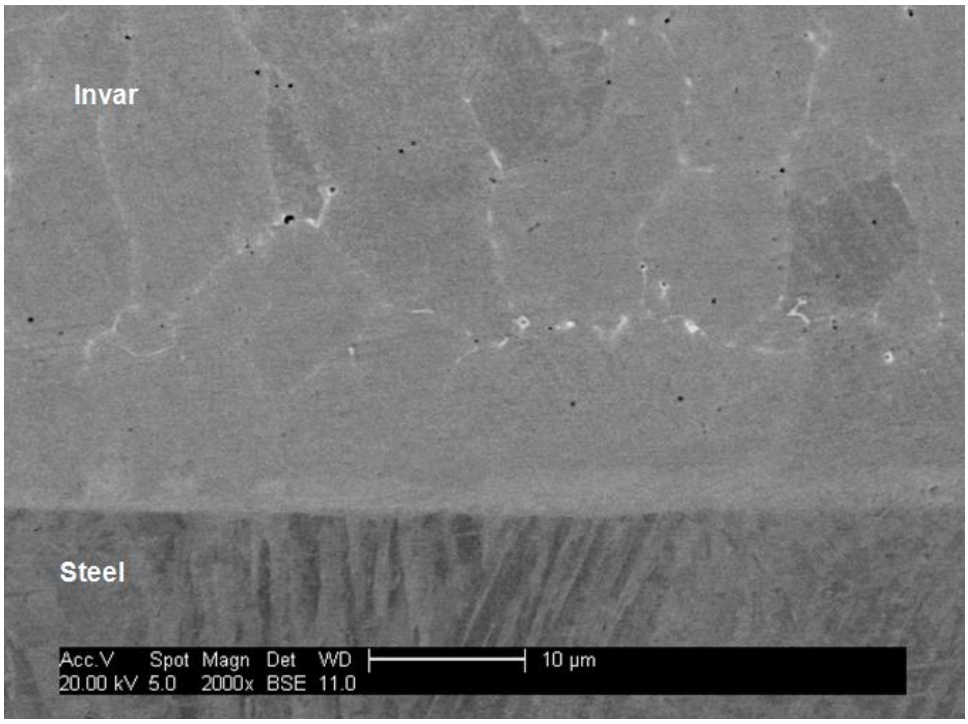

Figure 4-9 BSE image of WAAM Invar/Steel joint

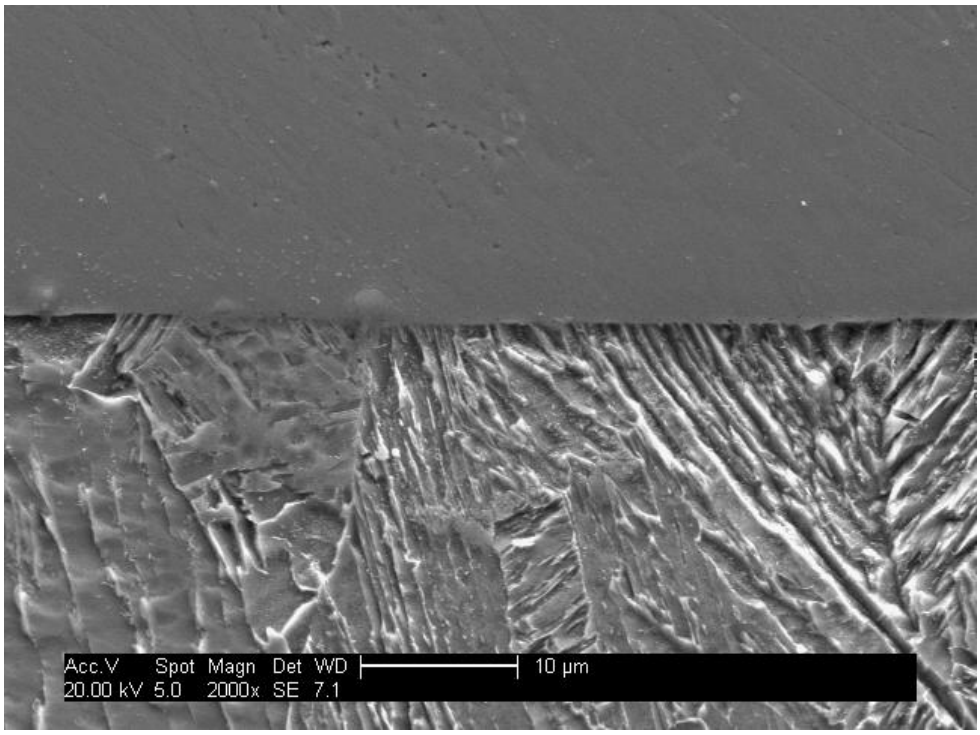

Figure 4-10 SEM image of WAAM Invar/Steel joint

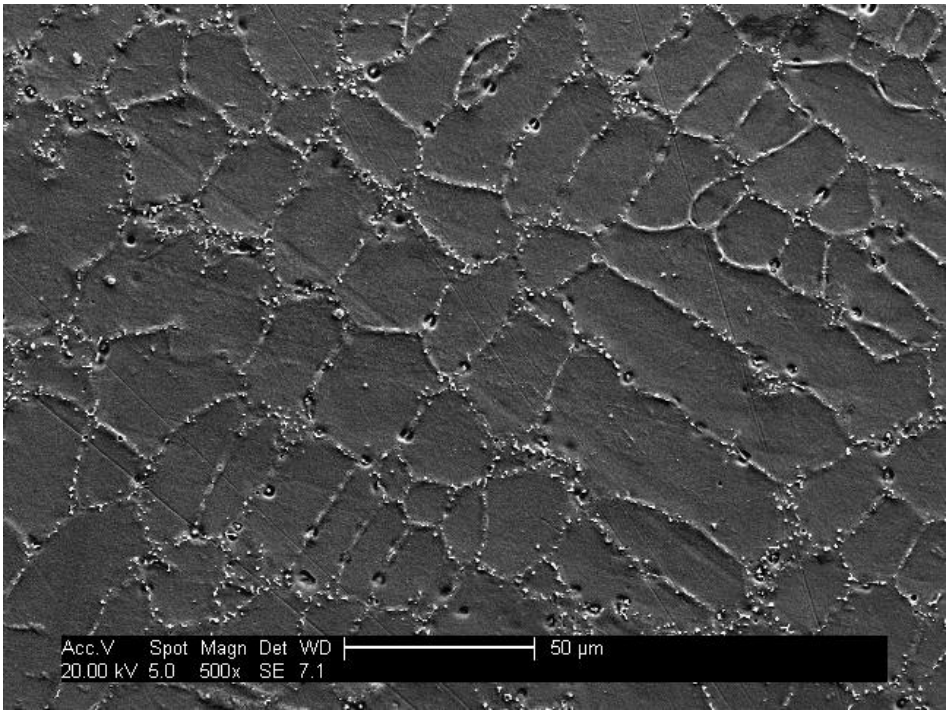

Figure 4-11 SEM image of WAAM deposited Invar alloy

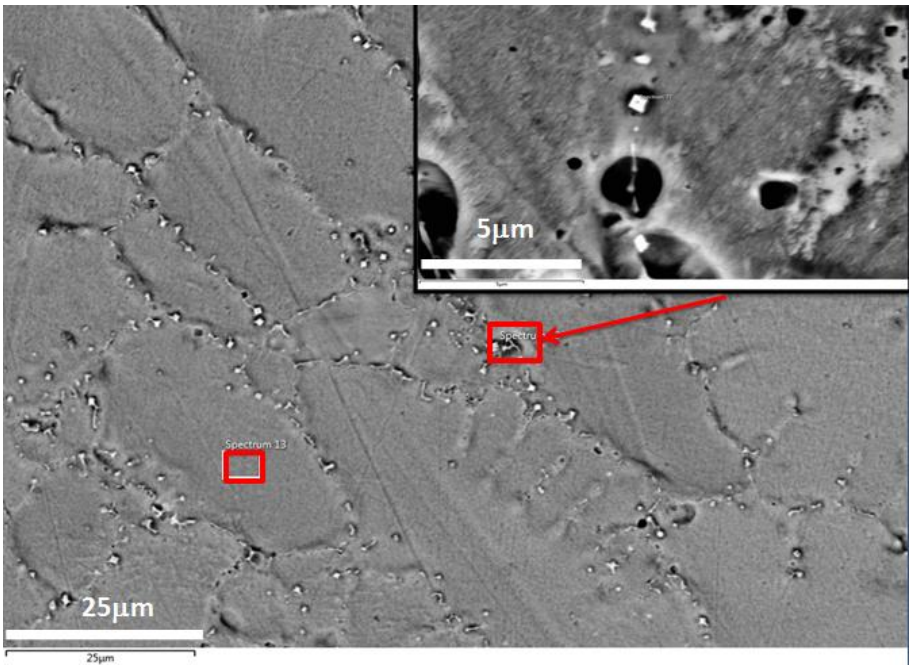

Figure 4-12 SEM image of grain boundary precipitation of WAAM deposited Invar alloy

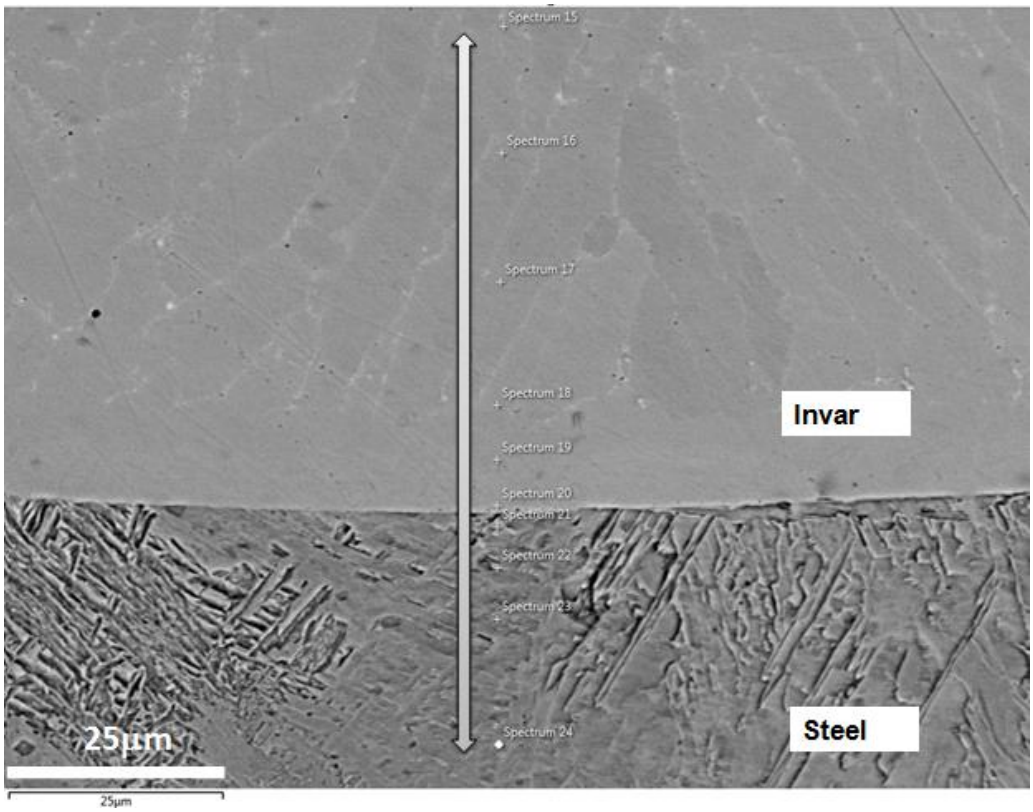

Figure 4-13 SEM analysis of the sample (pure Argon used)

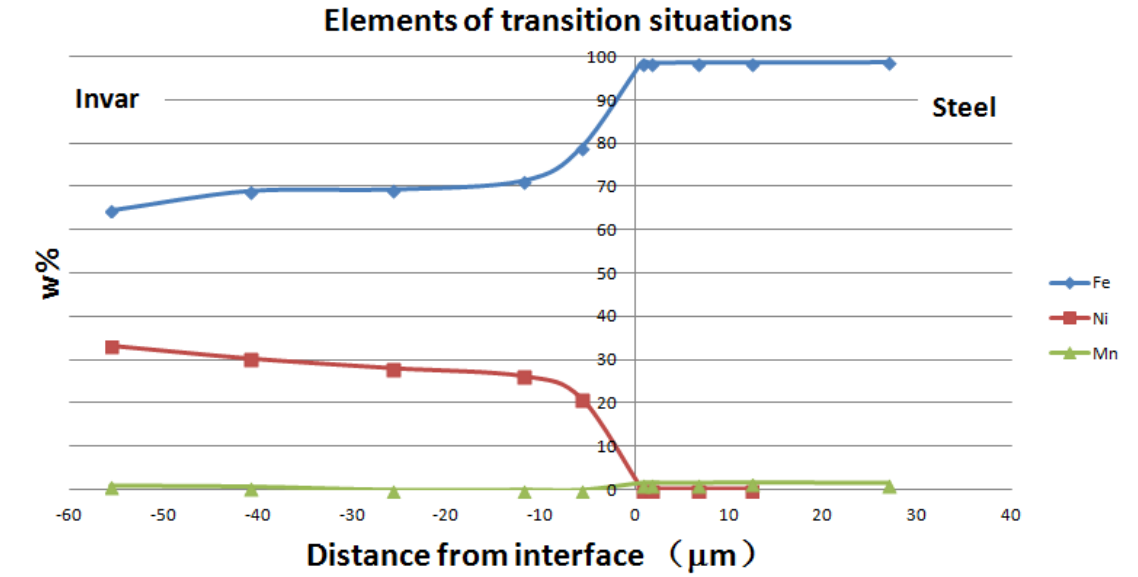

Figure 4-14 Composition of Fe and Nickel versus location for a graded interface between Invar and steel, shielding gas: Ar

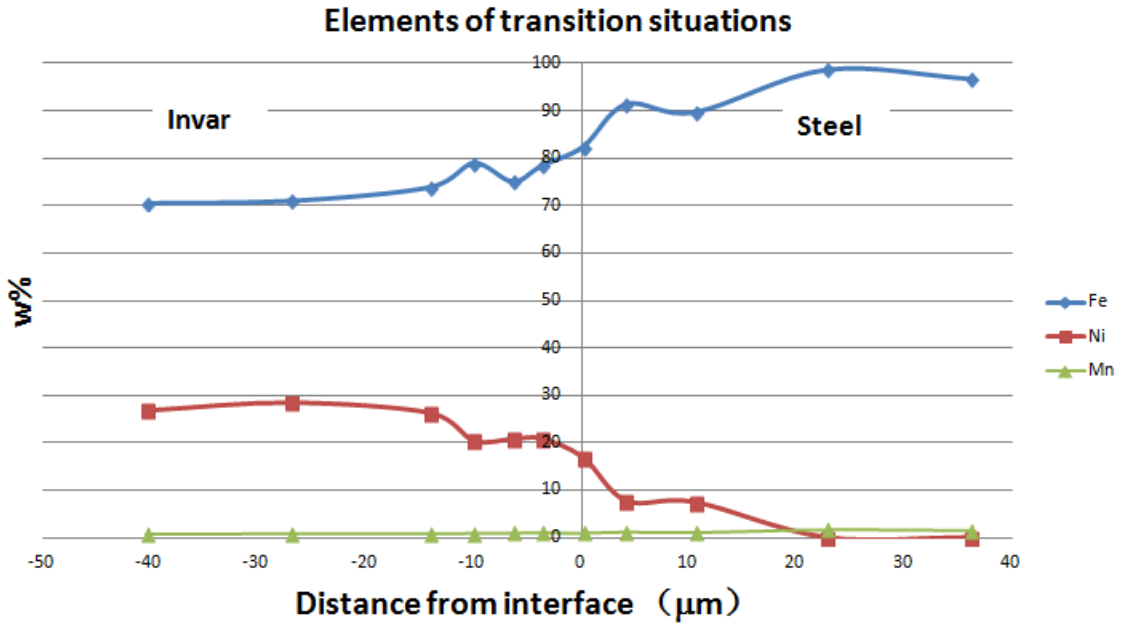

Figure 4-15 Composition of Fe and Nickel versus location for a graded interface between Invar and steel, shielding gas: Ar+2.5%CO2

Appendix C1 and C2 Electron show backscatter images at the interface of each sample with different shielding gases. The Energy Dispersive Spectrometer

（EDS）scanning results reflect the narrow transition layer from 100% of Invar alloy to 100% of stainless steel.

4.4 Mechanical properties Test

4.4.1 Tensile test

4.4.1.1 Tensile test results

The tensile test results are summarized in Table 4-3. Figure 4-16 shows one of six broken tensile test samples of Invar/steel joint. From Table 4-3 and Figure 4-16, it can be seen that all six Invar/steel joint samples, which are produced with different shielding gases, fail within the Invar remote from the joint. It reveals that Invar is successfully deposited on the steel with a high integrity joint. The average ultimate tensile strength of the Invar/steel joint, which is deposited with different shielding gases, is 503MPa. The UTS of the Invar/steel joint deposited with different gases has no significant difference. However, the elongation is considerably different. For pure Invar walls made using the WAAM process no difference was found in UTS and elongation for different directions.

Table 4-3 tensile test result

Group No.	Type	Note	UTS [N/mm^2]	Elongation (%)	Comments
1	Invar - Steel	Ar	512.0	21	All 3 samples fail within the Invar remote from the joint.
			512.0	20.0	
			513.0	20.0	
Average			***512.3***	***20.3***	
2	Invar - Steel	Ar+2.5%CO_2	496.8	57.5	All 3 samples fail within the Invar remote from the joint.
			492.5	46.5	
			492.0	39.1	
Average			***493.8***	***47.7***	
3	Invar	Longitudinal	491.9	54.5	Sample 2 slipped through the jaws at a peak load of 15031N. As a result no values for this item have been recorded.
			--	--	
			486.9	46.1	
Average			***489.4***	***50.3***	
4	Invar	Transverse	500.5	41.7	Invar alloy mechanical properties do not show significantly influence by direction.
			496.1	41.7	
			513.9	44.1	
Average			***503.5***	***42.5***	

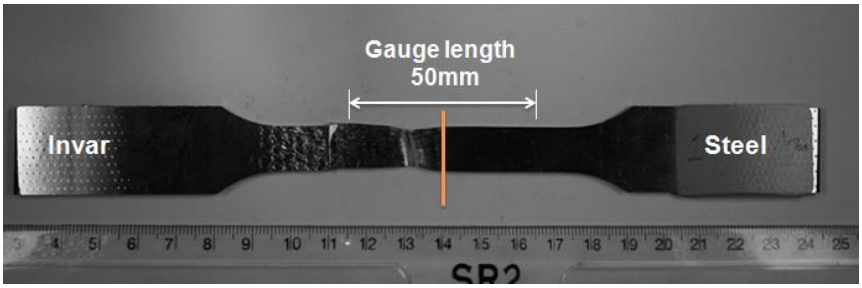

Figure 4-16 Invar-steel samples failed within the Invar remote from the weld

4.4.1.2 Fracture morphology inspection

Figure 4-17 shows the SEM fractograph images of tensile tests. It is clearly seen that all four samples are broken with typical ductile fracture surface morphology.

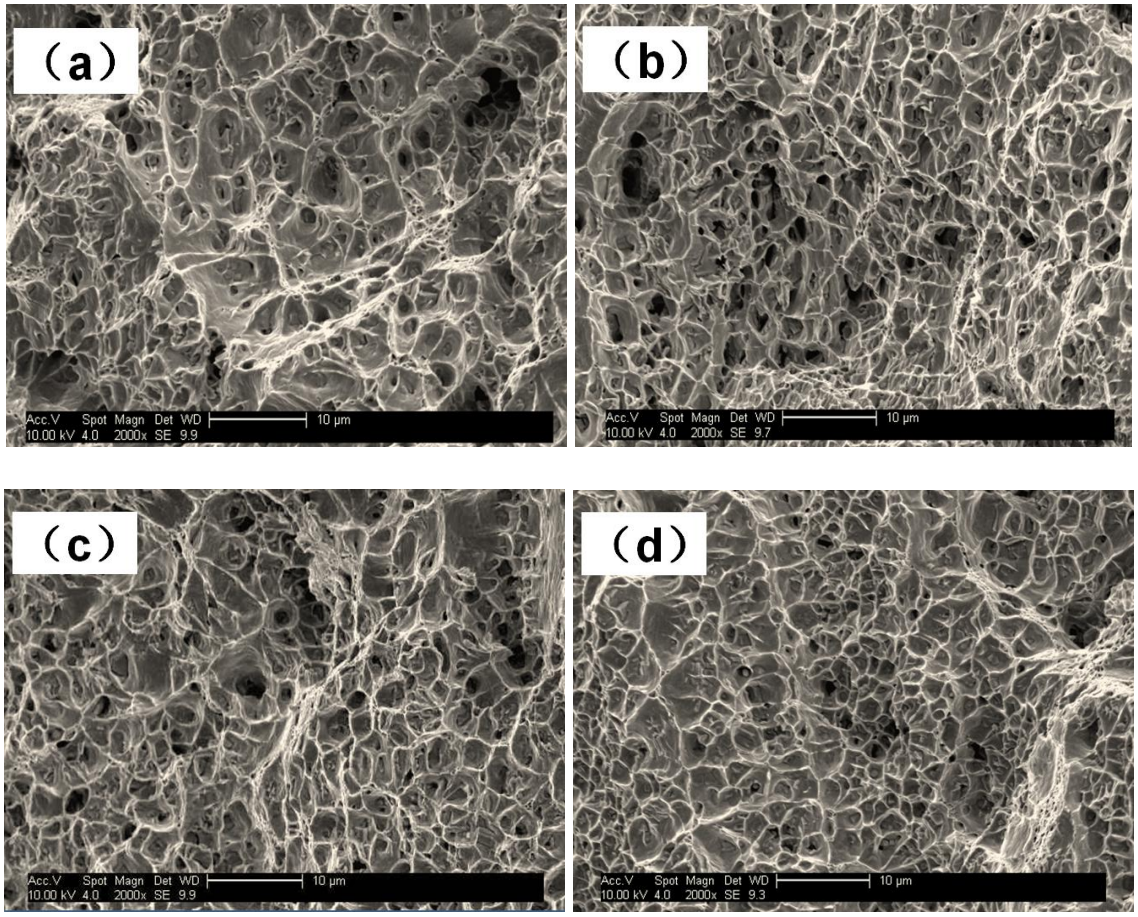

Figure 4-17 Fracture morphology of tensile specimen images by SEM. (a) Invar/steel joint with Argon shielding gas; (b) Invar/steel joint with Argon + 2.5% CO2 shielding gas; (c) Pure Invar tested longitudinally; (d) Pure Invar tested transversely.

4.4.2 Hardness test

A set of twenty-one points along a line perpendicular to the weld joint were tested as indicated in Figure 4-18. Hardness test results are shown in Figure 4-19. The hardness of Invar is lower value than that of steel. There is a hardness transition zone across the Invar and steel joint.

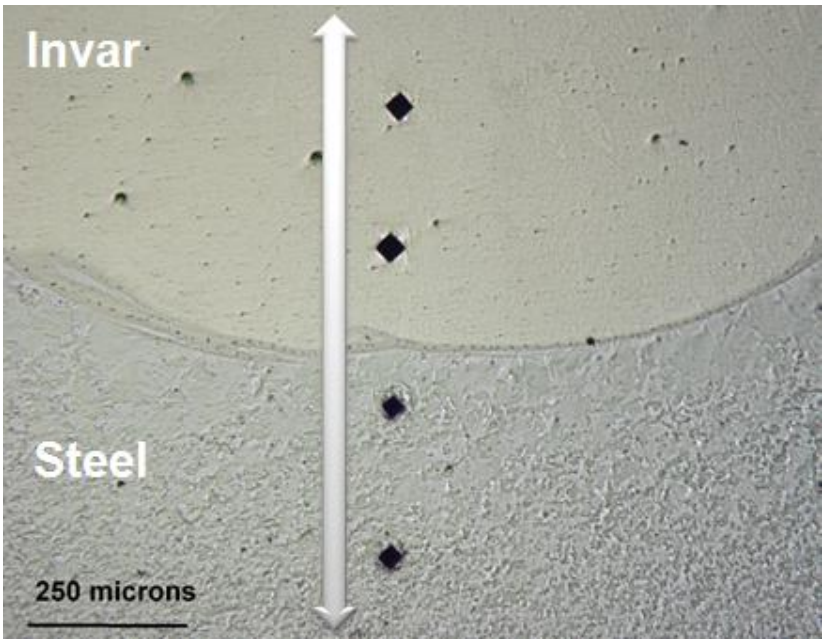

Figure 4-18 Interface hardness measurement, the points were set perpendicularly to the weld seam

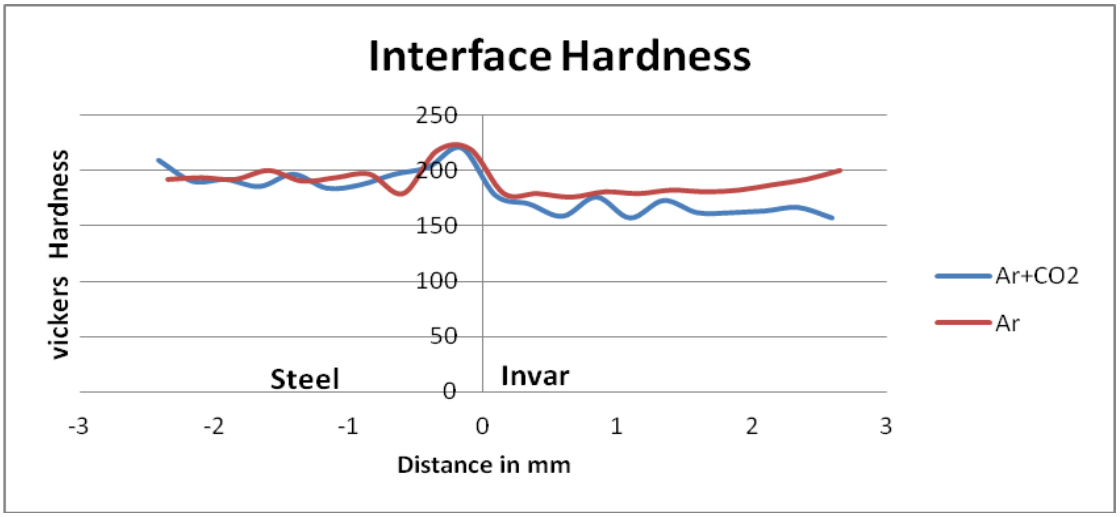

Figure 4-19 Vickers hardness across steel to Invar joint

5 FEM analysis

This chapter focuses on numerical simulation of the thermal expansion with different Invar volume fractions of the multi-material mould. The influence of Invar fraction in volume on the mould deformations level was investigated using the FE models.

5.1 Mould fabrication and set up of boundary conditions

5.1.1 Set up of the FE mould

A set of 1 m long and 0.2 m wide two-dimensional simplified rectangular models were produced to analyse the deformation of multi-material mould, as shown in Figure 5-1. The mould was made of two materials: Invar and steel. A total of 11 sets were made with different proportions of Invar in volume, which varied from 0%, to 100%, with 10% increments. The mould was uniformly heated from 20° C to 200° C. Abaqus was used and the grid size was 0.01m and the total number of elements was 2000; a type of 4-node bilinear plane stress quadrilateral grid was used to reduce integration. The middle of the model was fixed to control the movement of the object.

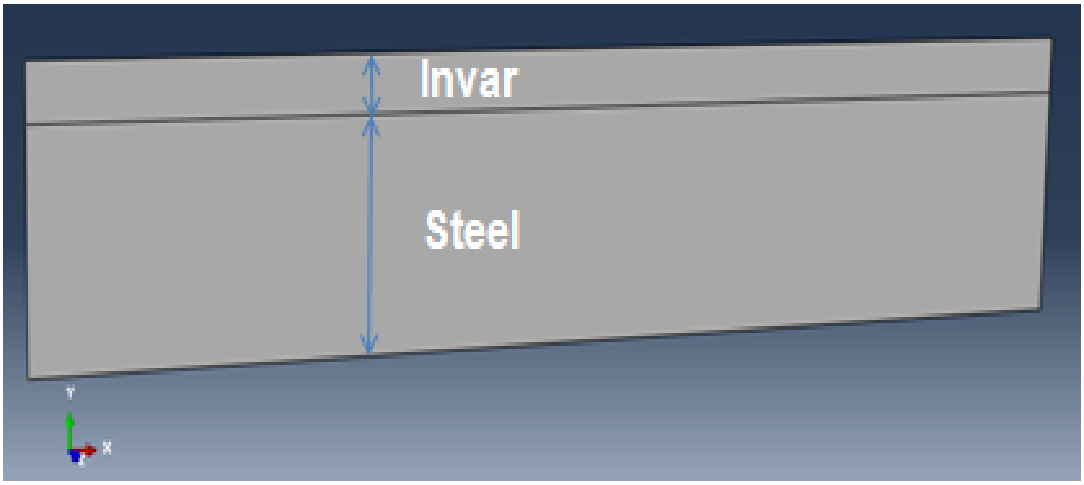

Figure 5-1 Two-dimensional rectangular model, Invar volume fraction varied from 0% to 100%

5.1.2 Measurements

The deformation generated after heated was measured as follows:

As shown in Figure 5-2, Line A-B-C was the original shape of the mould and Arc $A'-B'-C'$ was the corresponding deformed shape. So was D, E, F .

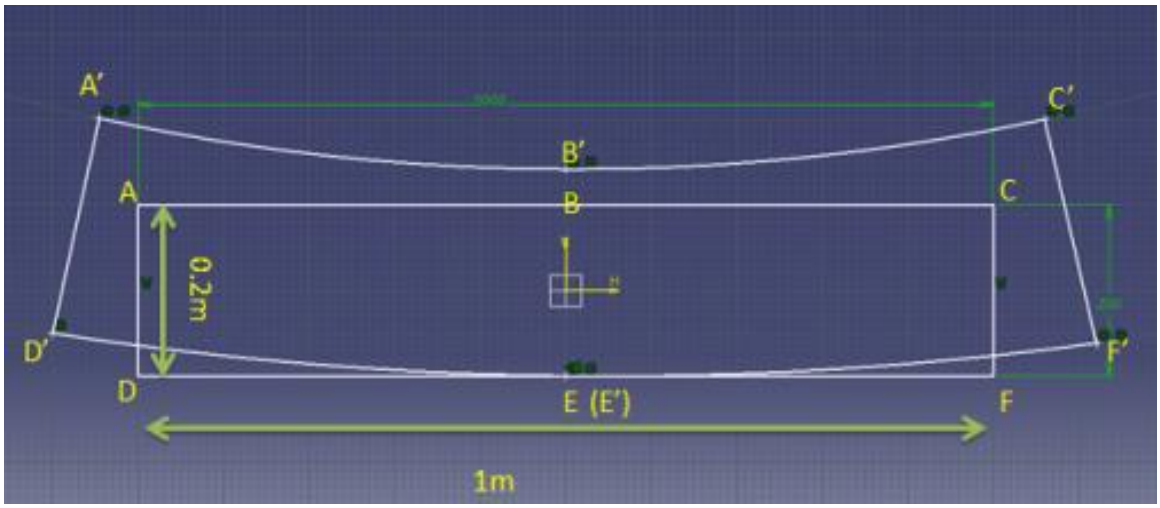

Figure 5-2 The mould initial and deformed shape when FEM wad used for numerical simulation of the curing process

Angle *A'B'C'* was set as a measurement of the curve (mould)'s bending degree, which was marked by $\angle A'B'C'$. Curve length A'B'C' was set as a measurement of the curve's elongation (mould's expansion), as shown in Table 5-1.

Table 5-1 Measurement parameters

Measurement	Description	Mark
Bend angle	measure of the curve's bending degree	$\angle A'B'C'$ (deformed)
Bend length	measure of the curve's elongation	$l_{A'B'C'}$ (deformed)

5.2 Numerical mould results

5.2.1 Typical example: Invar content = 60%

Considering for example the Invar volume fraction at 60%; strain contours and stress distribution diagram of the deformed shape are shown in Figure 5-3 and Figure 5-4, respectively. For both the deformation scale factor was 40. The measurement value is shown in Table 5-2. From Figure 5-3 and Figure 5-4, it can be seen that the model generated an upward deformation and the maximum stress occurred at the interface of steel and Invar.

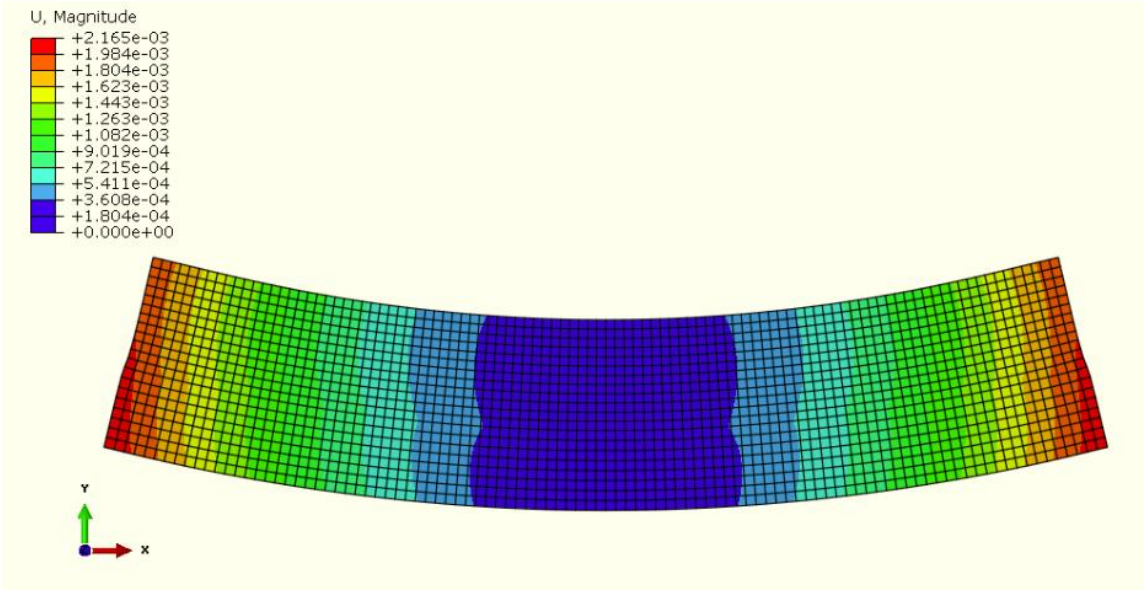

Figure 5-3 Strain contours of the deformed shape, Invar content =60%, deformation scale factor=40, unit: m.

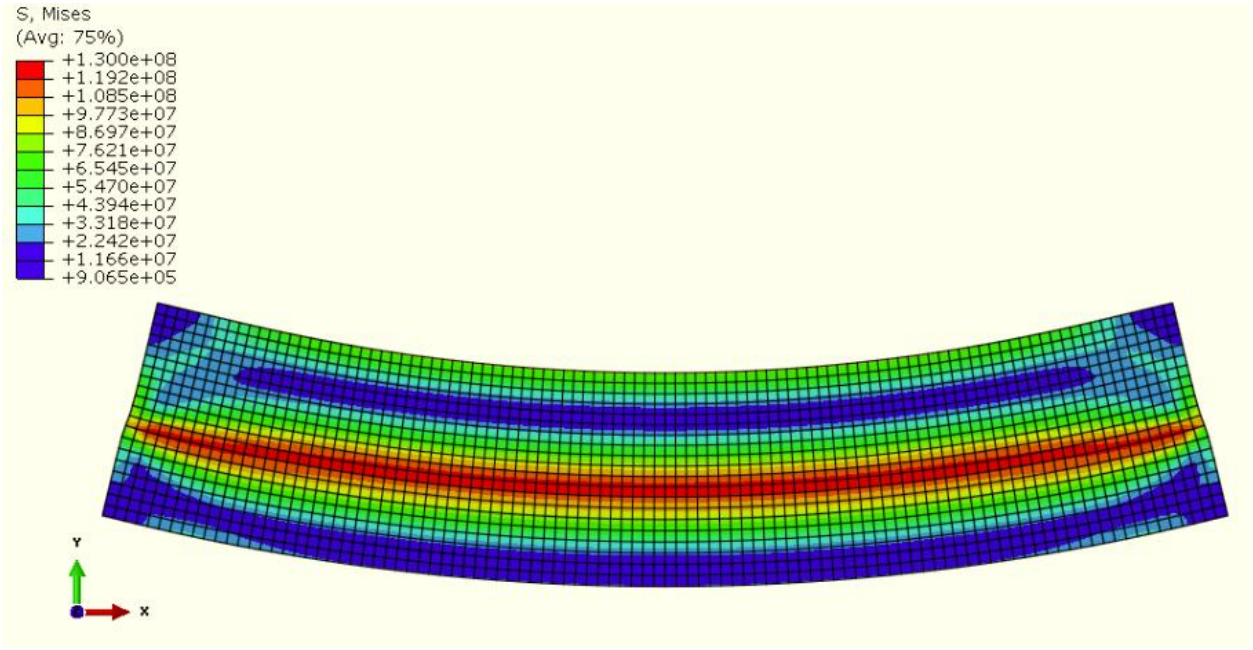

Figure 5-4 Stress distribution diagram of the deformed mould, Invar content =60%, deformation scale factor=40, unit: Pa

Table 5-2 Measurement values of the deformed shape

	above	below	Comments
bend angle (°)	179.607	179.603	
Bend length change(mm)	3.9	4.33	A positive value indicates elongation.

5.2.2 Result of 11 sets

When 11 sets of calculation were finished, measurement of the mould's bend angle change and bend length change according to Invar volume fraction was observed, as shown in Figure 5-5 and Figure 5-6. The specific results are shown in Appendix E1.

When Figure 5-5 and Figure 5-6 are compared, the following conclusions can be drawn:

1. From 0% Invar to 100% Invar, the mould's bending deformation is always larger than that of 100% Invar value; the mould would only generate expansion in two conditions: 100% steel and 100% Invar.
2. The mould's bending trend is aggravated when the Invar content increases and the maximum value of bending deformation occurres

when the Invar volume fraction is 50%. After that, model's bending deformation decreases as Invar volume fraction continued to grow.

3. The mould's surface length elongation value is always less than pure steel condition and this value decreases when the Invar content lies between 0% to 70%; after that, the length change gradually increases until 100% Invar limit is reached.

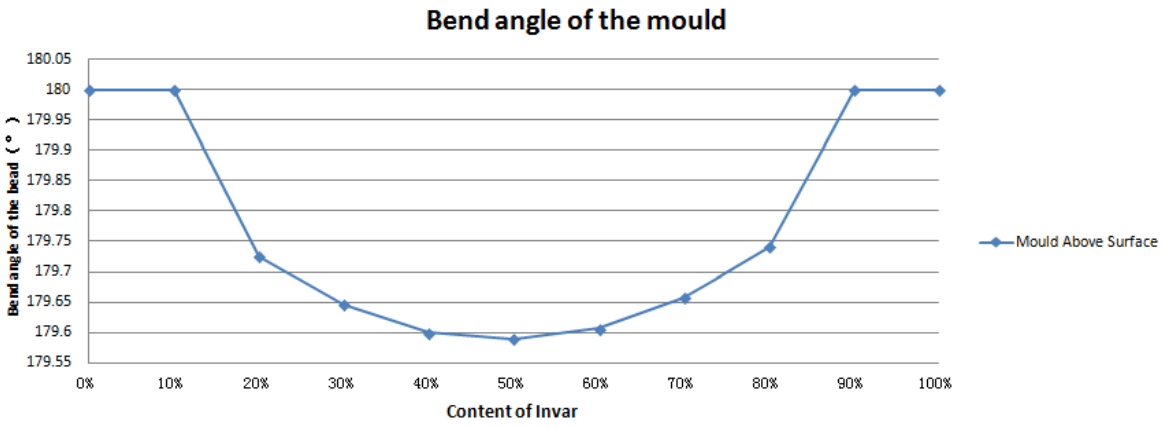

Figure 5-5 Measurement of mould's bend angle change according to Invar content in the heating process.

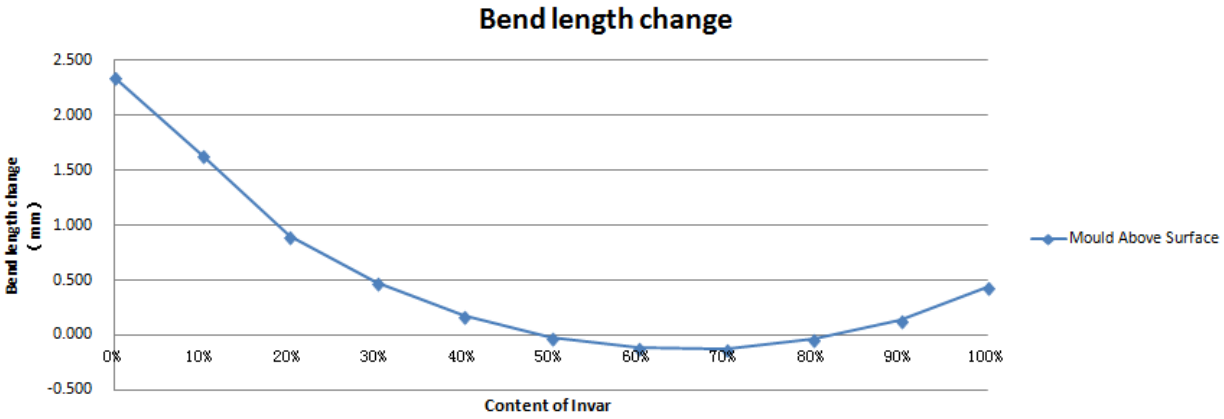

Figure 5-6 Measurement of mould's bend length change according to Invar content in the heating process.

5.3 Summary

In this chapter an FE model was produced to analyse the deformation of a multi-material mould when heated from 20° C to 200° C. In all 11 trials were

conducted, the results indicated that no bending value was less than 100% Invar model and the most serious bending status was generated when Invar occupied half of the mould's content.

The results of the analysis shows that the new mould's bending deformation predicted is actually larger than the original mould (made of 100% Invar). It means the steel/Invar mould in this chapter is not feasible. However, it is hoped that the new mould's deformation value can be equal or less than that of pure Invar mould case. One possible solution is the parameter compensation method in mould design and this will be introduced in chapter 6.

6 Parameter compensation method in mould

In this chapter, parameter compensation design method was applied to control the deformation of the mould. The effectiveness and logic of this compensation algorithm was verified by simulating an APU composite door fabrication mould as a typical example.

6.1 The parameter compensation method

Until now, the mould's deformation was a dominant factor in inaccurate dimension control of composite material components in autoclave forming process. The compensation design method was an effective way to control the deformation of the forming mould, which was getting increasingly important in the mould's design.

Traditional compensation design methods were typically relied on experience due to the limitation of calculation capacity. Using trial and error, the mould surface would be adapted by repeated adjustment and compensation processes. This procedure was often time-consuming and expensive.

With the rapid development of computer technology and finite element method, the compensation parameter method for mould design had become feasible. For instance, in Dong's PhD thesis (Dong, 2003) (the Florida state university, U.S.A), he developed FEA-based and regression-based dimension variation models for dimension variation prediction and control for mould design. This model was verified by experimental data.

The significance of the parameter compensation design method lay in good deformation prediction to get the correct modified shape at high temperature. More specifically, using the simulated displacement of the nodes after deformation process, the tooling's surface was adjusted on the specific displacement value calculated by Finite element model (FEM) method. Figure 6-1 shows the general flowchart of the parameter compensation design method process.

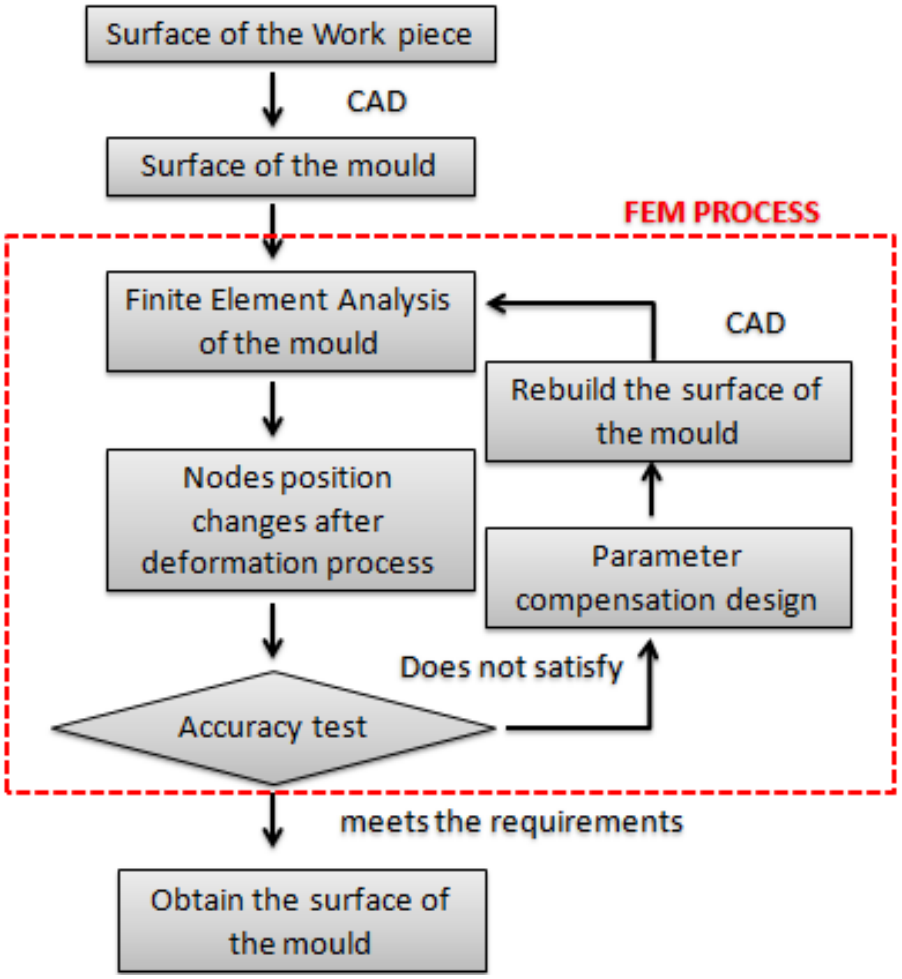

Figure 6-1 Parameter compensation design method flowchart

6.2 The implementation process

6.2.1 Mould deformation definition

As shown in Figure 6-2, $P_i(x_i, y_i, z_i)$ was defined as the original position and $P'_i(x'_i, y'_i, z'_i)$ as the deformed position. The corresponding compensation design position was $P''_i(x''_i, y''_i, z''_i)$. To control the mould's deformation, generally P_i'' should be defined in the opposite side.

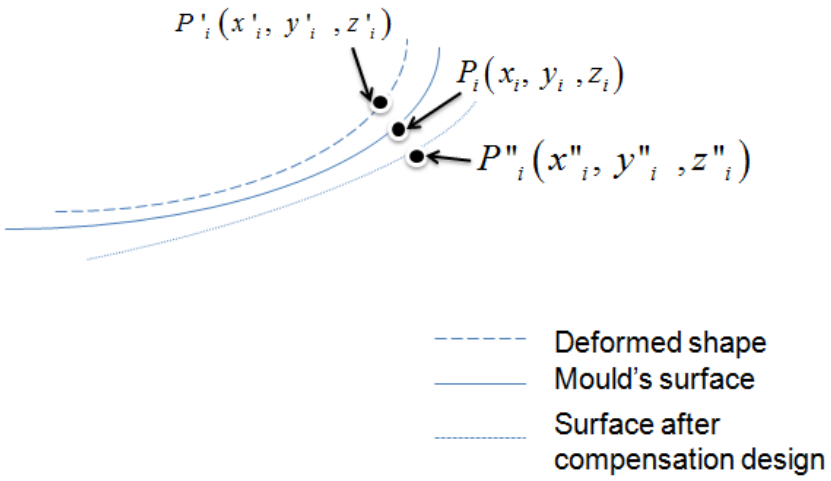

Figure 6-2 Deformation Schematic of the mould's surface

6.2.2 Principle of the parameter compensation method

In general, the compensation design equation is expressed as follows:

$$\overrightarrow{p''_i p_i} = \lambda \overrightarrow{p_i p'_i} \tag{6-1}$$

Where λ is compensation coefficient, $0 \le \lambda \le 1$.

Generally, when $0.5 \le \lambda \le 1$, the iteration converged quickly; When the calculated value was close to the expected data, $0 \le \lambda \le 0.5$, the iteration converged slowly to achieve more accurate results. Dong pointed out that from practical results, the initial value of λ can be 1 and this model has been verified by experiment (Dong, 2003).

To calculate the position of P_i'', from equation 6-1:

$$(x_i - x_i'', y_i - y_i'', z_i - z_i'') = \lambda(x_i' - x_i, y_i' - y_i, z_i' - z_i) \tag{6-2}$$

The following equation can be derived:

$$(x_i'', y_i'', z_i'') = (x_i - \lambda(x_i' - x_i), y_i - \lambda(y_i' - y_i), z_i - \lambda(z_i' - z_i)) \tag{6-3}$$

Where, $\Delta x = x_i' - x_i, \Delta y = y_i' - y_i, \Delta z = z_i' - z_i$,

So, the position of parameter compensation point is:

$$\begin{cases} x_i'' = x_i - \lambda \Delta x \\ y_i'' = y_i - \lambda \Delta y \\ z_i'' = z_i - \lambda \Delta z \end{cases} \qquad 0 \le \lambda \le 1 \tag{6-4}$$

Expressed as vectors this is,

$$P_i'' = P_i - \lambda \overrightarrow{p_i p_i'} \qquad 0 \le \lambda \le 1 \tag{6-5}$$

6.2.3 Principle of the calculation process

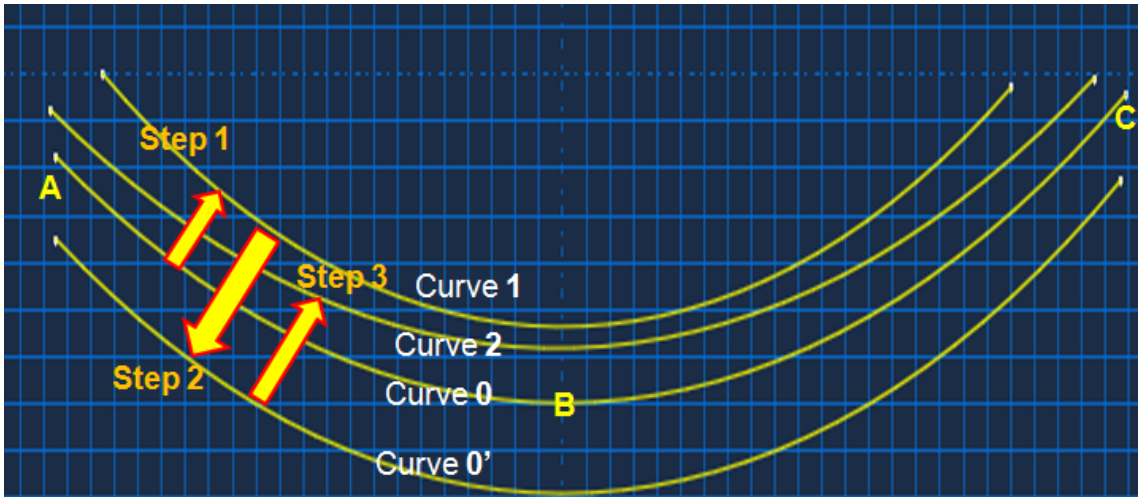

Figure 6-3 Basic calculation process of the mould surface

Figure 6-3 indicated the general design iteration step,

Where Curve 0- original shape (Expected value of the product),

Curve 1- deformed shape (deformation compensation was not applied),

Curve 0' - deformation compensation applied design,

Curve 2 - new deformed shape (deformation of compensated shape)

Specific operation was as follows:

1. Determine the mould's initial surface according to the appearance of composite material component;

2. Use Finite element analysis method for the mould and determine deformation and deformation displacement;
3. Measure the deformation displacement to check whether it meets the mould's requirements ;

   In fact, the deformation displacement value of each point can be expressed as follows:

$$\left|\overrightarrow{p_i p_i'}\right| = \sqrt{\left(x_i' - x_i\right)^2 + \left(y_i' - y_i\right)^2 + \left(y_i' - y_i\right)^2} \qquad \textbf{(6-6)}$$

   If the value of $\left|\overrightarrow{p_i p_i'}\right|$ is outside the allowable range, the compensated design will be needed in the next step;

4. Calculate the mould's compensated surface according to Equation 6-1;
5. Repeat steps 2 and 3, if the calculated results meet the mould's accuracy requirements after those steps, stop the calculation process and output the final results.
6. If the results did not meet accuracy requirements on the basis of steps 2 and 3, continue the process until step 5 is satisfied.

In fact, the aim of this whole process was to let curve 2 approximate as closely as possible to curve 0 (expected shape of the product); Meanwhile, Curve 2 was the deformed shape of curve 0' (deformation of compensated shape).

6.3 Application of parameter compensation method

6.3.1 Set up of the FE mould

Taking a commercial aircraft composite auxiliary power unit (APU) door forming mould as an example, the APU door shape and 2D-curing mould is shown in Figure 6-4 and 6-5. From section 5.3 results, which indicated that the most serious bending status was generated when Invar comprised 50% of the content.

To verify the parameter compensation method, the most serious deformation condition should be taken into consideration, when the Invar volume fraction

was 50%. The corresponding thickness of the Invar layer was 0.12 m and the steel layer 0.08m. The mould was uniformly heated from 20 °C to 200 °C.

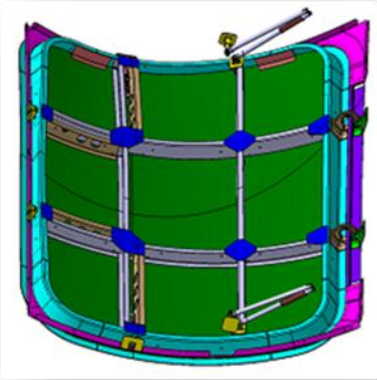

Figure 6-4 APU (auxiliary power unit) door from commercial aircraft

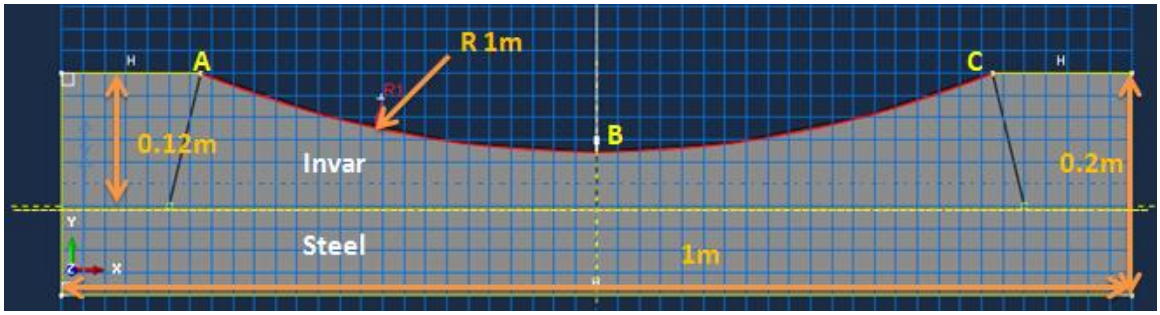

Figure 6-5 Female mould used for APU door forming

6.3.2 Initial deformation result

The strain contours and stress distribution diagram was shown in Figure 6-6 and Figure 6-7, respectively. Both the deformation scale factor was 2 times. The measurement value was shown in Table 6-1.

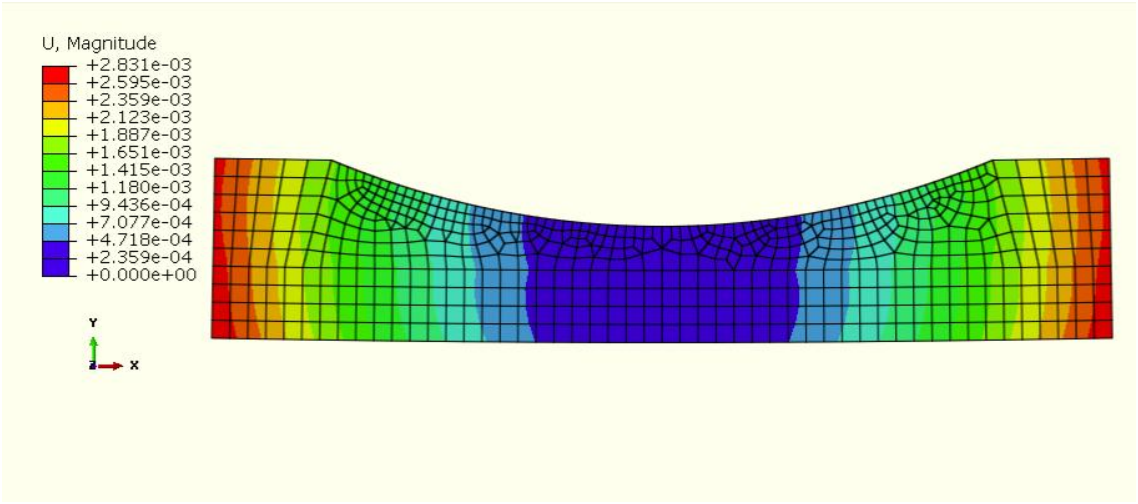

Figure 6-6 Strain contours of the deformed shape,

deformation scale factor=2, unit: m

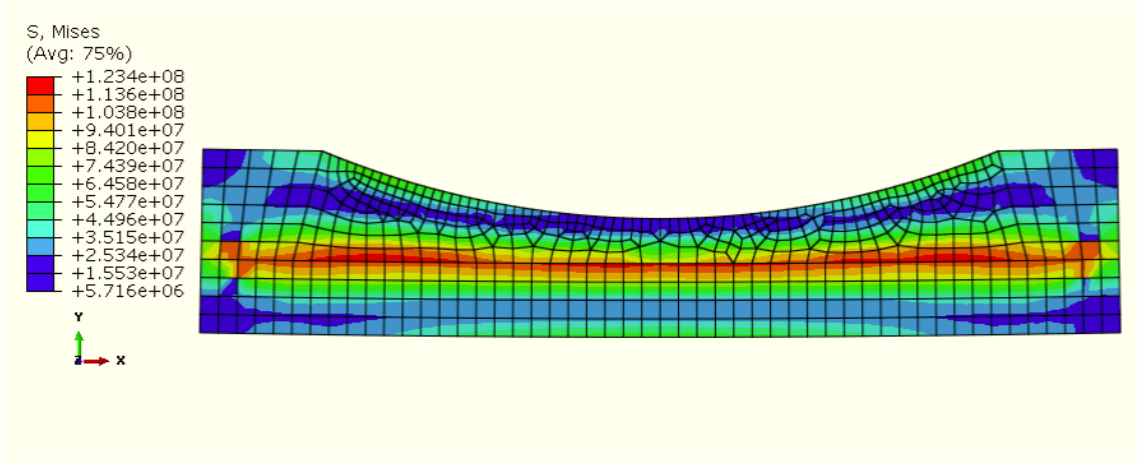

Figure 6-7 Stress contours of the deformed shape,

deformation scale factor=2, unit: Pa

Table 6-1 Angle change

	Bend angle	The amount of change
Original	158.284°	
Deformed	157.830°	0.454° (0.29%)

6.3.3 Parameter compensation design

All the node's positions were obtained as Figure 6-8 shows. The mould's compensated surface should be calculated according Equation 6-5. Thus, the new compensation designed shape was created from the interface of CATIA software and Abaqus, as Figure 6-9 to Figure 6-11shown.

	Original position		Position change value	
Node Label	COORD.COOR1 @Loc 1	COORD.COOR2 @Loc 1	U.U1 @Loc 1	U.U2 @Loc 1
1	-400.000E-03	-20.0000E-03	-535.443E-06	1.82640E-03
2	-370.000E-03	100.000E-03	371.076E-06	1.65782E-03
3	-500.E-03	100.000E-03	348.535E-06	2.67316E-03
4	-500.E-03	-20.0000E-03	-673.226E-06	2.67454E-03
5	-500.E-03	-100.000E-03	-1.40195E-03	2.45929E-03
6	500.E-03	-100.000E-03	1.40138E-03	2.45650E-03
7	0.	-20.0000E-03	187.929E-09	192.221E-06
8	400.000E-03	-20.0000E-03	535.591E-06	1.82421E-03
9	500.E-03	-20.0000E-03	673.164E-06	2.67171E-03
10	370.000E-03	100.000E-03	-370.286E-06	1.65608E-03
11	500.E-03	100.000E-03	-347.843E-06	2.67023E-03
12	0.	29.0318E-03	-948.822E-33	206.730E-06
13	-395.000E-03	0.	-378.603E-06	1.79542E-03
14	-390.000E-03	20.0000E-03	-224.487E-06	1.76466E-03
15	-385.000E-03	40.0000E-03	-74.4868E-06	1.73646E-03
16	-380.000E-03	60.0000E-03	74.9398E-06	1.70938E-03
17	-375.E-03	80.0000E-03	222.533E-06	1.68251E-03
18	-396.000E-03	100.000E-03	369.115E-06	1.84756E-03

Figure 6-8 Node positions

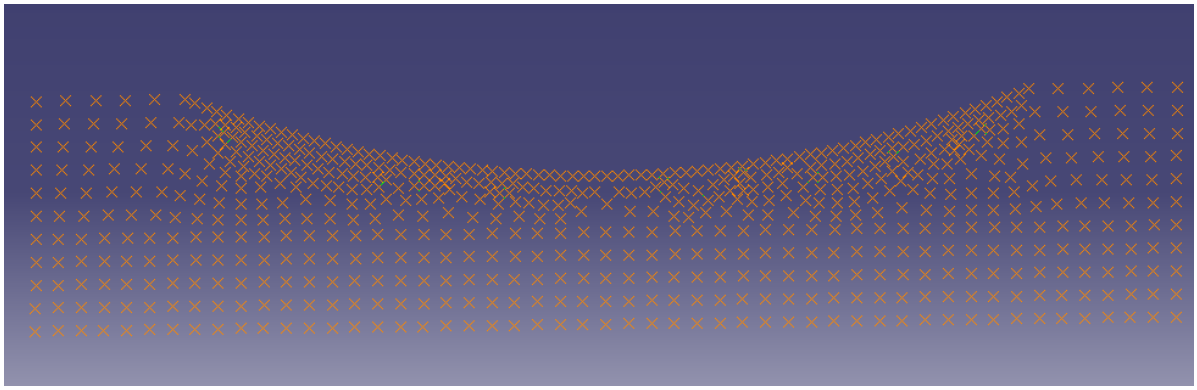

Figure 6-9 New design shape of the mould

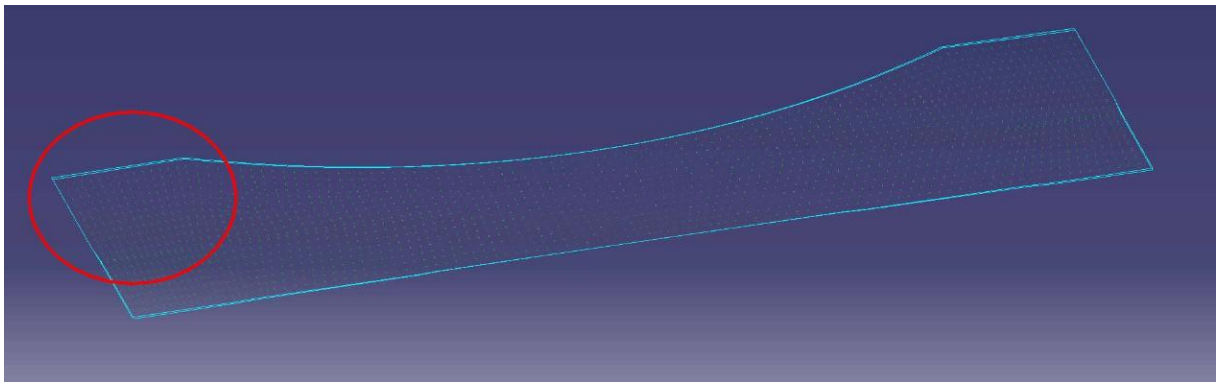

Figure 6-10 Shape created

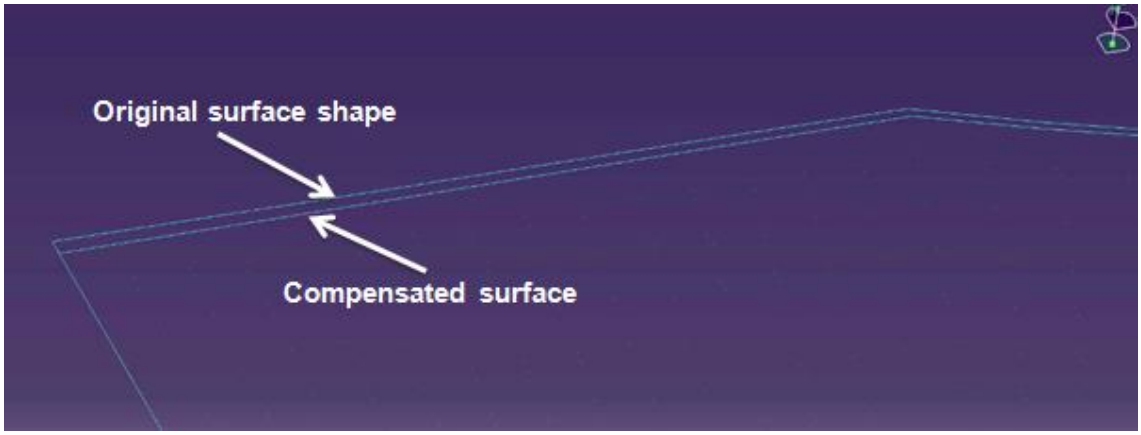

Figure 6-11 Partial enlarged view of Model modification

6.3.4 Compensated surface deformation results and analysis

The parameter compensation design mould results were used by the Abaqus software for calculation again; the results are shown in Figure 6-12, Figure 6-13 and Table 6-2.

This design method produced significant change, for the angle, the changed value only 4% of the initial deformation and the reference position changed from 1.497 to 0.353 mm.

In fact, for a 10m long mould,

H= 10m* sin0.454=0.079237m=79.237 mm

H'= 10m*sin0.009= 0.00157mm= 1.57 mm

This method can effectively control the deformation of the mould.

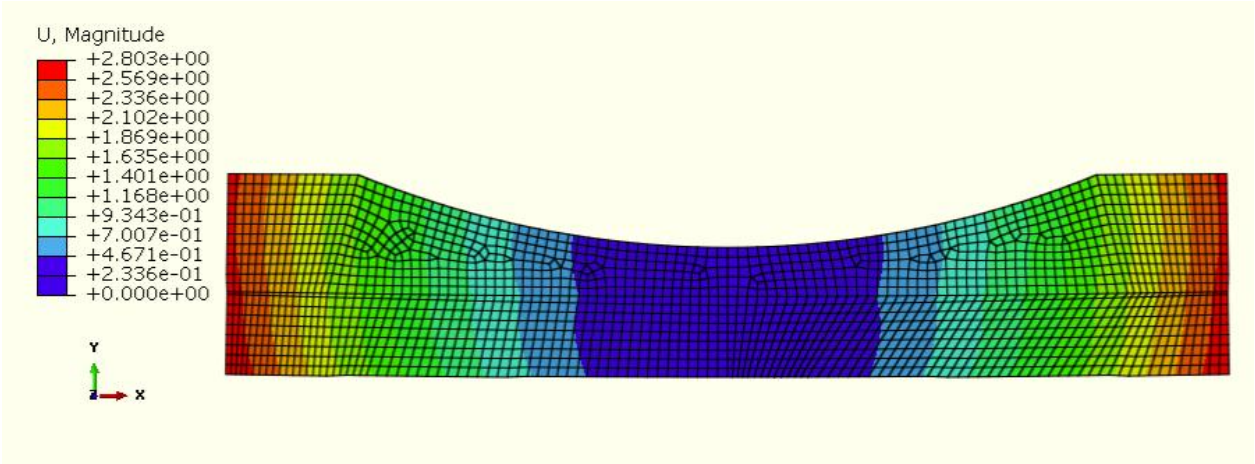

Figure 6-12 Strain contours of compensated surface deformation, deformation scale factor=2, unit: m

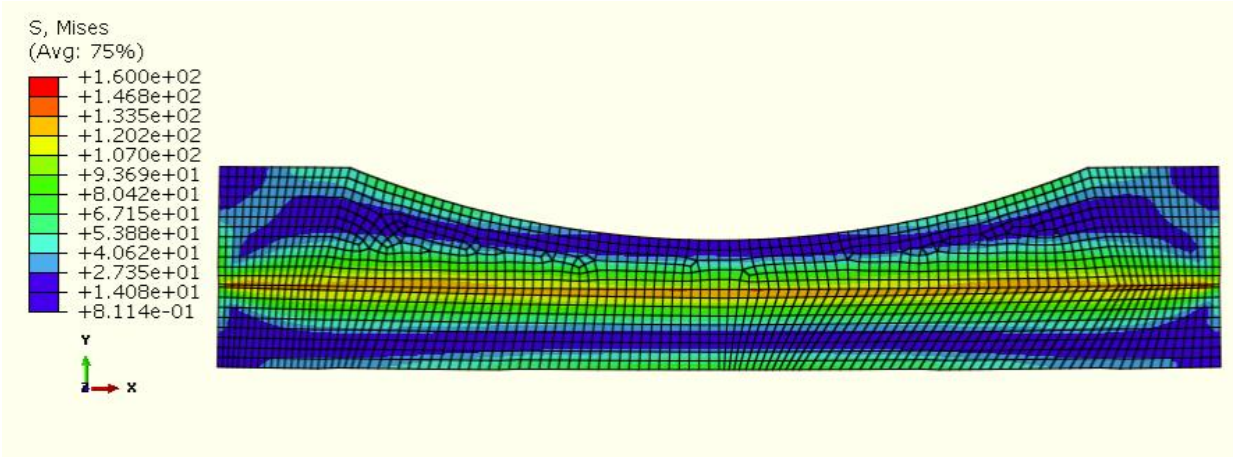

Figure 6-13 Stress contours of compensated surface deformation deformation scale factor=2, unit: Pa

Table 6-2 Compensated surface deformation result and comparison

Bend angle		CHANGED VALUE	CHANGED PERCENTAGE
Original surface	158.284°		
Deformed surface	157.83°	0.454°	0.29%
compensated surface deformation（heated）	158.275	0.009°	0.01%

96%

6.4 Summary

The compensation design method for forming moulds was increasingly gaining designers' attention; due to mould deformation was the main factor affecting the accuracy of composite components. With the rapid development of machine technology, the parameter compensation design became a reality. The parameter compensation method was carried in two steps: first accurate deformation prediction of the mould and second anti-deformation-based design. By simulating an APU composite door fabrication mould, the deformation of the mould was reduced from 0.454° to 0.009°, which satisfied the aerospace industry‘s requirements and the results verified the effectiveness and logic of this compensation algorithm.

7 Discussion

7.1 WAAM Invar on steel feasibility ability study

7.1.1 Bead on the plate deposition

Table 4-1 indicates that a stable welding bead cannot be achieved in low WFS/TS ratio. Discontinuity and lack of fusion in the welding bead is observed when WFS/TS ratio is lower than 8. The reason for this is that when the WFS/TS ratio is lower the heat input and the feed of the wire are lower. The arc heat is not high enough to melt the substrate and the wire at same time. This can be avoided by increasing the WFS/TS ratio, as shown in Figure 4-1.

Pedro Almeida's study (Sequeira Almeida, 2012) has shown that a high WFS/TS ratio can result in a larger cross-sectional area and wider welding bead. Benyounis and Hashmi(Benyounis et al., 2005)'s study has shown that more metal will be melted when a higher heat is input in the GMAW welding process.

Meanwhile, it can be seen that the quality of the welding beads has been improved with Argon + 2.5% CO_2 shielding gas, as shown in Table 4-1 and Table 4-2. Argon + 2.5 %CO_2 shielding gas gives a smooth and continuous welding bead whilst the trials with pure Argon cannot.

Subramaniam and White's study (Subramaniam and White, 2001) has pointed out that addition of carbon dioxide (CO_2) in pure Argon results in reduction of surface tension of the droplet and molten pool. This promotes bead shape in the GMAW process.

Pure Argon as a shielding gas has a higher heat input than Argon + 2.5% CO_2 at the same WFS because of a higher ionization potential of pure Argon. However, in reduction of surface tension of the droplet and molten pool CO_2 plays a more important effect in the welding process. This is why Argon + 2.5% CO_2 generates a wider welding bead and a larger contact angle compared with samples deposited with pure Argon shielding gas in the same WFS and TS parameter.

7.1.2 Multi-layer welding

Figure 4-5 shows cross sectional image of multi-layer WAAM wall. It can be seen that it has a narrower joint with the substrate. The reason for this is that the first layer is deposited on a cold substrate. The heat conduction is faster because it has a higher temperature gradient between the first layer and substrate. From the second layer, the subsequent Invar is always deposited on the previous layer. The temperature gradient between two adjacent layers is lower. Therefore the heat conduction within the wall is slower than in the first layer which in contact with the substrate. The residual heat existing in the previous layers raises the wall temperature. The high wall temperature reduces the surface tension; improve the wetting and spreading behaviour of the welding pool (Sequeira Almeida, 2012).

Comparing Figure 4-4 with Figure 4-5, it can be seen that the initial bead shape is wider with Argon + 2.5% CO_2 shielding gas. This is because CO_2 can reduce the surface tension; promote the mobility and the wetting of the pool. It has been found that the initial layers (1st, 2nd and so forth) shape has a significant effect on the wall's useable area efficiency (Sequeira Almeida, 2012). That is why the useable area efficiency is higher when Argon + 2.5% CO_2 is used.

Sequeira Almeida's study has shown that effective wall width has a significant increase when the ratio (WFS/TS) increases but the wall's surface waviness does not increase significantly (Sequeira Almeida, 2012).

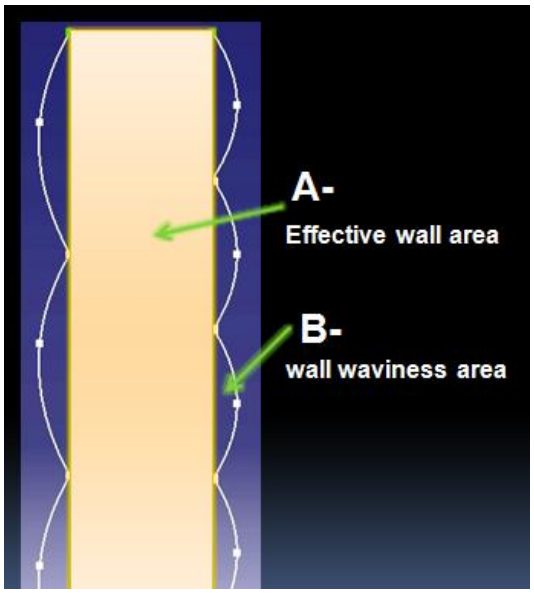

Figure 7-1 Cross section of the multi-layer welding

As shown in Figure 7-1, the useable area efficiency is calculated by equation 7-1.

$$UAE = \frac{A}{A+B} \tag{7-1}$$

Where UAE is the useable area efficiency

A is the effective wall area

B is the wall waviness area

When A increases, the UAE increases correspondingly. That is why a higher useable area efficiency can be achieved when ratio (WFS/TS) increases.

At present, the main methods to improve the effective wall thickness are reducing the TS when WFS is kept constant and pre-heating the substrate. Reducing the TS allows more material to be deposited per unit length. Pre-heating the substrate can reduce the temperature gradient between substrate and the first deposit layer. This can improve wetting and spreading behaviour of the welding pool. Leinonen optimised individual experimental parameters from the above two aspects and obtained a higher useable area efficiency (Mattias, 2011).

7.1.3 Microscopic analysis results

This study indicates that Invar is successfully deposited on steel in the WAAM process. Both Ar and Ar +2.5% CO_2 can be used as shielding gas when welding Invar alloy.

Cary pointed out that Carbon dioxide (CO_2) can improve fluidity of the melting puddle, increase the weld pool's penetration and promote bead shape (Cary and Helzer, 1979). That is why the element transition cross Invar/steel joint is wider (30 μm) when Argon + 2.5% CO_2 was used than Argon alone was used as shielding gas (10 μm), as shown in Figure 4-14 and Figure 4-15, respectively.

In addition, compared with Pulse and Dip transfer welding process, CMT is a relatively lower heat input process. This is likely to cause a narrow transition layer from 100% Invar to 100% steel.

7.1.4 Mechanical properties

From tensile tests, there is no significant difference in the ultimate tensile strength of Invar/steel joint with pure Ar and Ar+2.5% CO_2 as shielding gas. They are 512.3Mpa and 493.8Mpa respectively. However, the ductility is considerably different. It is 47.7% when Ar+2.5% CO_2 is used as shielding gas while it is 20% when pure Argon is used as shown in Table 4-3.

The reason for this is that there is a wider element diffusion zone in samples with Ar+2.5% CO_2 as shielding gas. This may make positive a contribution to the material's ductility. This need to be further investigated in the future. Another reason is that the wall built with pure Argon shielding gas does not have sufficient back shielding protection. And the surface of each layer is oxidised during the process. These oxides may get trapped between the layers and form inclusions which cause a decrease in ductility value. When building the second wall with Ar+2.5% CO_2 as shielding gas, a proper back shielding protection was given for each layer.

It has been found that the mechanical properties including UTS and elongation of WAAM Invar wall show no difference in different test directions. This can be

explained from the optical and SEM images of the solidification microstructure of the Invar wall as shown in Figure 4-8 and Figure 4-11. Equiaxial grains have been observed through the whole wall.

The hardness test results are in line with expectations and the Invar value is lower than steel. The value in the hardness transition zone between the Invar and steel joint is higher than in the Invar matrix. That means there is a hardness enhancement zone in the interface. This could be attributed to grain refinement in the recrystallization process.

In summary, it can be seen that the mechanical properties of the joints is stronger than Invar base material. The data also show that the welding process does not have any negative effect on the mechanical properties, neither Invar itself nor the interface.

The experimental results verify the desirability of fabricating a functional mould for composite material fabrication using WAAM technology, it also includes repair of tooling through WAAM technology.

7.2 WAAM Invar on steel feasibility ability study

7.2.1 Factors that influence mould deformation

In chapter 5, the model generated an upward deformation and the maximum stress occurred at the interface of steel and Invar when Invar volume fraction was 60%. This is as expected because steel's thermal expansion coefficient (CTE) is larger than Invar, which are $12\times10^{-6}/{}^{o}C$ and $2.5\times10^{-6}/{}^{o}C$, respectively. It results in a larger expansion value for Steel part than for the Invar part when the bimetal model is heated. In this case, the Invar part is under pressure and the steel part bears pulling force. Thus the mould bent upward. Also, due to the significant difference of the expansion values of these two materials, the maximum stress was generated in the interface between Invar and steel.

From Figure 5-5 and Figure 5-6, it can be seen that there is no bending when the Invar content is 0% or 100%. The reason is when Invar content is 0% or

100%, it means pure Invar or pure steel model status respectively and there should be only expansion and no bending process.

In addition, the results also indicate that there is a corresponding increase in mould's bending trend when Invar volume fraction is from 0% to 50%; however, the mould's bending reduces when the Invar volume fraction continually increases. The maximum bending situation occurs when the Invar volume fraction is 50%

In this FEM model, three factors influence the bimetal mould's deformation: difference in thermal expansion coefficient (CTE), volume fraction and Young's modulus.

In fact, as a type of high nickel alloy, there is no significant decrease in Young's modulus of Invar from 20° C to 200° C. However, the Young's modulus of steel is sensitive to the temperature change. At 200° C, the Young's modulus of Invar and steel is very similar, which is 142Mpa and 140Mpa, respectively. Thus, the ability to resist deformation is almost the same in these two materials at 200° C.

Now only the remaining two factors will influence the mould's deformation, which is the difference in CTE and volume fraction. Invar's lower CTE property effect on the model is progressively demonstrated when its volume fraction increases. When the Invar content is less than 50%, steel has a dominant effect on the mould's deformation. When the Invar volume fraction increases, its ability to resist deformation grows accordingly. This is demonstrated as higher bending degree. The serious situation occurs when Invar constitutes half of the mould. After that, the Invar fraction plays a leading part in the mould's deformation. When Invar volume fraction continually increases, the bending trend decreases. That is why the bend length change is less even in the same bending degree when the Invar content is higher than 50% compared to Invar content less than 50%, as shown in Figure 5-5 and Figure 5-6.

FEM analysis has also indicated that no bending value was less than in the 100% Invar case. That means the new mould's deformation will be a problem if

no effective solution was applied, as compared with the existing mould (100% Invar plan).

In addition, it can be seen from Figure 5-6 that in whole 11 trails the model's bend length (the above surface) is less than the pure steel case. The bend length change value is negative when the Invar content is between 50% to 80%. The reason is in the bending deformation process, Invar part is under internal stress at the interface. The inner stress results in bending and shrinkage on Invar's above surface. Invar's low CTE plays a more leading role in the whole model with the increasing Invar content. It is the reason that the bend length change value decreases when the Invar content increases until it reaches 70%. After that, the bend degree gradually decreases when the Invar content still increases. This is the reason that the bend length change value increases when the Invar content is between 70% to 100%.

7.2.2 Mould's stress analysis

FEM analysis showed that the inner stress is lower than yield stress in 9 trials except when the Invar content is 90%. The inner stress in the mould is 182Mpa, which is higher than the yield stress limitation 140Mpa when Invar content is 90%. It means that a plastic deformation process occurs and the mould cannot return back to the original shape.

In addition, in chapter 6, FEM analysis has checked that the inner stress is lower than yield stress value whatever parameter compensation has been applied. The parameter compensation method is useful in the typical female mould's deformation control.

It is noted that in Figure 4-15, the nickel content is less than 36% (nearly 30%) in Invar side (the first Invar layer). It means a wider scope of dilution happens when Ar+2.5% CO_2 is used compared with pure argon used. This situation gradually disappears in the subsequent deposit of Invar (almost 1or 2 layers). It can be seen from Figure 2-9 that nickel alloy's thermal expansion coefficient is larger than pure Invar when nickel's content is divided from 36%. Thus the CTE

at the interface is gradient with gradual change in distance from the interface. It will result in a gradient stress area at the interface.

In other words, because of the higher CTE in the diffusion area, it means the content of “steel” is slightly higher. For example, the original case is 20% of steel; in this situation the result of the mould’s bend angle and bend length change will be equal to more than 20% case (just a slight increase) in Figure 5-5 and Figure 5-6.

7.2.3 Effective way to control mould’s deformation

It can be clearly seen from Figure 5-5 and Figure 5-6 that the steel/Invar mould is not feasible because the bending deformation predicted is actually larger than pure Invar case.

To solve this problem, parameter compensation design method was introduced at the end of this thesis. To check the effectiveness and logic of the compensation algorithm, the most serious bending status was considered. That is when Invar accounted for the proportion of 50%. A numerical analysis result verifies that the mould’s bending deviation value is significantly decreased with a reduction of 96% compared to original dimension deviation.

Due to the time constraints, this phase did not contain experiments tests, real parts fabrication and the laser scanning approach. Future work is needed to improve the calculation of dimension deviation control.

Other ideas seem feasible to solve the bend deformation of bimetal mould; one of them is using a “Sandwich model”. That is Invar should be used as top and bottom part and steel as middle part, as shown in Figure 7-2. The key point in this proposal is both top and bottom Invar should have the same volume fraction. As a whole, the symmetrical mould will never bend upward or downward and only expansion will happen (correspondingly the surface will elongate when it is heated). In the future work to check whether this model is effective and how much the volume fraction ratio between each part should be carried out.

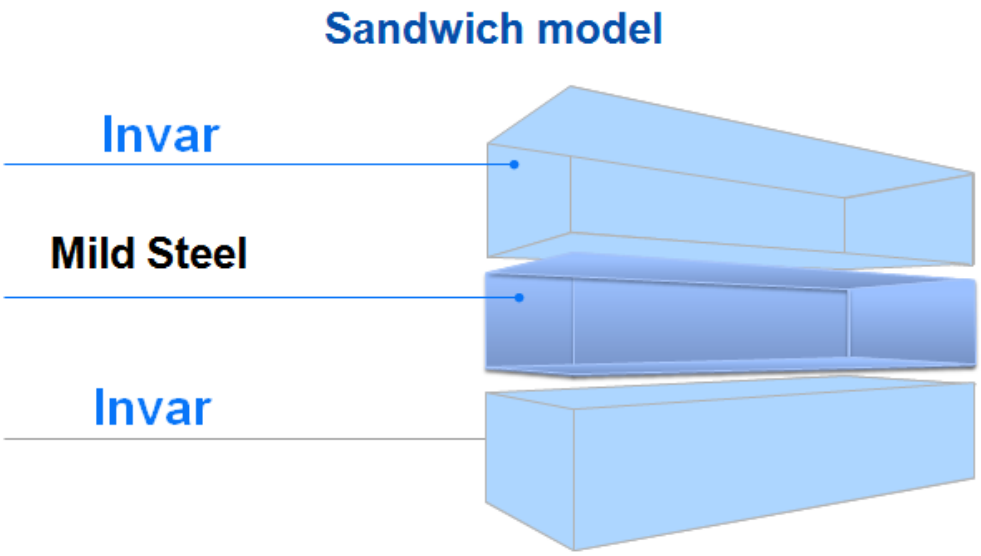

Figure 7-2 Sandwich model for bimetal mould

Another proposal is to find an alternative material which has a lower thermal expansion coefficient compared to mild steel in the chapter 5's model. A relatively lower thermal expansion coefficient material is likely to generate less bending. However, this material should have sufficient strength to bear the internal stress from the mould's bending deformation.

8 Conclusions

The project focused on the investigation of an alternative method to manufacture Invar moulds for composite component fabrication by WAAM technology to save costs for aero-industry.

The main conclusions are as follows:

1. Invar alloy has been successfully built on steel with a high integrity joint;
2. WAAM can be used for repairing an Invar mould because of the isotropy property of Invar deposit..
3. In this bimetal mould, the Invar content has a significant effect on the mould's thermal deformation; the mould made of pure Invar shows the minimum thermal deformation value.
4. The parameter compensation design approach is effective and logical for deformation control; and, using this method, the mould's deformation can be effectively controlled.

REFERENCES

Almeida, P. S. and Williams, S. (2010), "Innovative process model of Ti–6Al–4V additive layer manufacturing using cold metal transfer (CMT)", *Proceedings of the Twenty-first Annual International Solid Freeform Fabrication Symposium, University of Texas at Austin, Austin, TX, USA*.

BAKER, R. (1925), Method of making decorative articles, U.S. Patent No. 1,533,300. Washington, DC: U.S. Patent and Trademark Office.

Benyounis, K., Olabi, A. and Hashmi, M. (2005), "Effect of laser welding parameters on the heat input and weld-bead profile", *Journal of Materials Processing Technology,* vol. 164, pp. 978-985.

Cacciamani, G., De Keyzer, J., Ferro, R., Klotz, U., Lacaze, J. and Wollants, P. (2006), "Critical evaluation of the Fe–Ni, Fe–Ti and Fe–Ni–Ti alloy systems", *Intermetallics,* vol. 14, no. 10, pp. 1312-1325.

Cary, H. B. and Helzer, S. C. (1979), "*Modern welding technology*", University of Virginia.

Chen, J., Mehnen, J., Lockett, H. L. and Cranfield University. School of Applied Sciences (2012), *Hybrid design based on wire and arc additive manufacturing in the aircraft industry [electronic resource]*.

Chen, r. (2012), *Effectsof cladding heat input on TMCP steel pipes* (unpublished MSc Thesis thesis), Cranfield University.

Clark, D., Bache, M. and Whittaker, M. (2008), "Shaped metal deposition of a nickel alloy for aero engine applications", Journal of Materials Processing Technology, vol. 203, no. 1, pp. 439-448.

Corbacho, J., Suárez, J. and Molleda, F. (1998a), "Welding of invar Fe-36Ni alloy for tooling of composite materials", Welding international, vol. 12, no. 12, pp. 966-971.

Corbacho, J. L., Suárez, J. C. and Molleda, F. (1998b), "Grain coarsening and boundary migration during welding of invar Fe-36Ni alloy", Materials Characterization, vol. 41, no. 1, pp. 27-34.

da Costa Pépe, Nuno Vasco (2010), Advances in gas metal arc welding and application to corrosion resistant alloy pipes(Doctoral dissertation, Cranfield University).

Dong, C. (2003), *Dimension variation prediction and control for composites* (Doctoral dissertation, Florida State University).

EADS Deutschland GmbH (June 2004), *THE RESEARCH REQUIREMENTS OF THE TRANSPORT SECTORS TO FACILITATE AN INCREASED USAGE OF COMPOSITE MATERIALS,* Corporate Research Centre.

Elbit Systems Ltd. (2010), *Composite Technologies*, available at: http://www.elbitsystems.com/elbitmain/areain2.asp?parent=118&num=129&num2=129 (accessed 8th Oct. 2013).

Fessler, J., Nickel, A., Link, G., Prinz, F. and Fussell, P. (1997), "Functional gradient metallic prototypes through shape deposition manufacturing", Proceedings of the solid freeform fabrication symposium, SME, pp. 521.

Fronius Ltd. (2005), *CMT: Cold Metal Transfer*, available at: www.digitalweldingsolutions.com (accessed 1st March, 2013).

Haidar, J. and Lowke, J. J. (1997), "Effect of CO< sub> 2</sub> shielding gas on metal droplet formation in arc welding", Plasma Science, IEEE Transactions on, vol. 25, no. 5, pp. 931-936.

HE, Y., CAI, W. and ZHAO, P. (2006), "Moderate-temperature Cured Composite Moulds Used for Manufacturing Autoclaves [J]", Fiber Composites, vol. 1, pp. 016.

Hoa, S. V. (2009), Principles of the manufacturing of composite materials, DES tech Publications, Inc.

Hsu, C. and Soltis, P. (2002), "Heat input comparison of STT vs. short-circuiting and pulsed GMAW vs. CV processes.", 6 th International Conference: Trends in Welding Research, pp. 369.

Huang, g. (2011), "Investigation about Advanced mould the Invar manufacturing technology", Advances in Aeronautical Science and Engineering, no. 4, pp. 485-486.

Huebner, K. H., Dewhirst, D. L., Smith, D. E. and Byrom, T. G. (2008), The finite element method for engineers, John Wiley & Sons.

Hughes, T. J. and Hinton, E. (1986), Finite element methods for plate and shell structures, Pineridge Press International.

Jain, L. K., Hou, M., Ye, L. and Mai, Y. (1998), "Spring-in study of the aileron rib manufactured from advanced thermoplastic composite", Composites Part A: Applied Science and Manufacturing, vol. 29, no. 8, pp. 973-979.

Kussmaul, K., Schoch, F. and Luckow, H. (1983), "High Quality Large Components' Shape Welded'by a SAW Process".

Luling, Li Guidong Zhou Laishui An and Xiaojing, T. C. C. (2010), "A DESIGN METHOD OF THE COMPOSITES PART MOULD BASED ON THE PART DEFORMATION DURING THE MANUFACTURE PROCESS", 18th International conference on composites or Nano-Engineering, ICCE-18.

Lyttle, K. (2005), *Simplifying shielding gas selection*, available at: http://www.thefabricator.com/article/consumables/simplifying-shielding-gas-selection (accessed 1st March, 2013).

Mattias, L. (2011), *Additive-Layer-Manufacturing by CMT using Cu97Si3 wire on steel* (unpublished MSc Thesis thesis), Cranfield University, U.K.

Otsuka, T. (2006), "Evolution of an LNG terminal: Senboku terminal of Osaka GAS", *23rd World Gas Conference, Amsterdam,* pp. 1362.

Owusu-Ofori, S. P., Pai, D. M. and Sadler, R. L. (1997), *Research in Advanced Materials Processing and Process Modeling.*

Pierre, J. (2009), *3D Printer Technology – Animation of layering*, available at: http://www.createitreal.com/index.php/technology/process (accessed 31st January 2013).

PK Mallick (1993), *Fiber-reinforced composites: materials, manufacturing, and design,* CRC press.

Process Fab Inc. (2007), *Invar Mold*, available at: http://www.processfab.com/spv-43.aspx (accessed 9th Oct. 2013).

RobotWorx Co. (2009), *TIG vs. MIG Welding - What's the Difference?*, available at: http://www.used-robots.com/articles/viewing/tig-vs-mig-welding-what-s-the-difference (accessed 1st March 2013).

Saito, H. (1978), *Physics and applications of invar alloys,* Maruzen.

Sequeira Almeida, P. M. (2012), "Process control and development in wire and arc additive manufacturing", Cranfield University, U.K.

Shanping, L., Hidetoshi, F. and Kiyoshi, N. (2005), "Effects of CO2 shielding gas additions and welding speed on GTA weld shape", *Journal of Materials Science,* vol. 40, no. 9-10, pp. 2481-2485.

Shao, k. (2009), *Composite tooling deformation analysis* (unpublished Master's thesis thesis), Nanjing University of Aeronautics and Astronautics, China.

Sherman, L.M., (2007), *A whole new dimension – Rich homes can afford 3D printers*, The Economist, U.K.

Shin, K., Natu, H., Dutta, D. and Mazumder, J. (2003), "A method for the design and fabrication of heterogeneous objects", *Materials & Design,* vol. 24, no. 5, pp. 339-353.

Skiba, T., Baufeld, B. and Van der Biest, O. (2011), "Shaped metal deposition of 300M steel", *Proceedings of the Institution of Mechanical Engineers, Part B: Journal of Engineering Manufacture,* vol. 225, no. 6, pp. 831-839.

Smock, D. (2010), "Additive Systems Slash Aircraft Materials Costs", *Design News,* vol. 65, no. 6, pp. 6-7.

Sproule, K. (1990), "Nickel and its Uses", *Metals Handbook,* vol. 1, pp. 1114.

Subramaniam, S. and White, D. (2001), "Effect of shield gas composition on surface tension of steel droplets in a gas-metal-arc welding arc", *Metallurgical and materials transactions B,* vol. 32, no. 2, pp. 313-318.

Takehiko, E. (2006), *Realization of invar alloy LNG piping*, available at: http://www.igu.org/html/wgc2003/WGCpdffiles/10325_1045211427_4649_1.pdf (accessed 9th Oct. 2013).

Tom Moore (6 Dec. 2012), *Delta Air Lines takes off with 40 Bombardier jetliners*, available at: http://www.themanufacturer.com/articles/delta-air-lines-takes-off-with-40-bombardier-jetliners/ (accessed 8th Oct. 2013).

Ujiie, A. (1972), *METHOD OF CONSTRUCTING SUBSTANTIALLY CIRCULAR CROSS-SECTION VESSEL BY WELDING, U.S. Patent No. 3,665,143*. Washington, DC: U.S. Patent and Trademark Office.

University of Bath (08 July 2004), *COMPOSITE MATERIALS*, available at: http://people.bath.ac.uk/ck258/new%20materials%20documents/Composite%20materials.htm (accessed 8th Oct. 2013).

University of Tennessee - Knoxville (2010), *Composite molding*, available at: http://reformation.utk.edu/fabrication/composite-molding/ (accessed 9th Oct. 2013).

Varlowe Ltd. (2006), *Gas Shielded Arc Welding - GMAW - GTAW(TIG)*, available at: http://www.corrosionist.com/gas_shielded_arc_welding_gmaw.htm (accessed 1st March 2013).

Wang, F., Williams, S., Colegrove, P. and Antonysamy, A. A. (2013), "Microstructure and Mechanical Properties of Wire and Arc Additive Manufactured Ti-6Al-4V", *Metallurgical and Materials Transactions A,* vol. 44, no. 2, pp. 968-977.

Wassermann, E. (1991), "The invar problem", *Journal of Magnetism and Magnetic Materials,* vol. 100, no. 1, pp. 346-362.

Wei, P. and Chung, F. (2000), "Unsteady Marangoni flow in a molten pool when welding dissimilar metals", *Metallurgical and Materials Transactions B,* vol. 31, no. 6, pp. 1387-1403.

Wisconsin Wire Works, I. (2005), *Dissimilar metals*, available at: http://www.wisconsinwireworks.com/dissimilar_metals.html (accessed 8th August, 2013).

Yang, D. (2010), *Additive manufacture*, available at: http://additivemanufacturing.com/basics/ (accessed 7th September, 2013).

APPENDICES

Appendix A Material certification of Invar

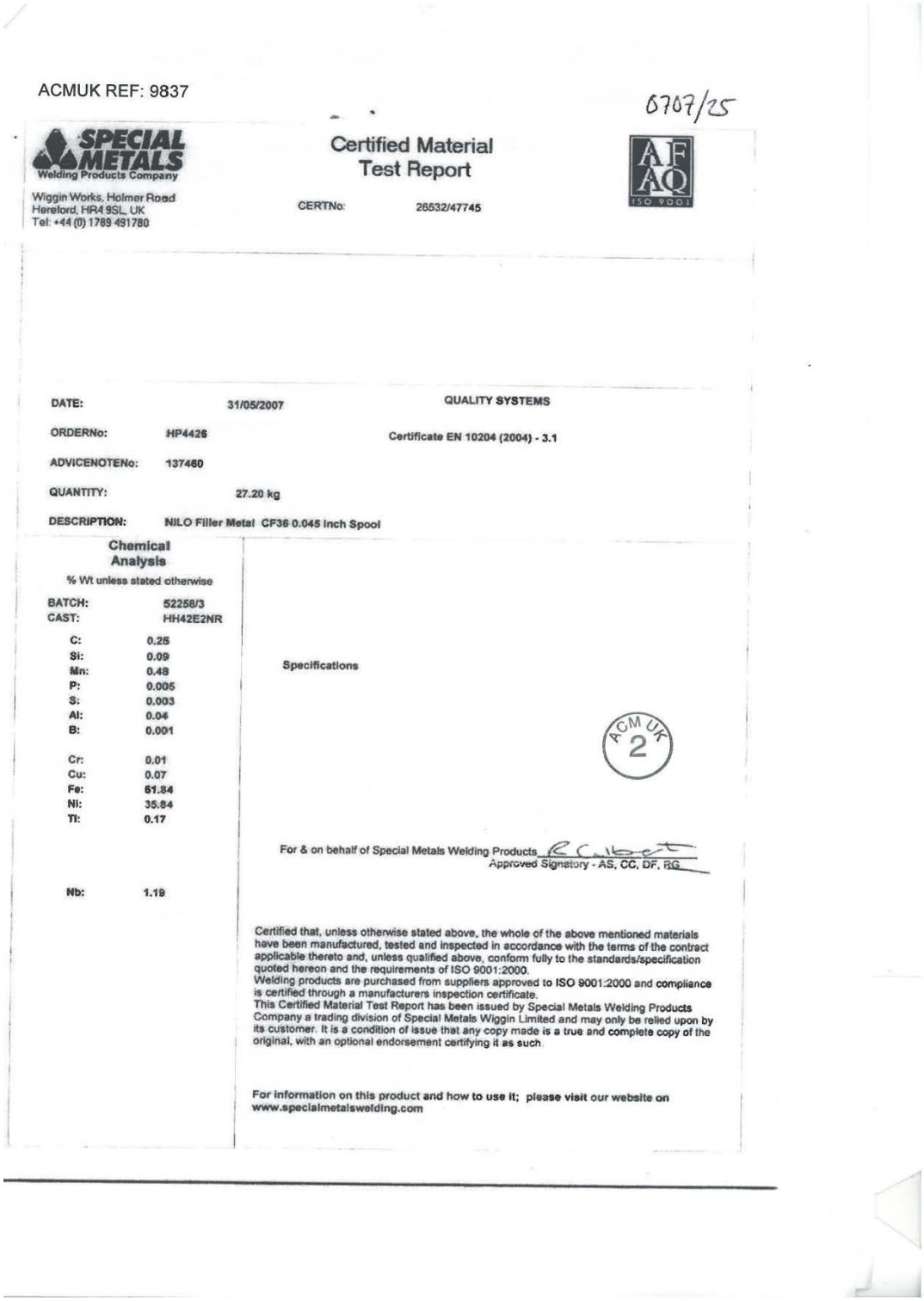

ACMUK REF: 9837

0707/25

SPECIAL METALS
Welding Products Company

Wiggin Works, Holmer Road
Hereford, HR4 9SL, UK
Tel: +44 (0) 1789 491780

Certified Material Test Report

CERTNo: 26532/47745

AFAQ ISO 9001

DATE: 31/05/2007

QUALITY SYSTEMS

ORDERNo: HP4426

Certificate EN 10204 (2004) - 3.1

ADVICENOTENo: 137460

QUANTITY: 27.20 kg

DESCRIPTION: NILO Filler Metal CF36 0.045 inch Spool

Chemical Analysis

% Wt unless stated otherwise

BATCH:	52258/3
CAST:	HH42E2NR
C:	0.25
Si:	0.09
Mn:	0.48
P:	0.005
S:	0.003
Al:	0.04
B:	0.001
Cr:	0.01
Cu:	0.07
Fe:	61.84
Ni:	35.84
Ti:	0.17
Nb:	1.19

Specifications

ACM UK 2

For & on behalf of Special Metals Welding Products
Approved Signatory - AS, CC, DF, RG

Certified that, unless otherwise stated above, the whole of the above mentioned materials have been manufactured, tested and inspected in accordance with the terms of the contract applicable thereto and, unless qualified above, conform fully to the standards/specification quoted hereon and the requirements of ISO 9001:2000.
Welding products are purchased from suppliers approved to ISO 9001:2000 and compliance is certified through a manufacturers inspection certificate.
This Certified Material Test Report has been issued by Special Metals Welding Products Company a trading division of Special Metals Wiggin Limited and may only be relied upon by its customer. It is a condition of issue that any copy made is a true and complete copy of the original, with an optional endorsement certifying it as such.

For information on this product and how to use it; please visit our website on www.specialmetalswelding.com

Figure A-1 Certification of Invar material

Appendix B Dog-bone specifications

All dog-bone samples were machined in accordance to the dimension below:

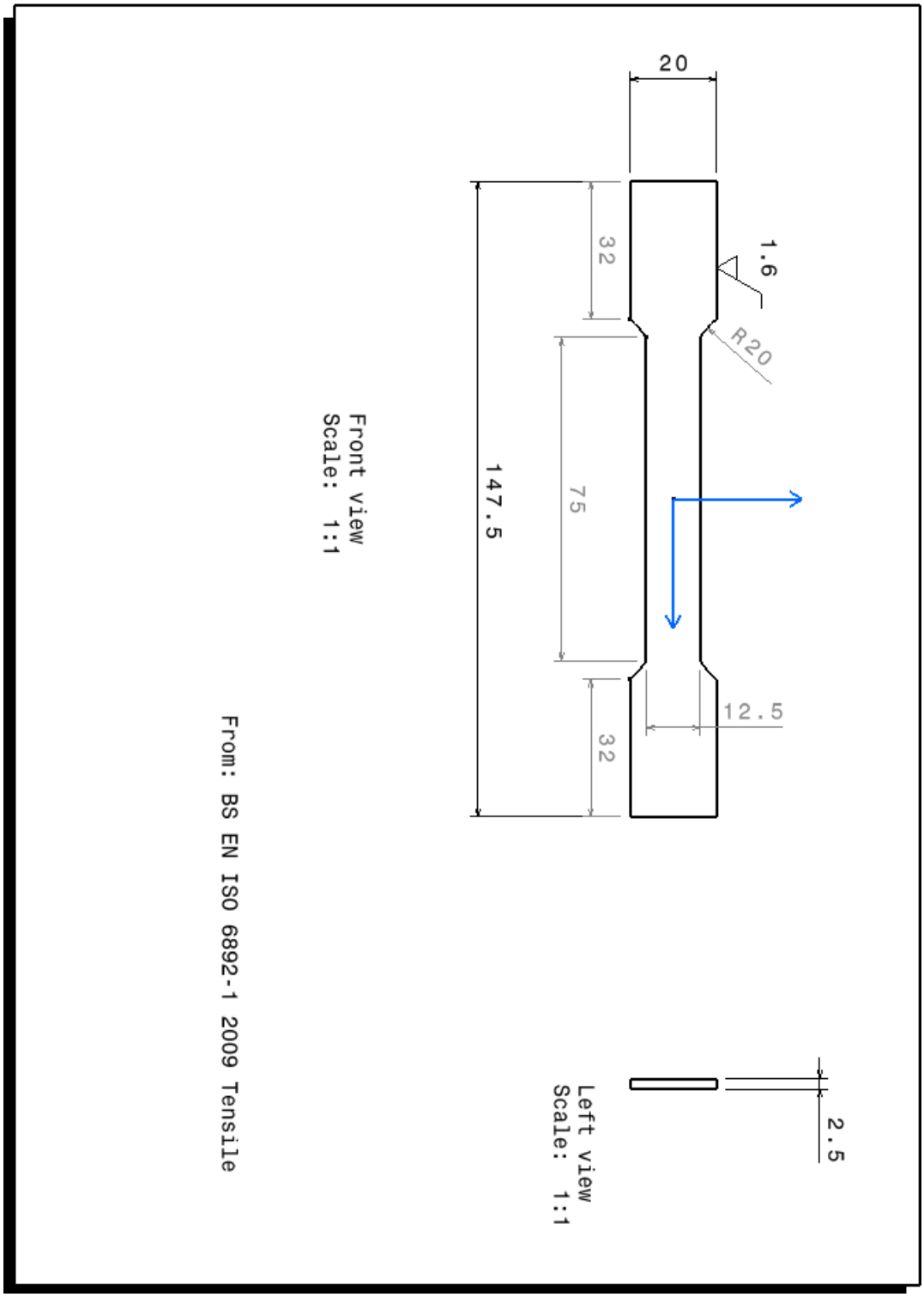

Figure B-1 Dog-bone sample dimension

Appendix C Dog-bone specifications

C.1 SEM image at the interface, shielding gas：Argon

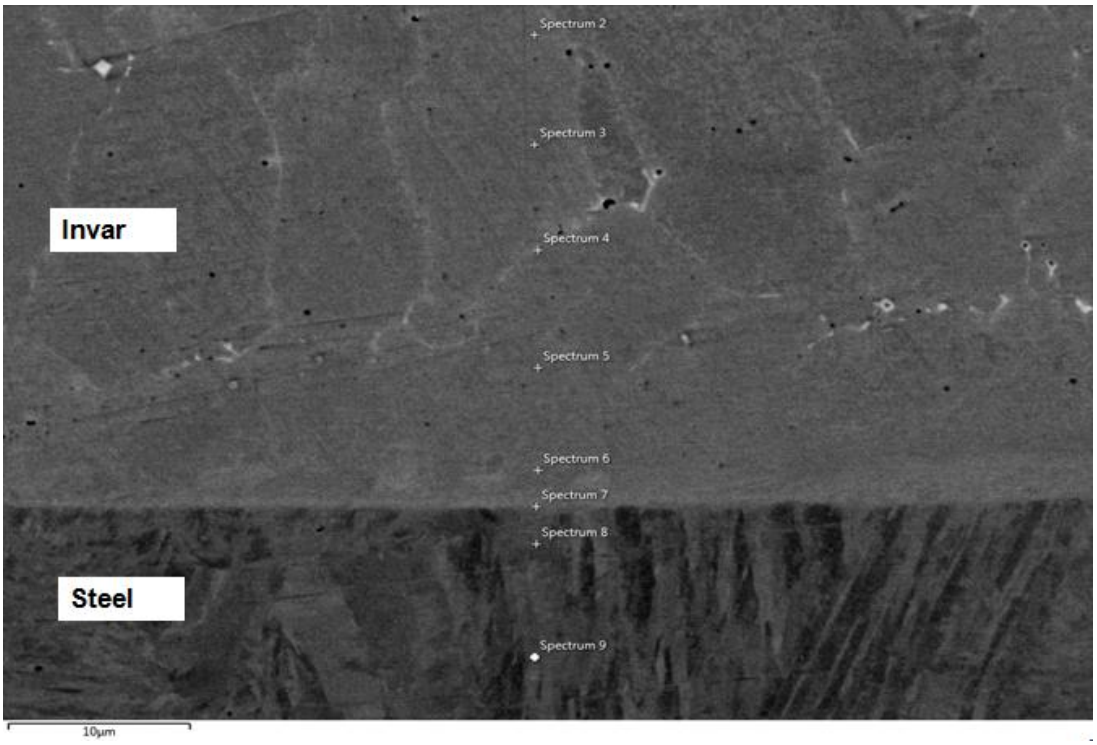

Figure C- 1 SEM image of Invar-steel sample

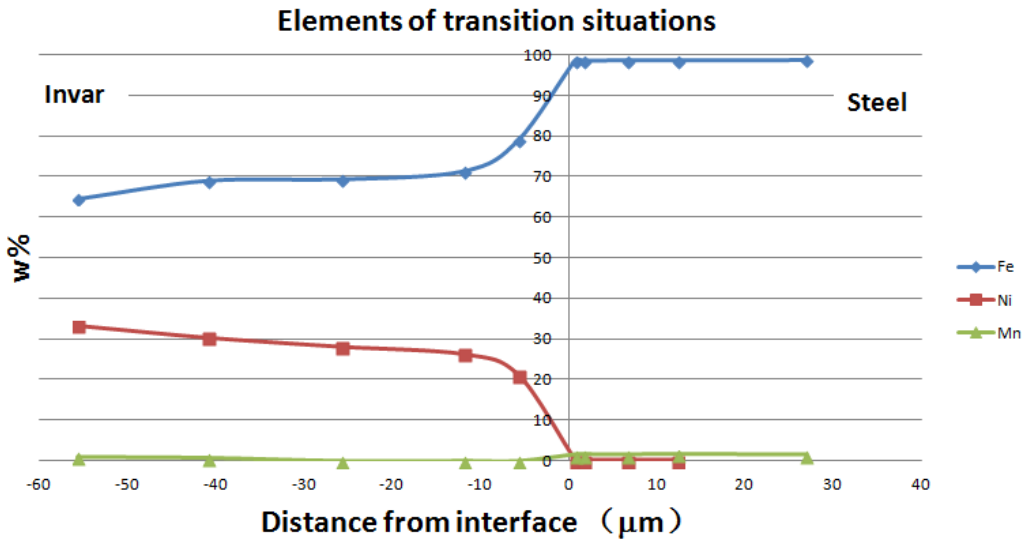

Figure C- 2 Composition of Fe and Nickel versus location for a graded interface between Invar and steel

C.2 SEM image at the interface，shielding gas：Ar+2.5%CO2

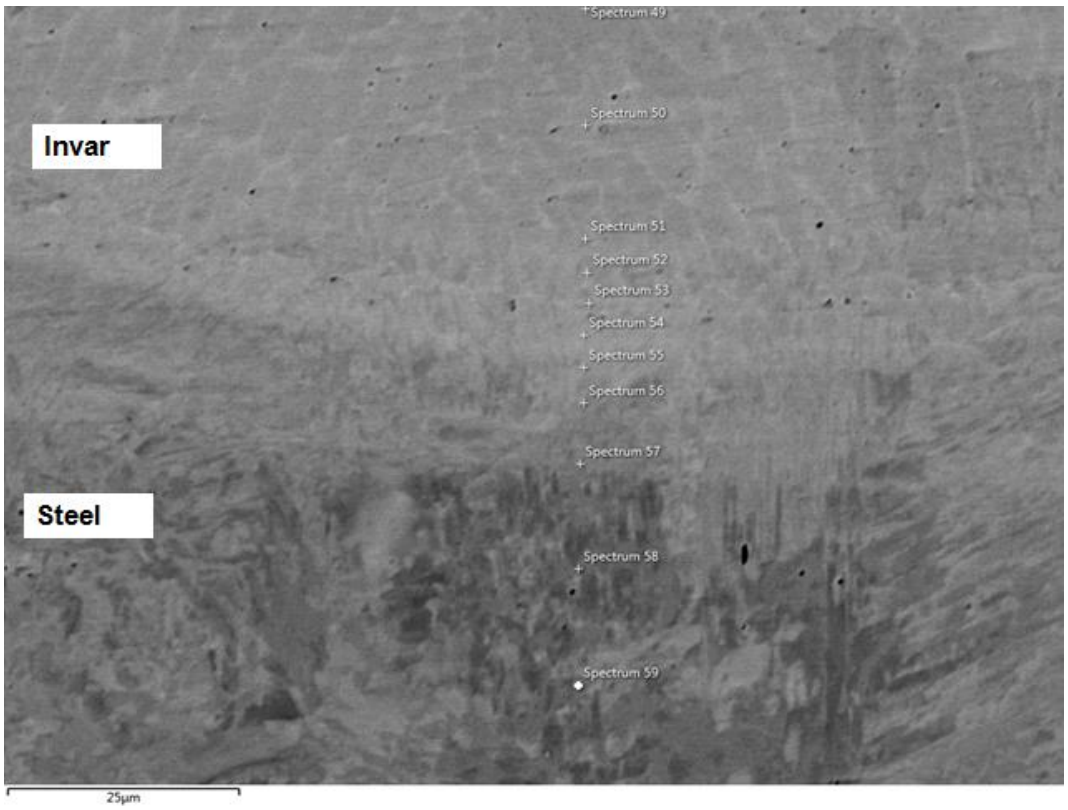

Figure C- 3 SEM image of Invar-steel sample

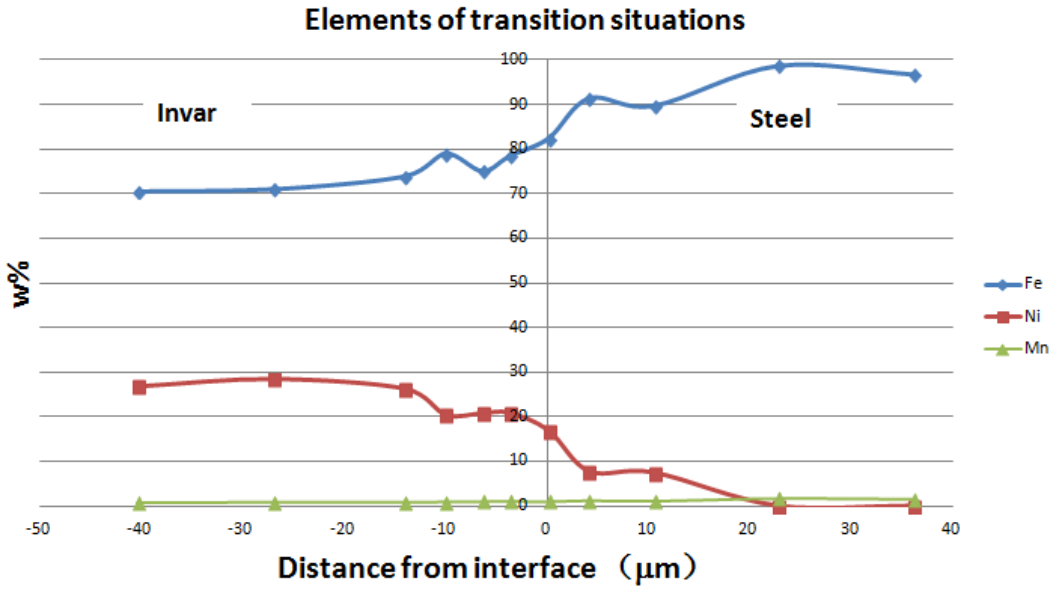

Figure C- 4 Composition of Fe and Nickel versus location for a graded interface between Invar and steel

Appendix D Dog-bone specifications

D.1 Invar –steel structure wall

D.1.1 Shielding gas of Argon for Invar part

Figure D- 1 Invar-steel wall, shielding gas of Argon; Invar 35 layers, steel 40 layers (Invar part waviness is higher due to less effective protection)

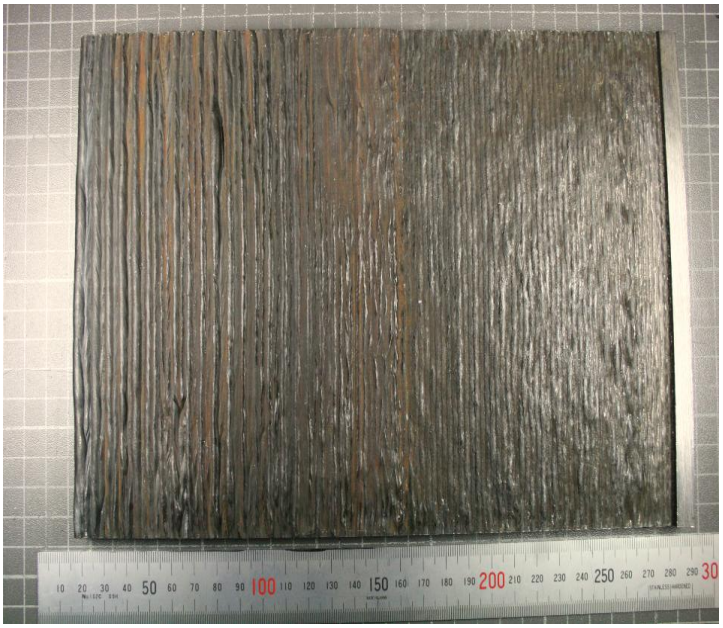

Figure D- 2 Image of Invar-steel wall cut from the substrate

D.1.2 Shielding gas of Argon+2.5%CO2 for Invar part

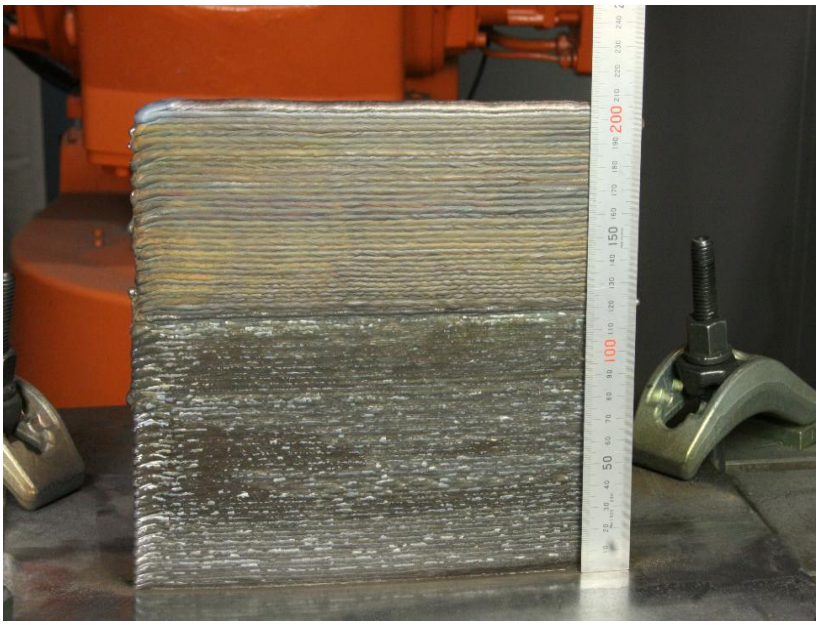

Figure D- 3 Invar-steel wall, shielding gas of Argon+2.5%CO2;

Invar 35 layers, steel 40 layers

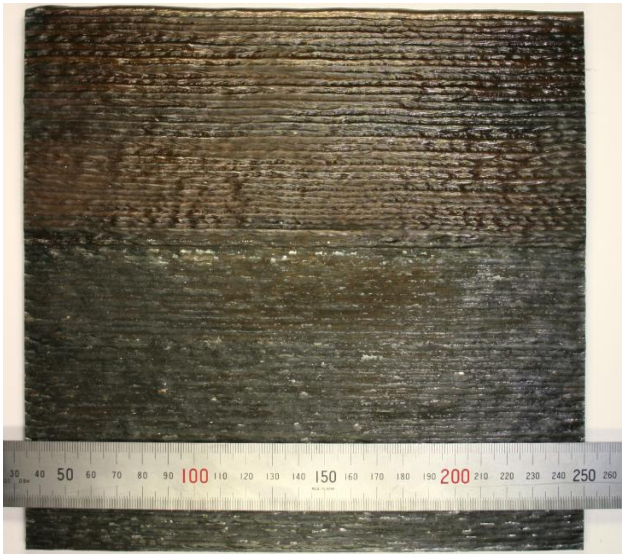

Figure D- 4 Image of Invar-steel wall cut from the substrate

D.2 Invar structure wall

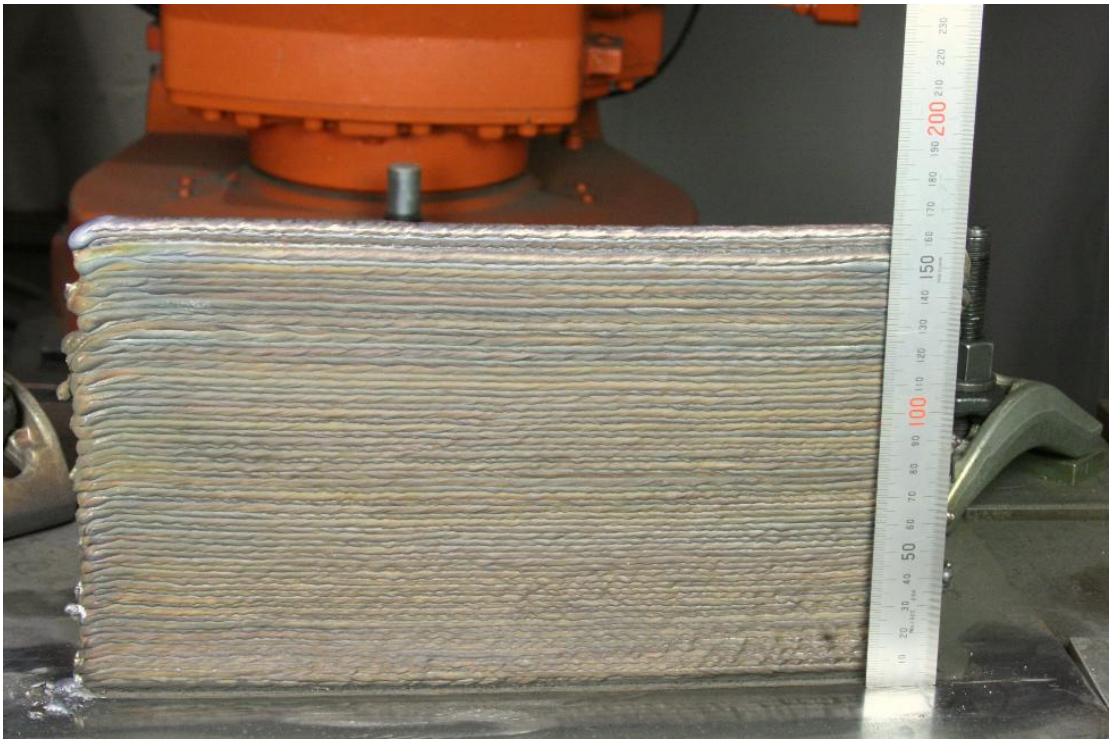

Figure D- 5 Invar-steel wall; Invar 65 layers

Figure D- 6 Image of Invar wall cut from the substrate

Appendix E FEM analysis

E.1 Rectangular models

E.1.1 Invar content =0%

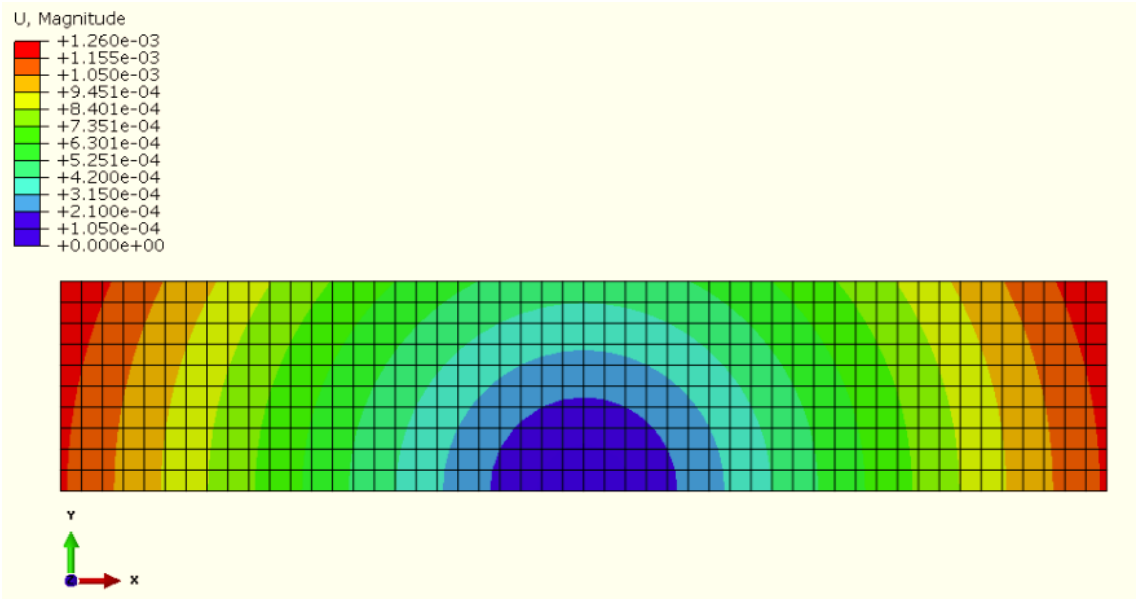

Figure E-1 Strain contours of the deformed shape, Invar content =0%, deformation scale factor=40, unit: m.

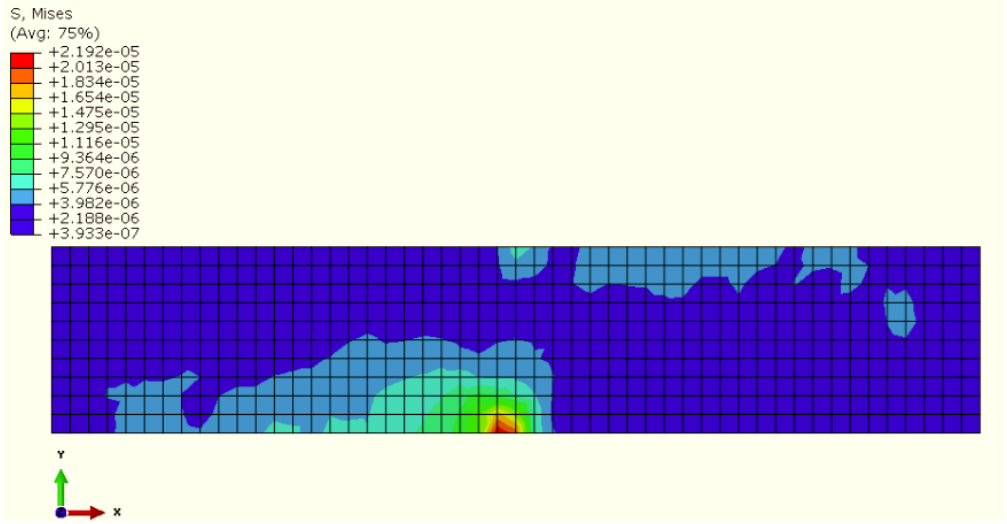

Figure E-2 Stress distribution diagram of the deformed mould, Invar content =0%, deformation scale factor=40, unit: Pa

E.1.2 Invar content =10%

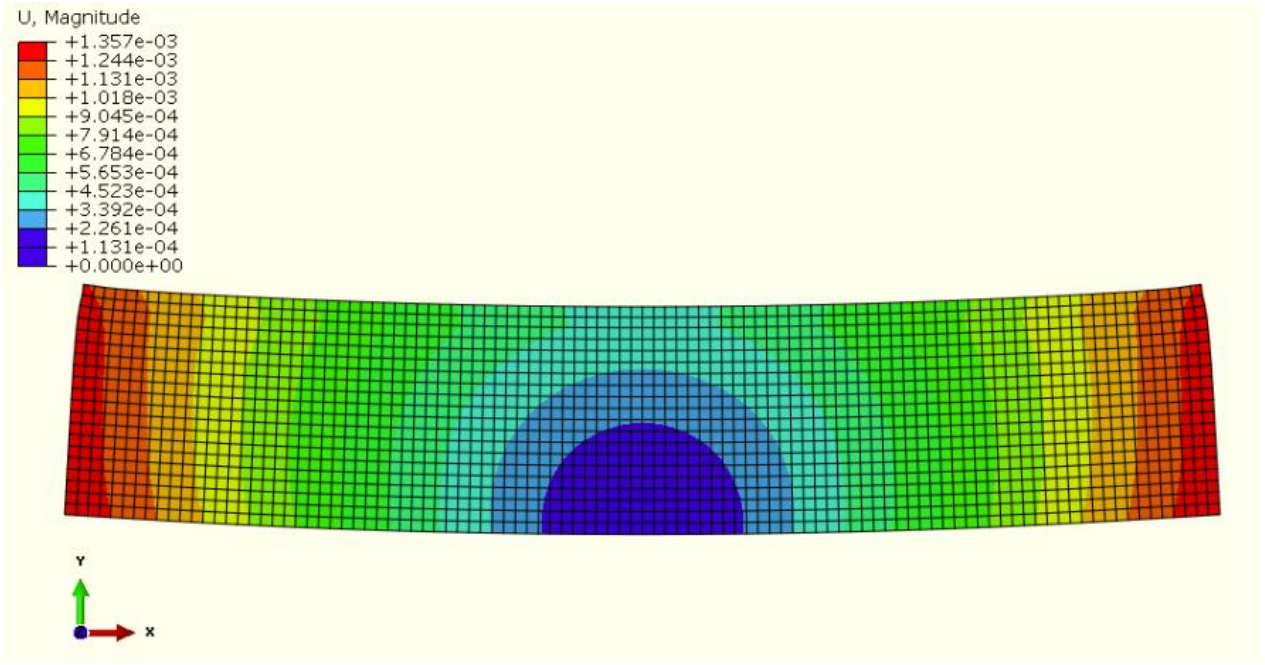

Figure E-3 Strain contours of the deformed shape, Invar content =10%, deformation scale factor=40, unit: m.

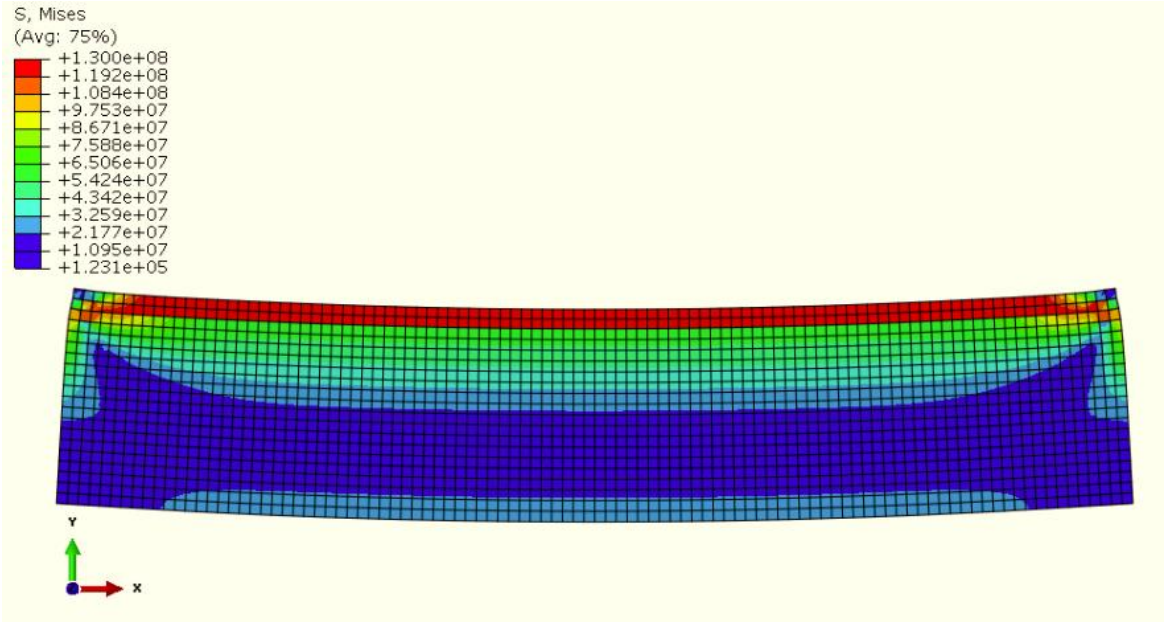

Figure E-4 Stress distribution diagram of the deformed mould, Invar content =10%, deformation scale factor=40, unit: Pa

E.1.3 Invar content =20%

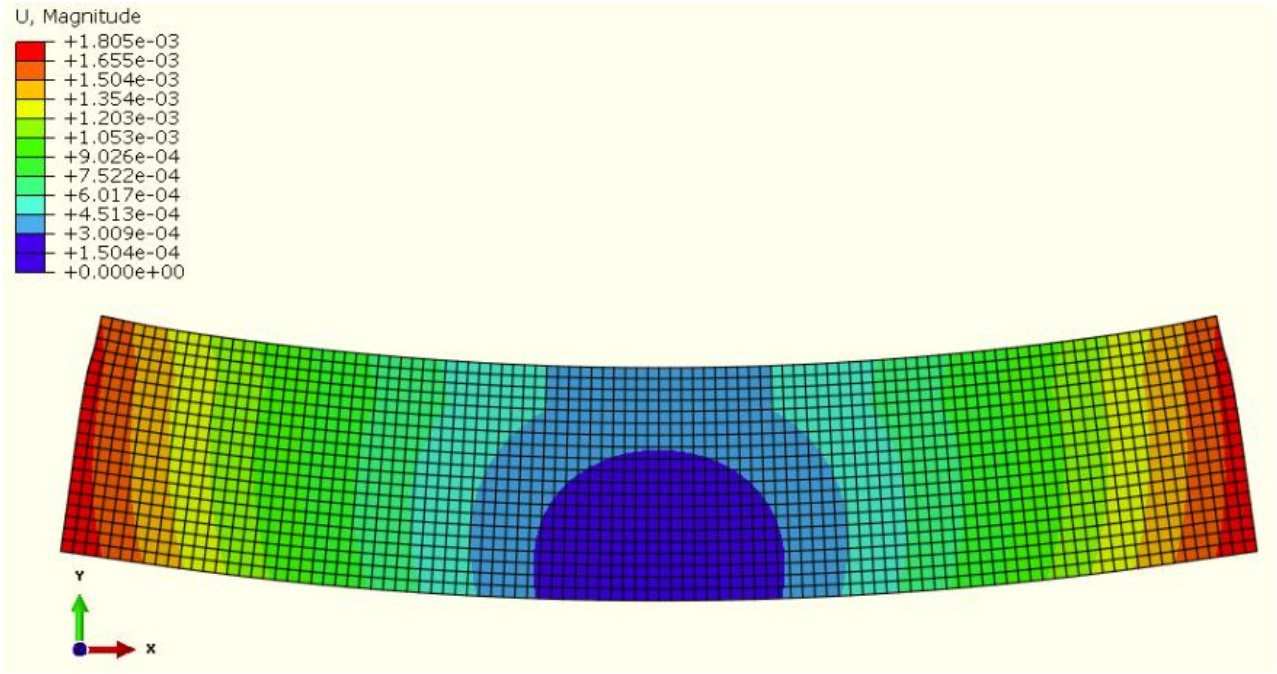

Figure E-5 Strain contours of the deformed shape, Invar content =20%, deformation scale factor=40, unit: m.

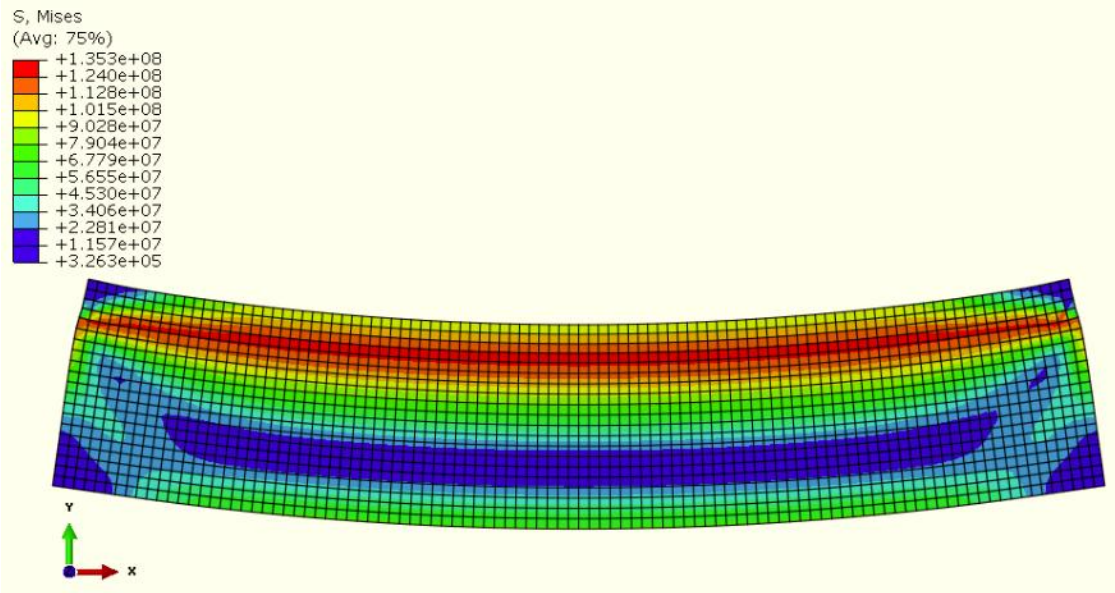

Figure E-6 Stress distribution diagram of the deformed mould, Invar content =20%, deformation scale factor=40, unit: Pa

E.1.4 Invar content =30%

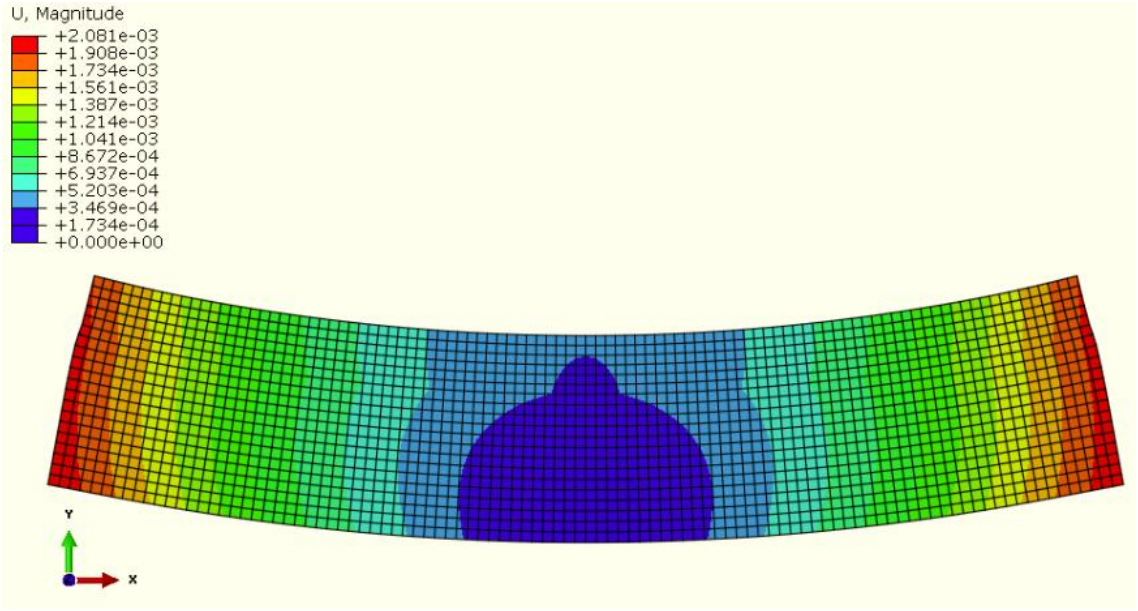

Figure E-7 Strain contours of the deformed shape, Invar content =30%, deformation scale factor=40, unit: m.

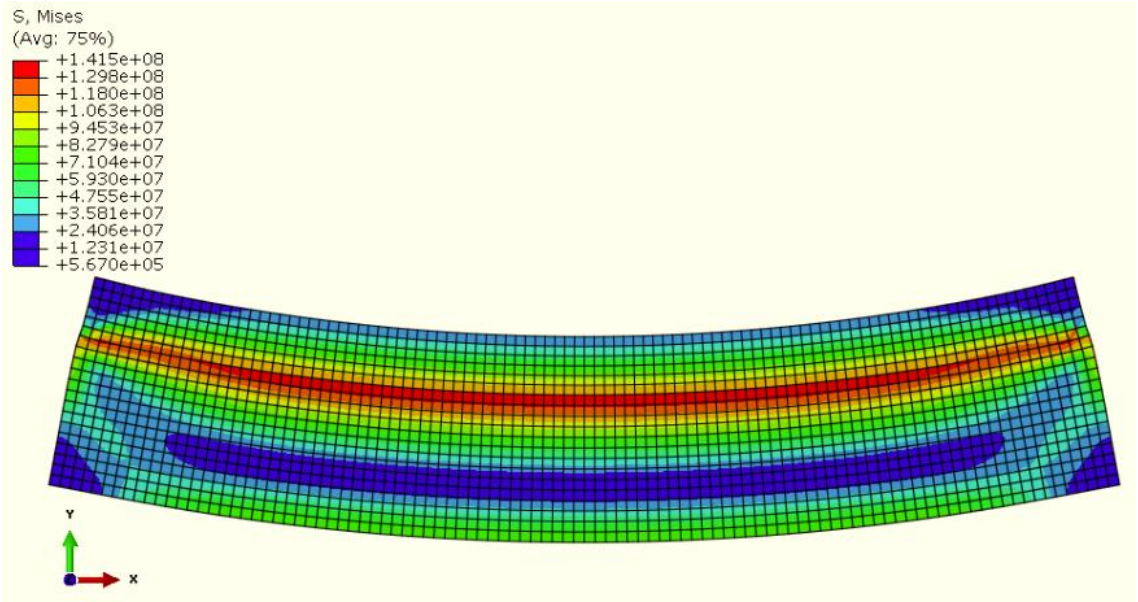

Figure E-8 Stress distribution diagram of the deformed mould, Invar content =30%, deformation scale factor=40, unit: Pa

E.1.5 Invar content =40%

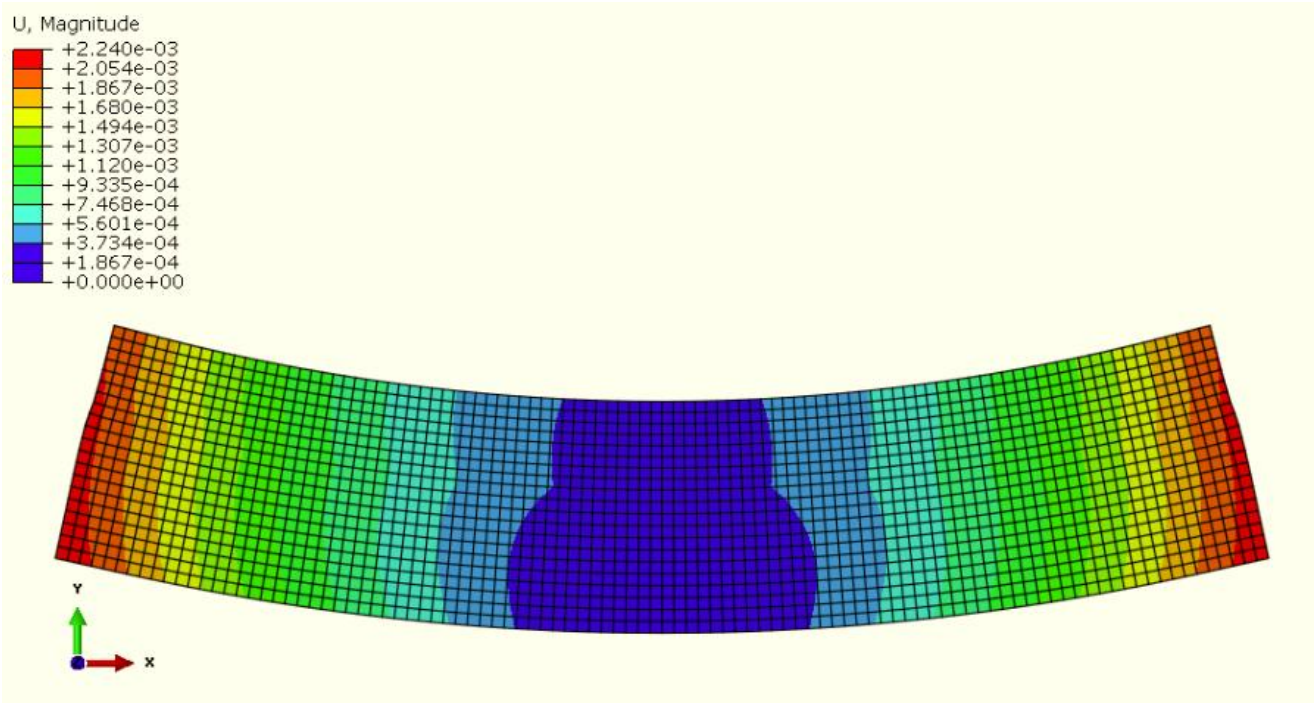

Figure E-9 Strain contours of the deformed shape, Invar content =40%, deformation scale factor=40, unit: m.

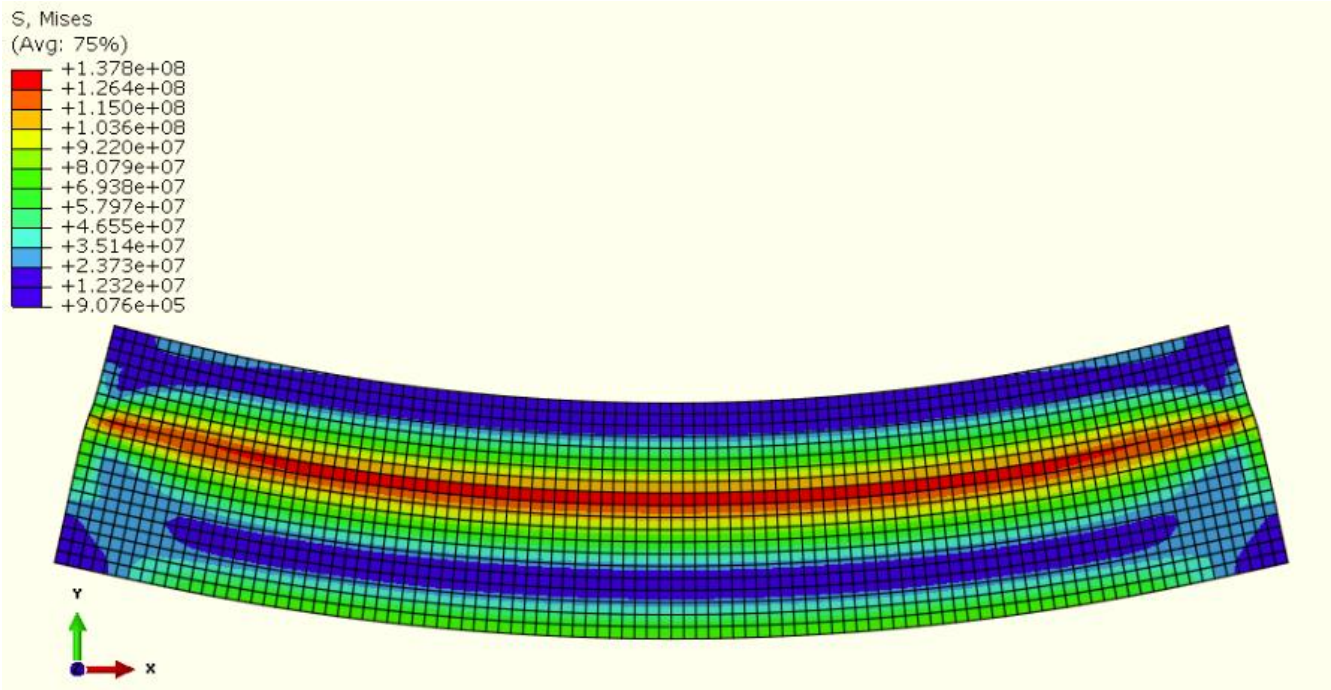

Figure E-10 Stress distribution diagram of the deformed mould, Invar content =40%, deformation scale factor=40, unit: Pa

E.1.6 Invar content =50%

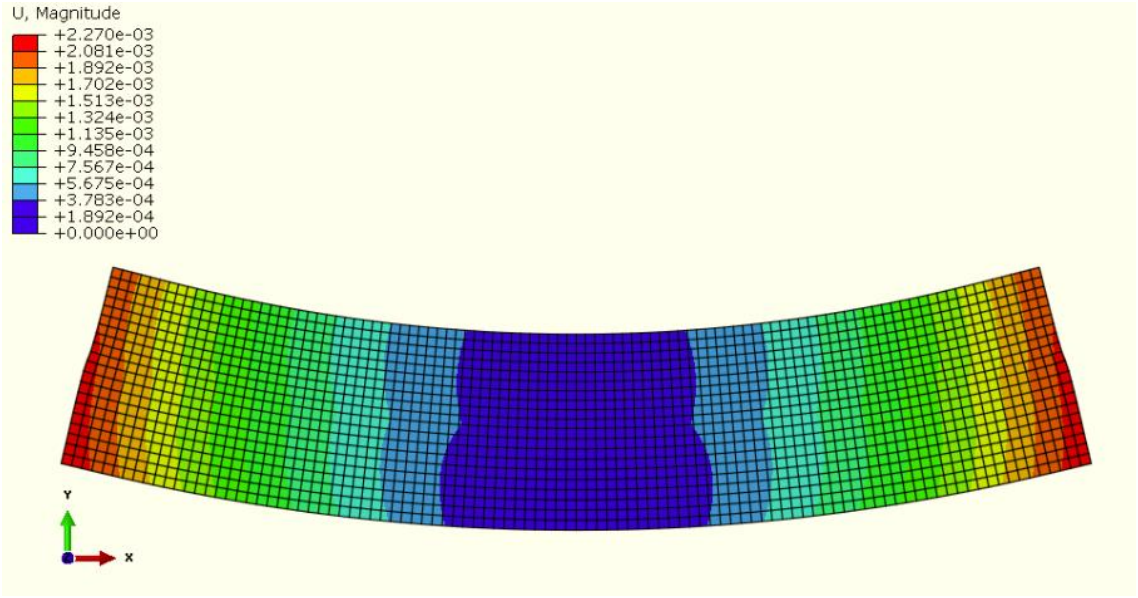

Figure E-11 Strain contours of the deformed shape, Invar content =50%, deformation scale factor=40, unit: m.

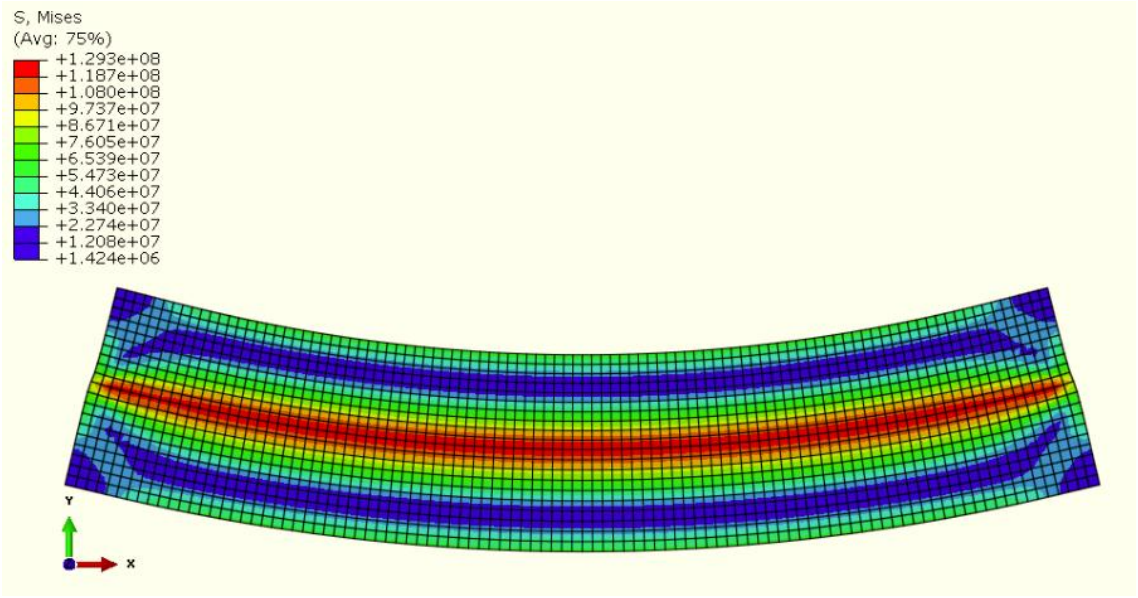

Figure E-12 Stress distribution diagram of the deformed mould, Invar content =50%, deformation scale factor=40, unit: Pa

E.1.7 Invar content =60%

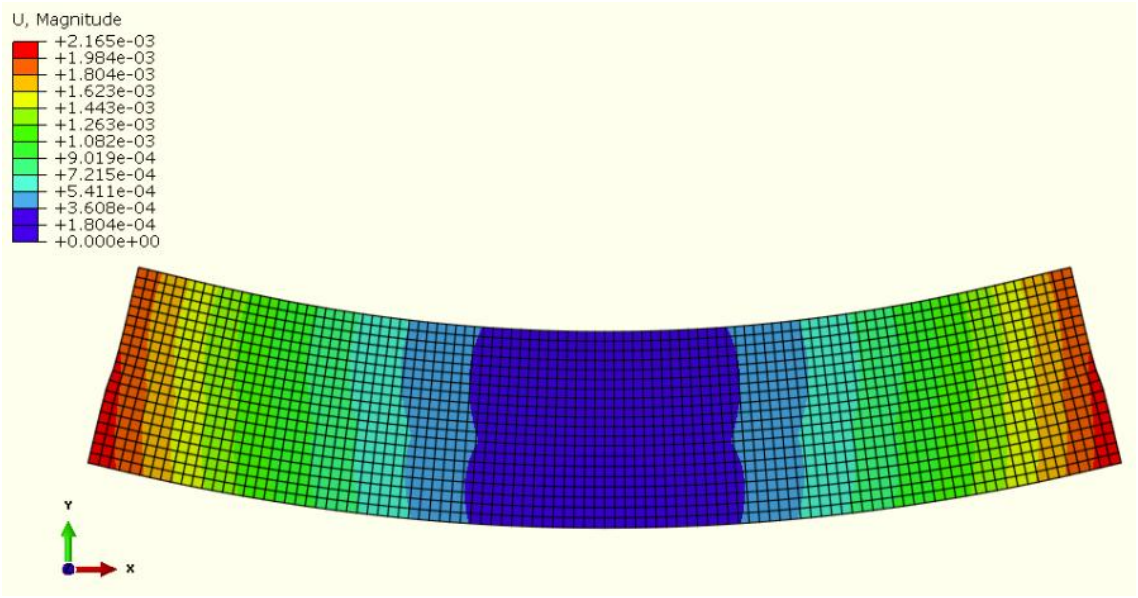

Figure E-13 Strain contours of the deformed shape, Invar content =60%, deformation scale factor=40, unit: m.

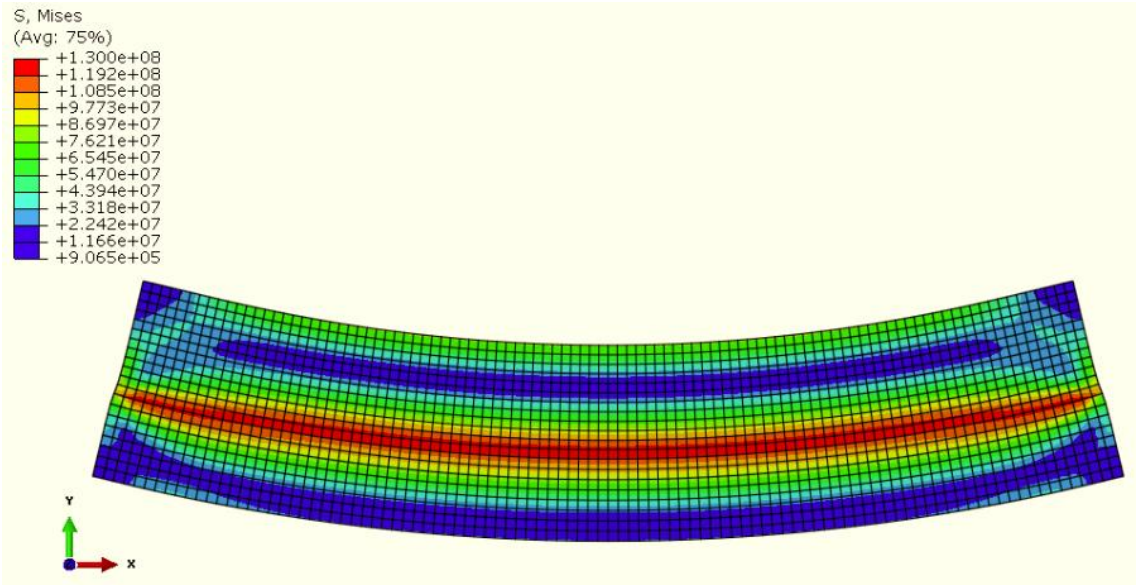

Figure E-14 Stress distribution diagram of the deformed mould, Invar content =50%, deformation scale factor=40, unit: Pa

E.1.8 Invar content =70%

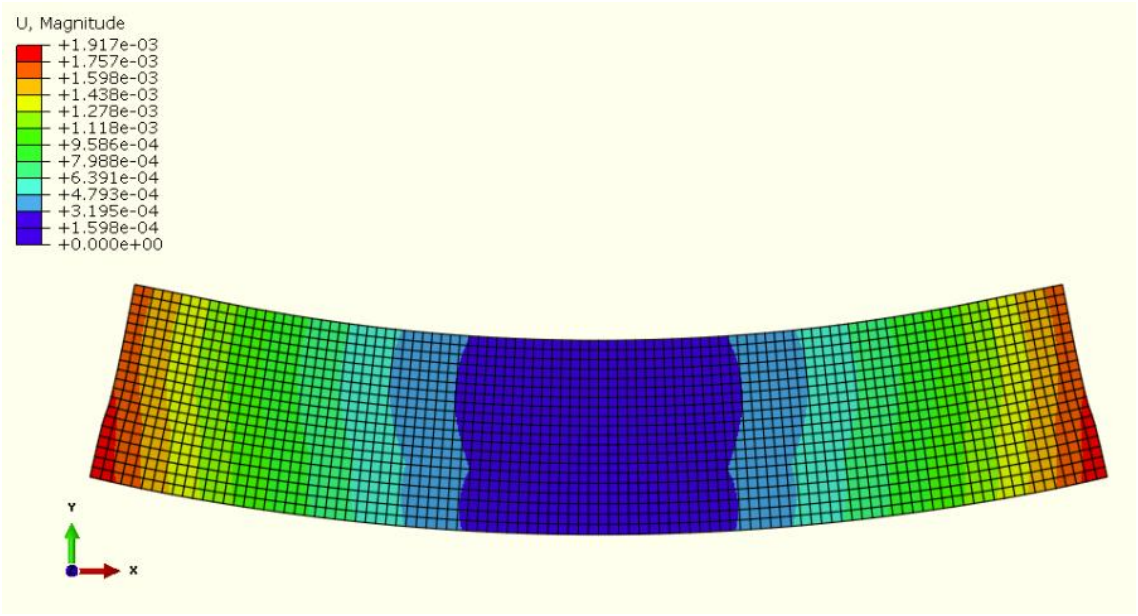

Figure E-15 Strain contours of the deformed shape, Invar content =70%, deformation scale factor=40, unit: m.

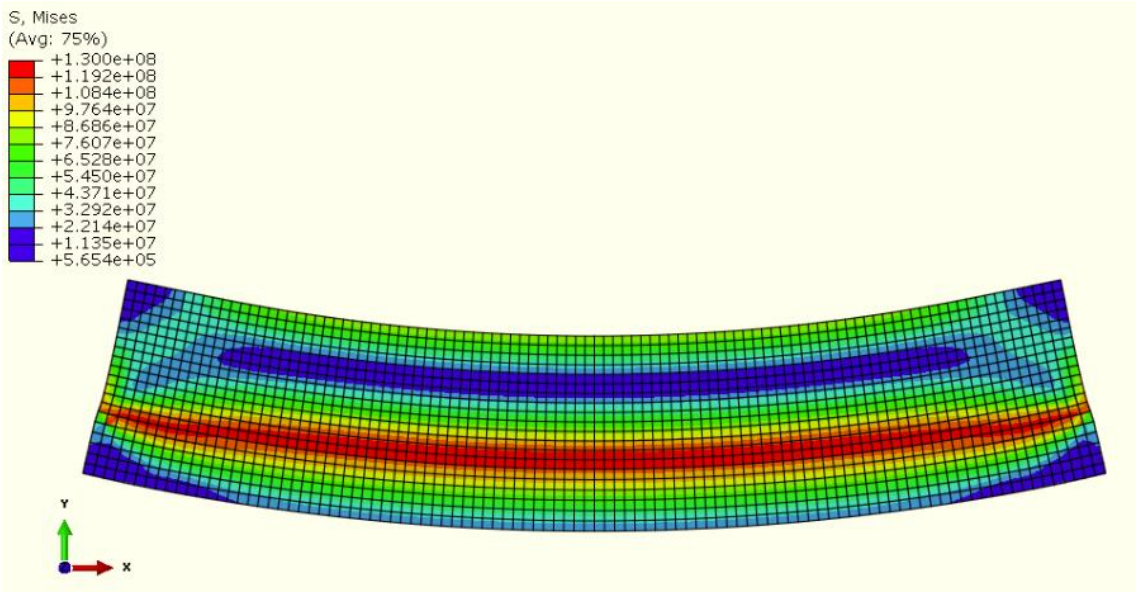

Figure E-16 Stress distribution diagram of the deformed mould, Invar content =50%, deformation scale factor=40, unit: Pa

E.1.9 Invar content =80%

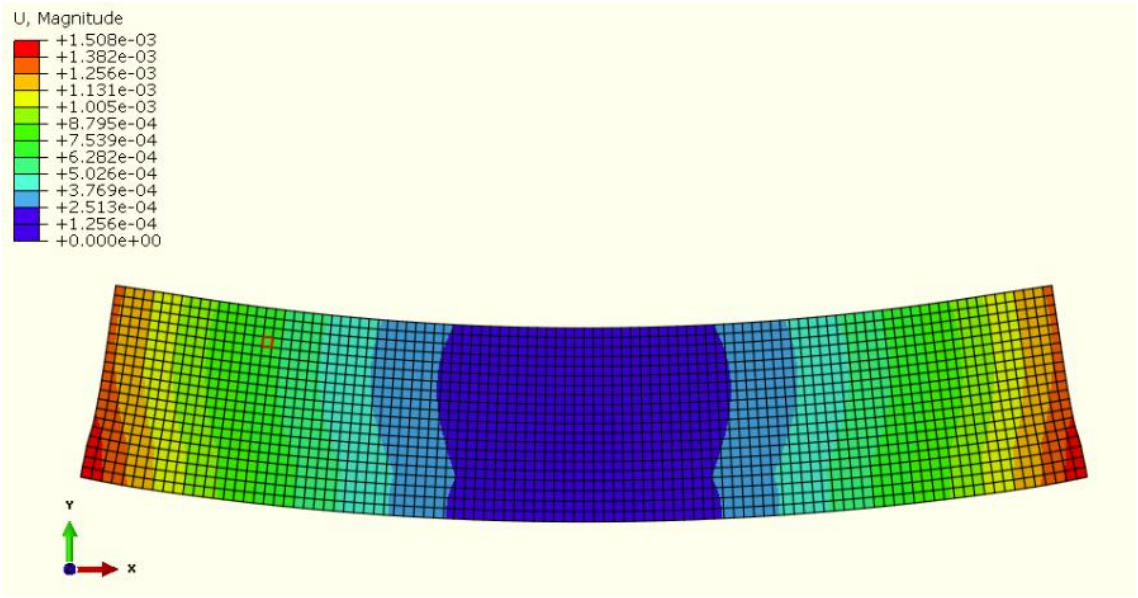

Figure E-17 Strain contours of the deformed shape, Invar content =80%, deformation scale factor=40, unit: m.

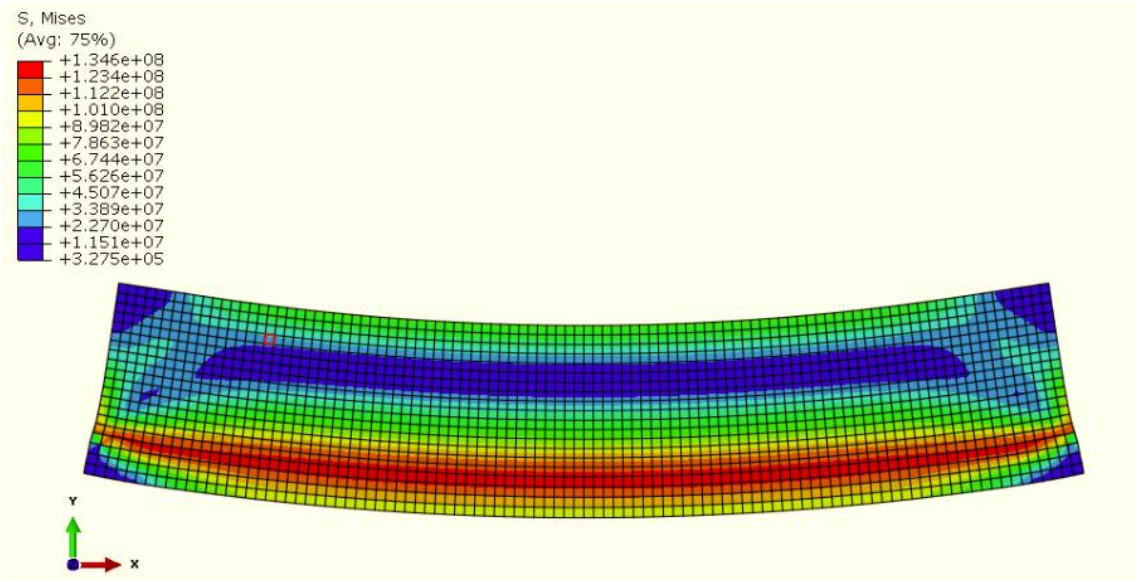

Figure E-18 Stress distribution diagram of the deformed mould, Invar content =50%, deformation scale factor=40, unit: Pa

E.1.10 Invar content =90%

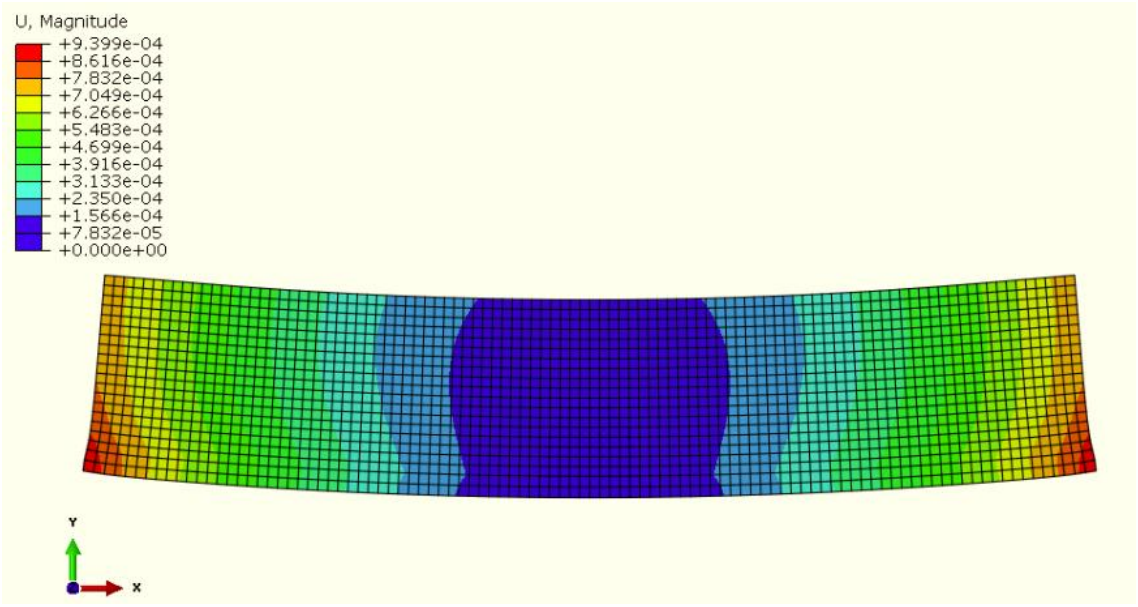

Figure E-19 Strain contours of the deformed shape, Invar content =90%, deformation scale factor=40, unit: m.

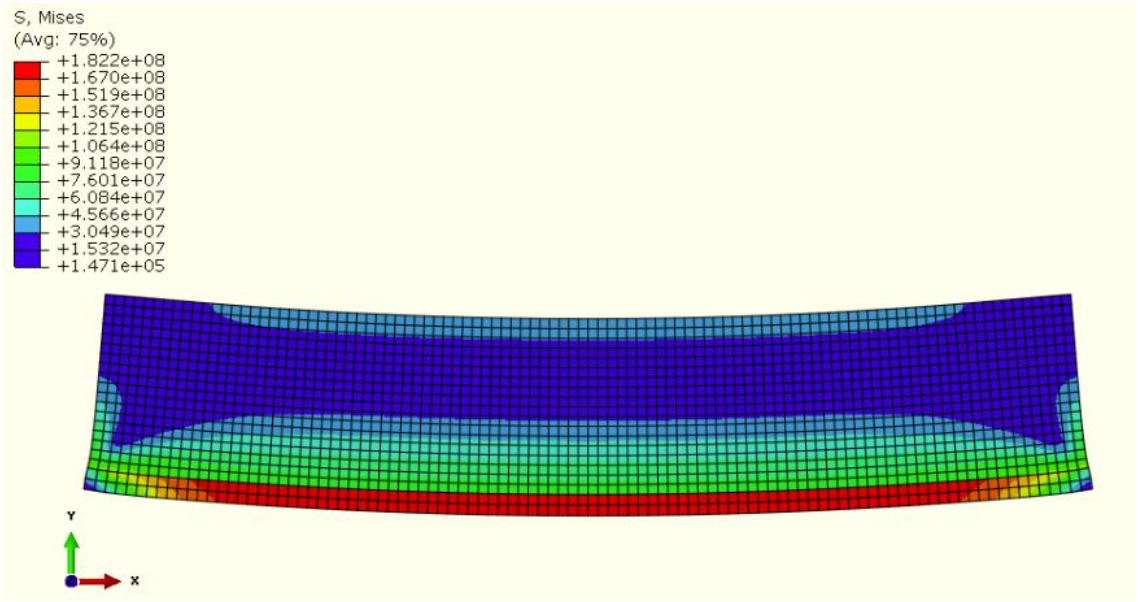

Figure E-20 Stress distribution diagram of the deformed mould, Invar content =50%, deformation scale factor=40, unit: Pa

E.1.11 Invar content =100%

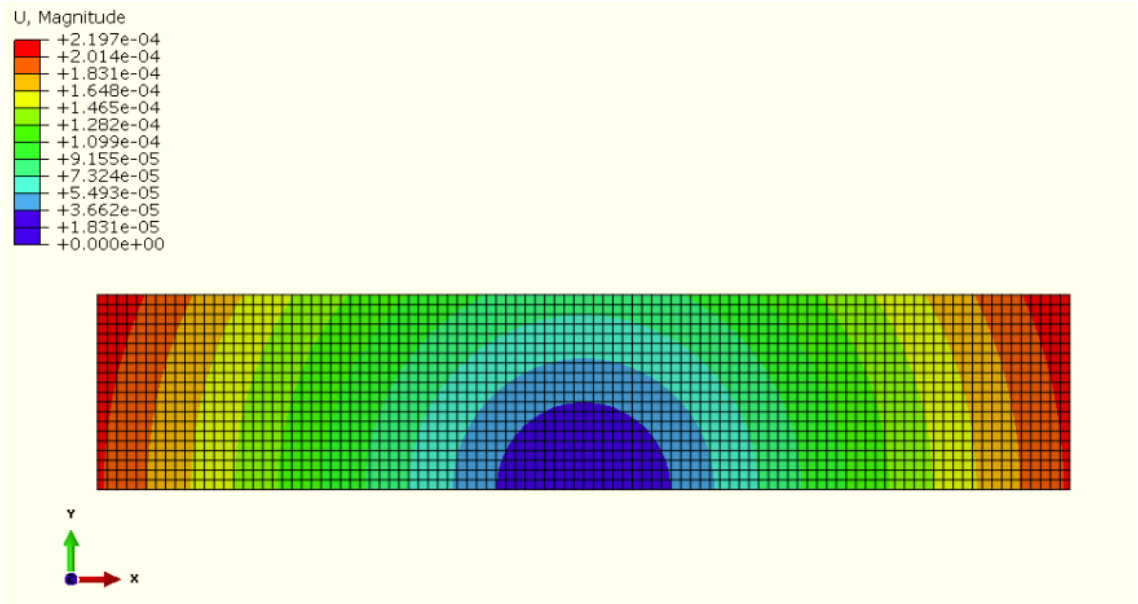

Figure E-21 Strain contours of the deformed shape, Invar content =100%, deformation scale factor=40, unit: m.

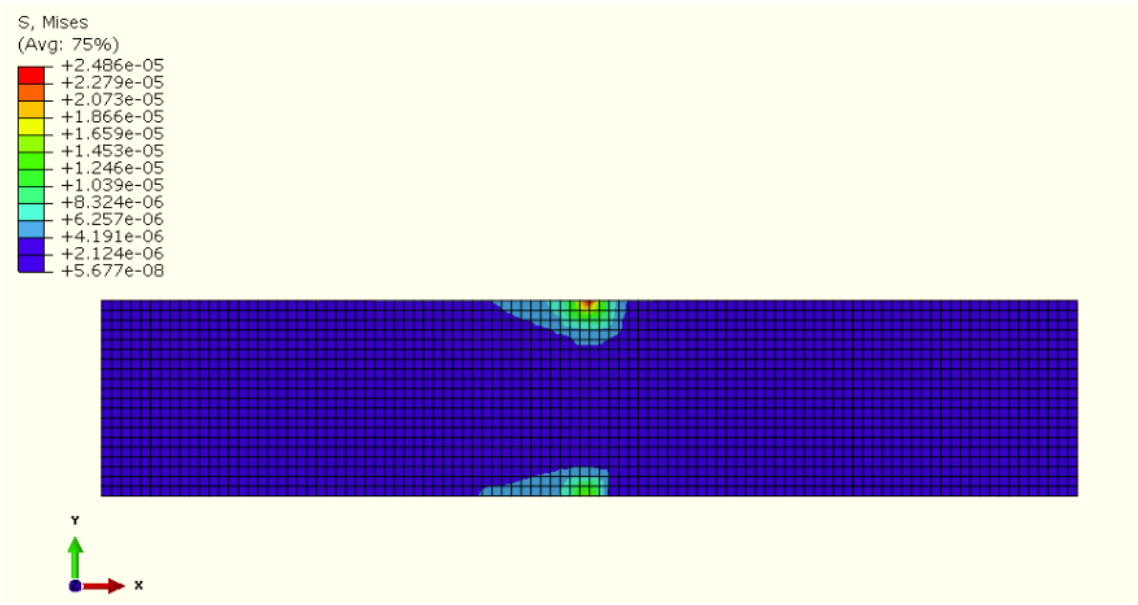

Figure E-22 Stress distribution diagram of the deformed mould, Invar content =50%, deformation scale factor=40, unit: Pa

E.2 Female models

E.2.1 Initial surface deformation

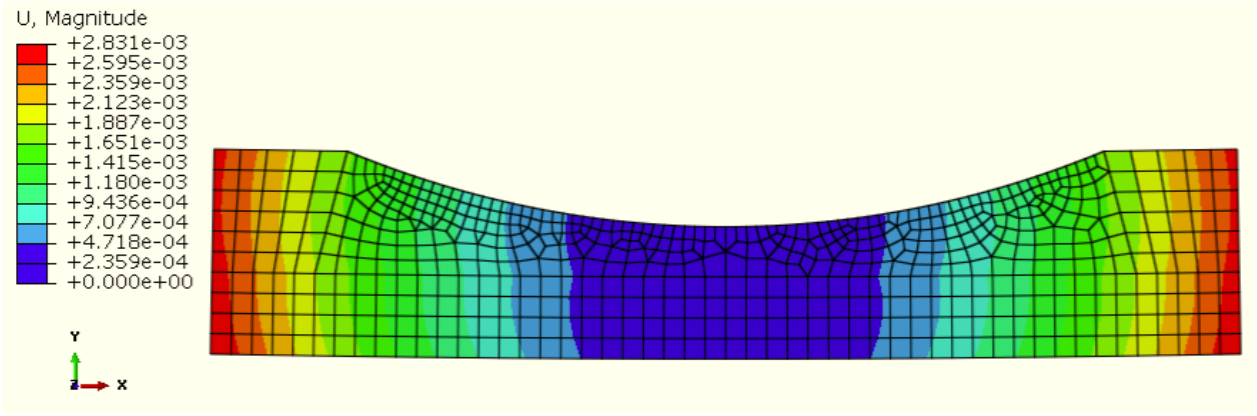

Figure E-23 Strain contours of original surface deformation, deformation scale factor=2, unit: m

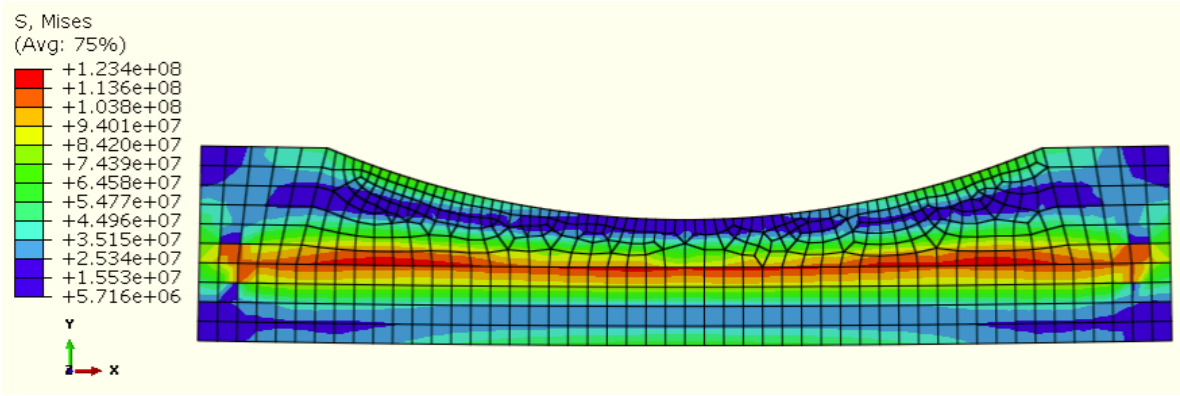

Figure E-24 Stress contours of original surface deformation, deformation scale factor=2, unit: Pa

E.2.2 Compensated surface deformation

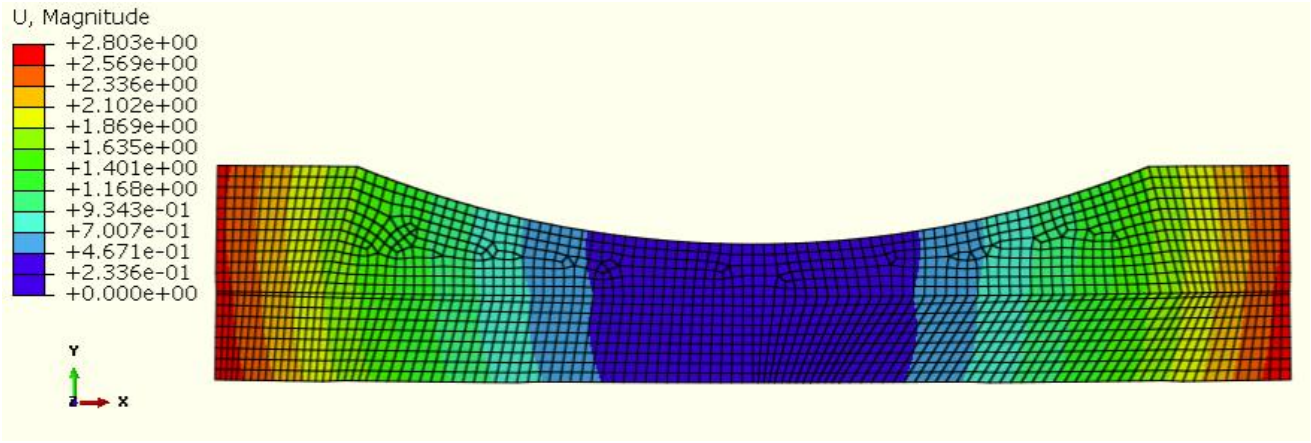

Figure E-25 Strain contours of compensated surface deformation (heated), deformation scale factor=2, unit: m

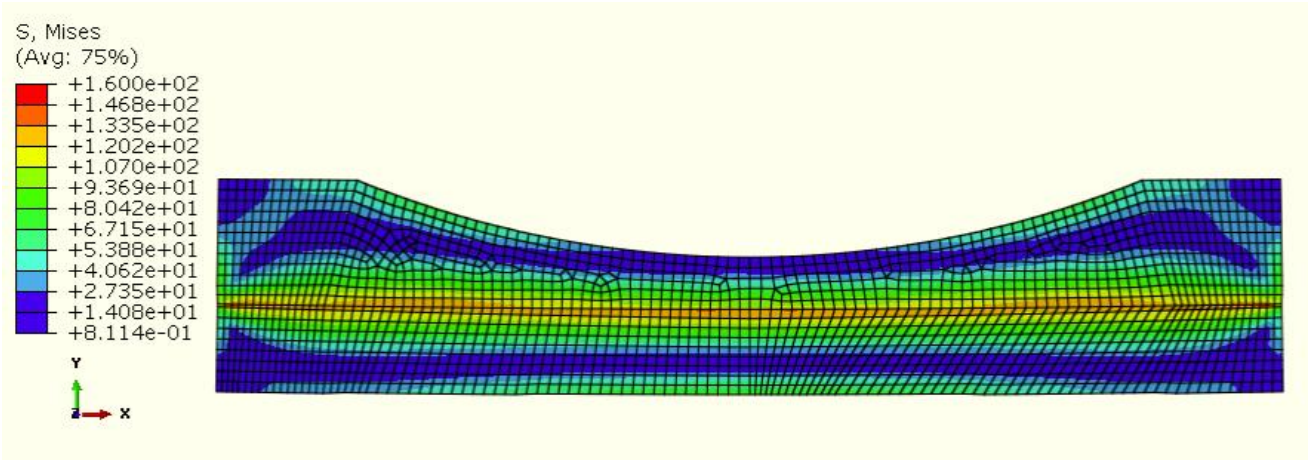

Figure E-26 Stress contours of compensated surface deformation (heated), deformation scale factor=2, unit: Pa